ACTA UNIVERSITATIS SZEGEDIENSIS

ACTA PHYSICA ET CHEMICA

NOVA SERIES

TOMUS XXV FASCICULI 1—2

AUSHAF 25 (1—2) (1—86) (1979)
HU ISSN 0001—6721

SZEGED, HUNGARIA
1979

ACTA UNIVERSITATIS SZEGEDIENSIS

ACTA PHYSICA ET CHEMICA

NOVA SERIES

TOMUS XXV. FASCICULI 1—2

AUSHAF 25 (1—2) 1—86 (1979)
HU ISSN 0001—6721

SZEGED, HUNGARIA
1979

Adiuvantibus

M. BARTÓK, M. BÁN, G. BERNÁTH, L. CSÁNYI, J. CSÁSZÁR, P. FEJES, F. GILDE, P. HUHN, I. KETSKEMÉTY, F. MÁRTA, F. SOLYMOSI, L. SZALAY et F. SZÁNTÓ

Redigit

PÁL FEJES

Edit

Facultas Scientiarum Naturalium Universitatis Szegediensis de Attila József nominatae

Editionem curant

J. ANDOR, M. BÁN, I. BÁRDI, J. HORVÁTH, Á. MOLNÁR, B. NÉMET et Á. SÜLI

Nota

Acta Phys. et Chem. Szeged

Szerkeszti

FEJES PÁL

A szerkesztő bizottság tagjai:

BARTÓK M., BÁN M., BERNÁTH G., CSÁNYI L., CSÁSZÁR J., FEJES P., GILDE F., HUHN P., KETSKEMÉTY I., MÁRTA F., SOLYMOSI F., SZALAY L. és SZÁNTÓ F.

Kiadja

a József Attila Tudományegyetem Természettudományi Kara (Szeged, Áradi Vértanúk tere 1.)

Szerkesztő bizottsági titkárok:

ANDOR J., BÁN M., BÁRDI I., HORVÁTH J., MOLNÁR Á., NÉMET B. és SÜLI Á.

Kiadványunk rövidítése:

Acta Phys. et Chem. Szeged

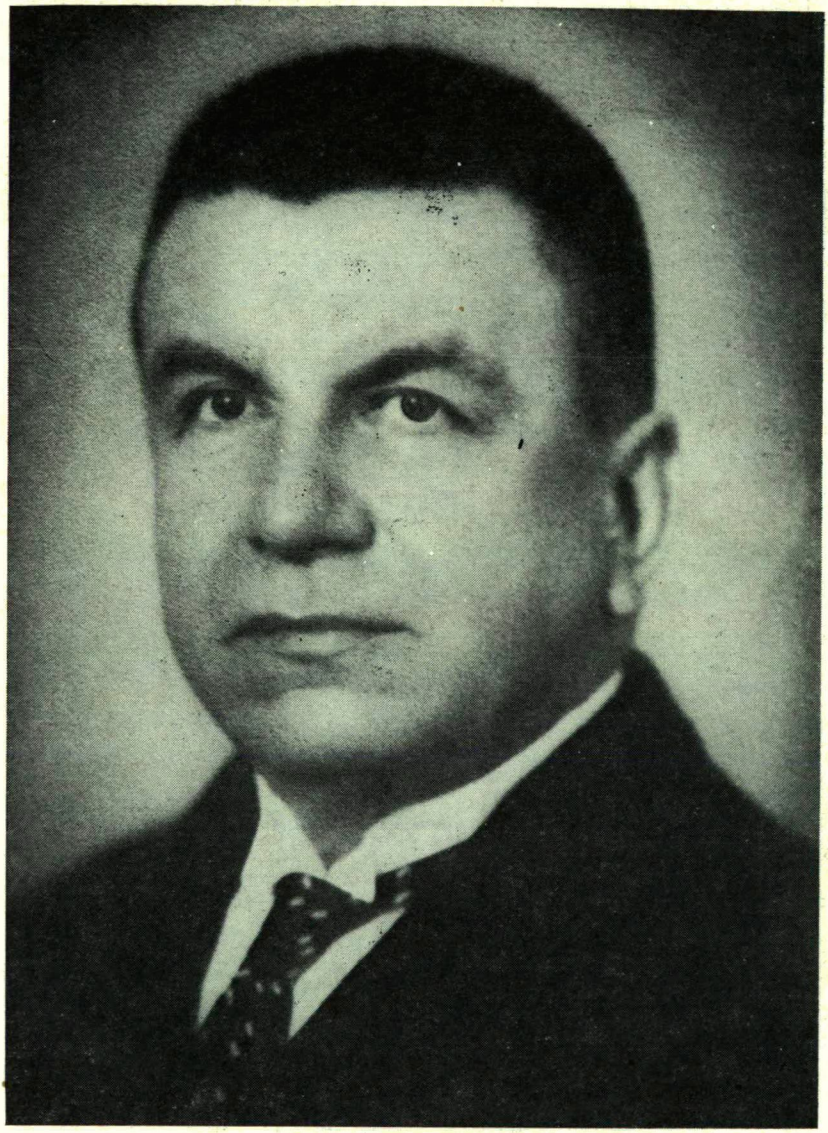

TIBOR SZÉKI
1879—1950

TIBOR SZÉKI
A TRIBUTE ON THE OCCASION OF THE 100th ANNIVERSARY OF HIS BIRTH

Tibor Széki was born on 18 April 1879 in Kolozsvár, where he also completed his university studies. He first obtained his diploma as a pharmacist, and in 1902 was awarded doctorates not only in pharmacy, but also in chemistry. Although his father, Miklós Széki, had a well-known pharmacy in Kolozsvár, after receiving his diplomas, Tibor did not opt for a pharmacy career. Instead, as he was strongly attracted towards university teaching and organic chemistry research, he was very pleased to accept the offer of a post as an assistant lecturer by Professor Rudolf Fabinyi, his mentor and ideal. This soon led to the possibility for him to develop his organic chemical knowledge further, particularly in the field of laboratory methods, in the Department of Organic Chemistry, at the Charlottenburg Technical University, in Berlin, under the guidance of Professor Karl Liebermann.

As was the custom at that time, following his appointment as a professor in Kolozsvár University, Rudolf Fabinyi had travelled abroad, and worked in the institutes of two famous organic chemists, Wislicenus and Adolf Baeyer. On returning to Kolozsvár, from 1876 on he had dealt mainly with research work in organic chemistry, as evidenced by a number of publications. Fabinyi may be regarded as the pioneer of Hungarian organic chemistry research. However, his wide interests soon diverted his attention to other areas of chemistry, and the organic chemistry research work in his institute only commenced a revival when he selected Tibor Széki as one of his assistants. Their first joint paper appeared in 1905, in Berichte der Deutschen Chemischen Gesellschaft, and was followed at short intervals by further publications. The successful activity of Tibor Széki, who had in the meantime been promoted to the position of lecturer, is indicated by the fact that in 1907 he was further upgraded for his work on "The chemistry of benzene-ring compounds", and in 1917 was appointed assistant professor. This rapid advance in his scientific career underwent a sudden break after the First World War, however: Kolozsvár was occupied by Roumanian troops, and then, as a consequence of the Peace Treaty of Trianon, the Roumanian government discontinued the activities of the Franz Joseph University in Kolozsvár, which had been founded in 1872. For this reason, the professors of the University were forced to leave Kolozsvár, and for the time being awaited their subsequent fate in Budapest. In 1921, the then Hungarian government denoted Szeged as the new site for the Franz Joseph University, but Professor Fabinyi did not live to know this, as he died in Budapest in 1920. Accordingly, Tibor

Széki was invited to take the only chair in chemistry at the Faculty of Mathematics and Natural Sciences of the University. He accepted this offer, even though the work in his father's pharmacy would have provided him with a safe and comfortable living. It is again a tribute to his attraction towards university teaching and organic chemistry research that he was able to overcome the strong sentimental attachment which he felt for the beloved town of his birth. The conditions under which he began work as an assistant professor in Szeged in 1922 were extremely primitive: the Department was housed in the basement and in 5 second-floor rooms of what had previously been a secondary school; there was practically no laboratory equipment, and the entire stock of the library consisted of 20 or so annual volumes of Berichte and Chemisches Zentralblatt, the personal property of Széki, brought with him from Kolozsvár.

Széki was faced with the task of somehow acquiring the equipment that was indispensable for the reasonably acceptable operation of the Department. In addition, he attached importance to the introduction of modern laboratory methods. In this connection, for example, in 1928 he arranged a scholarship for the writer of the present article to travel to Graz to become acquainted with all of the then known procedures of quantitative determination in organic microanalysis, in the institute of the Nobel Prize winner, Professor Fritz Pregl. This made it possible that as early as 1929 an organic microanalysis laboratory could commence operation in the Szeged department, as the first in Hungary. Here, all of the then known determination procedures were used to perform analyses not only for the Szeged group, but also for the Budapest departments and other institutes. (In his later period in Budapest, Széki immediately set up a similar laboratory.) The tasks of organization accompanying the development of the Department were solved in an exemplary way by Széki. All this demanded very much work, but in addition it was necessary to provide all of the special courses in chemistry for the chemistry and pharmacy students, involving 12–14 hours of lectures weekly. Some of this great load was taken off his shoulders only in 1924, when a second chemistry department was organized in the Faculty of Mathematics and Natural Sciences. However, even then there still remained for him the teaching work in organic chemistry and pharmaceutical chemistry, together with a special course of 2 hours a week on important topics in organic chemistry, such as the chemistry of carbohydrates, terpenes and alkaloids.

He was aided in his research and teaching work by only a small staff (1 lecturer, 3 assistant lecturers and 2 unpaid probationers), with no other technical help at all (laboratory technicians, office workers), even though the total number of students in the various categories soon rose to 180.

When I joined him as an assistant lecturer in 1926, I was amazed to observe what deep insight his lectures provided on the most important aspects of organic chemistry, including the chemistry of heterocyclic compounds, which was barely mentioned at the Technical University in Budapest at that time. His special organic chemistry courses gave a clear picture of the mental processes involved in structure research. He was a master in the art of lecturing, and as an ardent laboratory research worker he frequently presented interesting and instructive experiments, while he regularly shed light on questions of stereochemistry with the aid of models he had himself made. In spite of his great preoccupation with the teaching work, he continued the scientific researches he had been forced to abandon in Kolozsvár, as far as this was possible within the scope of the poor equipment and financial support of the

Department. Those striving for higher degrees were drawn into this work. A better possibility for the research opened only at the beginning of the nineteen-thirties when modern university buildings were constructed in Dóm Square; with the mediation of Albert Szent-Györgyi, the Rockefeller Foundation supported the up-to-date equipping of many of the departments of the Faculty of Medicine and the Faculty of Mathematics and Natural Sciences; at the same time, there was a considerable increase in the annual financial support of these departments on the basis of an agreement reached with the then Ministry of Education. Nevertheless, Tibor Széki enjoyed these improved conditions for only a short time, as in 1935 he was invited by the Péter Pázmány University to take the chair made vacant by the retirement of Professor Lajos Winkler. Here again he carried out much teaching and organizig work, primarily because he reorganized the existing department to be the Department of Organic and Pharmaceutical Chemistry. It was to his credit that Budapest University could finally begin to provide the necessary number of lessons weekly as regards the theoretical and laboratory teaching in organic chemistry, which was compulsory for the chemistry and pharmacy students. These students numbered around 250–300 each year, whereas merely 5 teaching staff were available (2 professors, 3 assistant lecturers, 1 unpaid probationer).

Evidence as to the scientific work of Tibor Széki is given by the 42 publications he prepared, and by the same number of doctoral theses in organic chemistry produced under his guidance. Most of his publications appeared in Berichte der D. Ch. Gesellschaft, Liebigs Annalen and Archiv der Pharmazie. In addition, he wrote a university text-book "Pharmaceutical Chemistry", published in 1941.

It is not possible to give a detailed account of his publications here, and I should like simply to refer to a few of his results. A fair number of his first papers, jointly written with Fabinyi, deal with the study of azarone (2,4,5-trimethoxypropenylbenzene). This naturally-occurring organic compound was isolated from the oil of *Asarum Europaeum,* which grows wild in the vicinity of Kolozsvár. The most interesting of their investigations in this respect relate to the unusual reactions of azarylaldehyde with various Grignard reagents. These reactions did not yield the expected secondary alcohols, but the ethers produced by bimolecular condensation of the latter. Széki and a small numbers of his staff dealt with azarone, and particularly with the azarone oil, in Szeged too; they isolated and identified some of the previously unknown components of the oil. A very interesting further feature of his examinations with Fabinyi was a condensation reaction that can be induced between pyrogallol and various ketones, and that leads to the formation of tetracyclic compounds. One of the especially interesting results of the research work in Szeged was the discovery of a correlation between pungent taste and molecular structure. With organic compounds synthetized for this purpose, Miklós Jancsó, the then Professor of Pharmacology, was able to attain just such an interesting anti-inflammatory effect in experimental animals as with, for example, capsaicine, the pungent-tasting component of paprika. Another interesting research field begun in Szeged was the study of the dimerization of phenolic ethers possessing a propenyl side-chain. These studies were later continued in Budapest by Sándor Müller, who discovered the mechanism of the dimerization and the steric structures of the stereoisomeric dimers.

In recognition of the results of his scientific research, Tibor Széki was elected a Corresponding Member of the Hungarian Academy of Sciences in 1934, and

a Full Member in 1945 (among others, his nomination was supported by László Zechmeister, Gyula Gróh and Frigyes Konek). In connection with his university activities, he was Dean of the Faculty of Mathematics and Natural Sciences in Szeged University in 1926/27, and Rector there in 1933/34. Of the organic chemists who worked under his professorial guidance, 3 in Szeged (Zoltán Földi, László Vargha and Győző Bruckner) and 1 in Budapest (Sándor Müller) acquired much higher qualifications and positions as a consequence of his initiatives, and all of them joined in the teaching of organic chemistry within special courses. The public activities of Tibor Széki are indicated by the facts that he was elected Vice-Chairman of the Hungarian Pharmaceutical Society from 1938 to 1943, and was subsequently its Chairman until 1947, while he was Chairman of the Hungarian Chemical Society in 1941.

Tibor Széki, one of the pioneers of Hungarian organic chemistry research, died suddenly in Budapest in 1950, after a life filled with much honourable work and not free from trial. After his death, his family presented his official portrait to the Várpalota Museum. However, it was in vain that I sought for it there among the portraits of the great Hungarian chemists. It might appear that Tibor Széki is not worthy of being remembered! However, I for one, who was his colleague for 8 years, will always treasure his memory with respect and affection, and I am convinced that numerous Hungarian organic chemists and pharmacists look back on him with similar feelings.

Győző Bruckner

Member of the Hungarian
Academy of Sciences

INTERMOLECULAR POTENTIAL FUNCTIONS FOR NONPOLAR MOLECULES

By

C. MALINOWSKA-ADAMSKA*

State University of New York at Binghamton
Binghamton, New York 13901

(Received, May 1, 1979)

The potential energy curves appropriate for rare gas atoms have been analysed. Relative merits of these curves (in particular Morse hybrid potential functions) have been tested by calculating the values of the vibrational energy eigenvalue differences and comparing them with the experimental ones. Reliable estimates of the function parameters have been collected and compared with those obtained from molecular beam experiments.

Introduction

Knowledge of intermolecular forces is necessary for an understanding of many of the physical properties of rare gas systems. A number of recent studies, both theoretical and experimental, have contributed to this knowledge. The calculation of potential energy curves can in principle be accomplished by means of quantum mechanical calculations. However, computational difficulties prevent these curves from being calculated routinely for rare gas molecules. The short-range repulsive portion of these curves has been obtained from either Self-Consistent-Field or Thomas–Fermi–Dirac calculatios. In addition, the long-range attractive portion of these curves is known to have the form $-C_6r^{-6}-C_8r^{-8}-C_{10}r^{-10}$ [1]. In the last few years approximate theoretical calculations of the short-range repulsions [2–5] and accurate estimates for the C_6, C_8 and C_{10} coefficients for a variety of pairwise interactions of rare gas atoms have been reported [6–8]. Other advances have increased our knowledge of rare gas interactions. Potential energy curves have been obtained from *ab initio* calculations based on an electron gas model [9]. Also, *ab initio* potential curves for He_2 have been obtained [10–12]. The vacuum ultraviolet absorption spectra have been reported for a variety of rare gas systems [13, 38]. Molecular beam experiments have been carried out and the results have been analysed to obtain the potential energy curves of a number of combinations of rare gas atoms [34, 36, 37]. Other workers have produced semi-empirical potential functions by fitting a model potential form to experimental data.

* On leave from the Institute of Physics, Technical University of Łódź, Wólczańska 219, 93—005 Łódź, Poland.

The primary difficulty with such semi-empirical schemes is in the choice of the potential function model.

In this paper we analyse the potential energy curves appropriate for the rare gas atoms. Relative merits of these curves have been tested by calculating the values of the vibrational energy eigenvalue differences and comparing them with the experimental values. Reliable estimates of the function parameters have been collected and compared with those obtained from molecular beam experiments.

Potential energy functions appropriate for rare gas atoms

The Lennard–Jones (12–6) potential has been widely used in the study of intermolecular forces [13–15]. This potential has the form:

$$U(r) = 4\varepsilon\left[\left(\frac{\delta}{r}\right)^{12} - \left(\frac{\delta}{r}\right)^{6}\right]. \tag{1}$$

Here ε and δ are parameters which represent an energy and a length which is characteristic of the system under consideration. This potential was widely used previously because of its simple analytic form, but has since been considered too inflexible to reproduce of dilute gas properties [17–21], therefore, some attempts to evaluate low density equilibrium and transport data have been directed towards finding more flexible functions [19]. Notable, among these are the Kihara potential [22]:

$$\begin{aligned} U(r) &= 4\varepsilon\left[\left(\frac{\delta-2a}{r-2a}\right)^{12} - \left(\frac{\delta-2a}{r-2a}\right)^{6}\right] \quad r \geqq 2a \\ &= \infty \qquad\qquad\qquad\qquad\qquad\qquad\quad r \leqq 2a. \end{aligned} \tag{2}$$

In Eq. 2 a third parameter "a" is added to represent the molecular core size, the Guggenheim–Mc Glasham potential [23], which introduces additional anharmonic terms in the neighbourhood of the potential minimum in order to explain solid properties, the formulation of BOYS and SHAVIT [24] which expands the potential in a complete set of Gaussian function, and the potential functions of DYMOND, RIGBY and SMITH [25] which represent the intermolecular energy by two-parameter in five terms, inverse power expression:

$$U(r) = \varepsilon\left[0.331\left(\frac{r_m}{r}\right)^{28} - 1.2584\left(\frac{r_m}{r}\right)^{24} + 2.07151\left(\frac{r_m}{r}\right)^{18} - 1.74452\left(\frac{r_m}{r}\right)^{8} - 0.39959\left(\frac{r_m}{r}\right)^{6}\right] \tag{3}$$

where r_m is the intermolecular separation at the minimum energy $-\varepsilon$. The attractive term in r^{-24} has no theoretical basis but was found necessary to give a broad bowl to the potential function to fit experimental data. This potential gave a sound treatment of second virial coefficients and gave the correct lattice energies when used in conjunction with AXILROD's nonparwise corrections [26]. It also gave satisfactory agreement when applied to the calculation of third virial coefficients [25].

BUCKINGHAM [16,17] and BUCKINGHAM–CORNER [27] have proposed three parameter potential functions. These potentials are respectively given by:

$$U(r) = \varepsilon[\alpha/(\alpha-6)]\{(6/\alpha)\exp[\alpha(1-rr_m^{-1})]-r_m^6 r^{-6}\}, \tag{4}$$

$$U(r) = \varepsilon\left\{g_1(\alpha,\beta)\exp\left[\alpha\left(1-\frac{r}{r_m}\right)\right]-g_2(\alpha,\beta)\left(\frac{r_m}{r}\right)^6\times\left[1+\beta\left(\frac{r_m}{r}\right)^2\right]\right\}, \quad r \geqq r_m. \tag{5}$$

$$U(r) = \varepsilon\left\{g_1(\alpha,\beta)\exp\alpha\left(1-\frac{r}{r_m}\right)-g_2(\alpha,\beta)\left(\frac{r_m}{r}\right)^6\times\left[1+\beta\left(\frac{r_m}{r}\right)^2\right]\exp 4\left(1-\frac{r}{r_m}\right)^3\right\}. \quad r \leqq r_m.$$

$$g_1(\alpha,\beta) = (6+8\beta)/[\alpha(1+\beta)-(6+8\beta)],$$

$$g_2(\alpha,\beta) = \alpha/[\alpha(1+\beta)-(6+8\beta)],$$

where α is the parameter which is a measure of the steepness of the exponential repulsion. The parameters $\alpha, \beta, \varepsilon, r_m$ have been determined from the crystal data, second virial and the Joule–Thomson coefficient data. (The function of Eq. (4), in fact, is that portion of the modified Buckingham (exp−6) potential which is defined for $r \geqq r_{max}$. Here r_{max} is the position of the spurious maximum in the potential due to the unrealistic importance of the r^{-6} term for small r; r_{max} is the smallest root of $\exp[\alpha(1-r_m^{-1}r_{max})]=r_m r_{max}^{-1}$ [28]).

The success and failures of three-parameter potential functions are well known [29]. They have the advantage of their flexibility but two limitations, in particular, restrict their use for the prediction of data [30]. On the basis of the data available at this time one finds:

1. For any property, a set of parameters used to fit the data taken in a given temperature range cannot be relied upon to predict this property correctly in another temperature range.
2. A set of parameters used to fit one kind of property (*e.g.* viscosity) cannot be relied upon to predict correctly data for another property (*e.g.* second virial coefficient).

Furthermore parameters chosen with a model function do not always agree with values obtained from direct independent information such as the results of scattering experiments. Several authors have tried to remove the limitations of the three-parameters functions by proposing more elaborate potentials.

Successful examples are the semitheoratical Barker potential [31] and the *m*-6-8 potential based Barker one [30].

Barker function has the form:

$$U(r) = \varepsilon\left\{\exp[\alpha(1-r)]\sum_{i=0}^{3}A_i(r-1)^i-\sum_{l=0}^{2}C_{2l+6}/(\delta+r)^{2l+6}\right\}. \tag{6}$$

Here $r=R/R_m$, where R is the internuclear distance, R_m is the separation between atoms which corresponds to the minimum of the potential well, and ε is the value of the potential at its minimum. The C_6, C_8 and C_{10} coefficients are set equal to their calculated values. The remaining parameters are used to fit the function to

second virial coefficient data, molecular beam scattering measurements and low-pressure gas transport properties. The resulting potentials afford excellent agreement with a variety of experimental results other than those used in fixing their parameters. However, the method is limited by the large amount of experimental data which is needed.

Other semi-empirical schemes have been proposed by BERNSTEIN and MORSE [32], BRUCH and MC GEE [33] and KONOWALOW and ZAKHEIM [1]. These workers used a Morse function of the form:

$$U(r) = 4\varepsilon(y^2 - y), \tag{7}$$

$$y = \exp\left[c\left(1 - \frac{r}{\delta}\right)\right],$$

Here δ is the value of the separation of the nuclei such that $U(r)=0$.

LEE [34] has proposed a hybrid potential function which he has fit to molecular beam scattering data. This potential is called the exponential-spline-Morse-spline-van der Waals (ESMSV) potential and has the following form:

$$f(x) = U(r)/\varepsilon, \quad x = r/r_m.$$

$$f(x) = A\exp[-\alpha(x-1)], \quad 0 \leqq x \leqq x_1.$$

$$f(x) = \exp\left(a_1 + (x-x_1)\{a_2 + (x-x_2)[a_3 + (x-x_1)a_4]\}\right),$$

exponential spline function, $x_1 \leqq x \leqq x_2$.

$$f(x) = b_1 + (x-x_3)\{b_2 + (x-x_4)[b_3 + (x-x_3)b_4]\}, \tag{8}$$

spine function, $x_3 \leqq x \leqq x_4$.

$$f(x) = -C_6 r^{-6} - C_8 r^{-8} - C_{10} r^{-10}, \quad x_4 \leqq x \leqq \infty.$$

This potential gives good results for Ne_2 when compared with experimental data other than the solid state measurements from which its parameters were deduced [35]. For the heavier rare gas systems, instead of ESMSV potential, Morse-spline-van der Waals (MSV) potential [36, 38] was used. This potential has the form [36]:

$$f(x) = U(r)/\varepsilon,$$

$$f(x) = \exp[-2\beta(x-1)] - 2\exp[-\beta(x-1)], \quad 0 \leqq x \leqq x_1.$$

$$f(x) = b_1 + (x-x_1)\{b_2 + (x-x_2)[b_3 + (x-x_1)b_4]\}, \tag{9}$$

spline function, $x_1 \leqq x \leqq x_2$.

$$f(x) = -c_6 x^{-6} - c_8 x^{-8} - c_{10} x^{-10}, \quad x_2 \leqq x \leqq \infty,$$

where $c_i = C_i/\varepsilon r_m^i$.

Other workers have reported potential functions which are constructed from a Morse function, a long-range tail function, and an interpolating polynomial to join the two segments [5, 28]. KONOWALOW and ZAKHEIM [1] have reported Morse-6 hybrid potentials. Their potentials were constructed from three parts: *1)* A short-range term of the form $U(r)=A\exp(-\lambda r)$, *2)* a long-range dipole-dipole dis-

persion attraction $U(r) = -C_6 r^{-6}$, where the C_6 coefficients are obtained from highly accurate semiempirical estimates; *3)* A Morse function of the form:

$$U(r) = \varepsilon\left\{\exp\left[-2\frac{c}{\delta}(r-r_m)\right] - 2\exp\left[-\frac{c}{\delta}(r-r_m)\right]\right\}, \tag{10}$$

which is used to connect the long and short-range segments.

Recently, KONOWALOW and co-workers described a modification of their procedure [41]. The term $-C_6 r^{-6}$ is replaced by $-C_6 r^{-6} - C_8 r^{-8} - C_{10} r^{-10}$, which is a more accurate representation of the long-range behaviour. The parameters A, λ, C_6, C_8 and C_{10} are available from theoretical calculations [3–8]. The other parameters: ε, c, δ or r_m, and q_0, where q_0 is the contact point between the Morse function and the long-range portion of the curve, are obtained by fitting second virial coefficient data.

Experimental second virial coefficient have traditionally been used in the study of intermolecular forces because of their ready availability and the ease at which they can be calculated for model potentials. The virial equation state for real gases is [14]:

$$pV_0 = RT(1 + B(T)/V_0 + C(T)/V_0^2 + \ldots),$$

where B and C are the second and third virial coefficients, respectively and V_0 is the molar volume. It is shown from statistical mechanics [14] that

$$B(T) = B_\Omega(T) + \frac{h^2}{m} B_1(T), \tag{11}$$

where:

$$B_\Omega(T) = 2\pi N_A \int_0^\infty [1 - \exp(-U(r)/kT)] r^2 dr$$

and

$$B_1(T) = \frac{N_A}{24\pi k^3 T^3} \int_0^\infty \left(\frac{dU(r)}{dr}\right)^2 \exp(-U(r)/kT) r^2 dr$$

$B_\Omega(T)$ is the classical second virial coefficient and $B_1(T)$ is the first quantum correction to it. Here N_A is Avogadro number, k is Boltzman constant, h is Planck constant, m is the mass of the particle and $U(r)$ is some central field potential function. $U(r)$ is usually expressed in terms of a number of parameters.

In order to calculate the second virial coefficients at a given temperature T, the form of the potential must be specified. The potential under consideration has the form [41]:

$$U(r) = \varepsilon\left\{\exp\left[-2\frac{c}{\delta}(r-r_m)\right] - 2\exp\left[-\frac{c}{\delta}(r-r_m)\right]\right\}, \quad 0 \leqq r \leqq q_0. \tag{12}$$

$$U(r) = -C_6 r^{-6} - C_8 r^{-8} - C_{10} r^{-10}, \quad q_0 \leqq r \leqq \infty.$$

Another equivalent formula for the Morse potential is [1]:

$$U(r) = 4\varepsilon\left\{\exp\left[2c\left(1-\frac{r}{\delta}\right)\right]-\exp\left[c\left(1-\frac{r}{\delta}\right)\right]\right\}.$$

In order to determine the parameters c, δ, ε, C_6, C_8, C_{10} and q_0 KONOWALOW and co-workers applied the following procedure [41]: The C_6, C_8 and C_{10} coefficients set equal to their theoretical value. The repulsive portion of the Morse potential is set equal to the short-range repulsion [40] of the form: $A\exp(-\lambda r)$, where A and λ are obtained from quantum mechanical calculations.

$$A\exp(-\lambda r) = 4\varepsilon\exp\left[2c\left(1-\frac{r}{\delta}\right)\right].$$

Then

$$A = 4\varepsilon\exp(2c) \tag{13}$$

and

$$\lambda = 2c/\delta. \tag{14}$$

The parameter q_0 is found by finding the largest root of the equation:

$$-C_6r^{-6}-C_8r^{-8}-C_{10}r^{-10}-4\varepsilon\left\{\exp\left[2c\left(1-\frac{r}{\delta}\right)\right]-\exp\left[c\left(1-\frac{r}{\delta}\right)\right]\right\} = 0.$$

The largest root is chosen because the long-range portion of the curve is valid only for large values of r. The parameter c is varied until the minimum of the difference between the sum of the squares of the calculated and experimental second virial coefficient is obtained. If c is obtained ε and δ can be calculated by means of Eqs. (13) and (14). The value of r_m is found by use of the relation:

$$r_m = (\delta/c)(c+\ln 2) \quad [42].$$

The parameters of the potential energy functions for nonpolar molecules were calculated without using the first quantum correction [41]. Here we include the estimates, where the first quantum correction was used in the calculation of the second virial coefficient also. From these potentials vibrational energy eigenvalue differences are calculated and are compared to experimental spectroscopic evidence [38, 39]. The function's parameters are compared to those obtained from various recent intramolecular potential calculations [1, 28, 30, 31, 41–58].

Empirical, semiempirical and theoretical parameters of the potential energy functions for nonpolar molecules

Reliable estimates of the parameters potential energy curves for nonpolar molecules are collected in Tables I–III.

Table I

*Summary of parameters for the Lennard-Jones, Buckingham, Buckingham-Corner and Morse potential models for rare gas atoms**

Position	Potential function	System	Parameters				Method of calculation	Ref.
			ε			r_m		
1.	Lennard-Jones (12-6) Eq. (1)	Ne-Ne Ar-Ar Kr-Kr Xe-Xe	50.113 164.698 219.506 314.763			3.16 3.87 4.04 4.46	Crystal data (CD)	[42]
			α	ε		r_m		
2.	Buckingham (Exp-6) Eq. (4)	Ne-Ne Ar-Ar Kr-Kr Xe-Xe	14.5 14.0 12.3 13.0	52.460 170.082 218.539 319.181		3.147 3.866 4.056 4.450	CD, second virial coefficient (SVC) and viscosity coefficient	[27]
			β	α	ε	r_m		
3.	Buckingham Corner (exp. 6-8) Eq. (5)	Ne-Ne Ar-Ar Kr-Kr Xe-Xe	0.2	13.9 13.6 11.7 12.8	51.218 170.082 219.230 324.703	3.87 3.16 4.08 4.45	CD and SVC	[17]
			c	δ	r_m	ε		
4.	Morse Eq. (7)	Ne-Ne Ar-Ar Kr-Kr Xe-Xe	5.1 5.0 4.5 4.9	2.775 3.386 3.510 3.872	3.152 3.855 4.038 4.420	60.729 199.902 252.224 379.234	The combination of CD and SVC data	[42]

* ε in units of 10^{-23} J; δ and r_m in units of 10^{-10} m.

Discussion

Table III clearly shows the effect of adding higher-order terms in the long-range London dispersion potential. The effect of adding the C_8 and then the C_{10} term was to decrease the depth of the well as the additional terms were included. In addition the value of δ and r_m was increased by 0.0003–0.0004 nm with the addition of the C_8 term and by about 0.0001 nm with the addition of the C_{10} term to the $-C_6r^{-6}-C_8r^{-8}$ tail. The effect of adding the C_8 term to the $-C_6r^{-6}$ tail is more pronounced than the addition of the C_{10} term to the tail which already includes the $-C_6r^{-6}-C_8r^{-8}$ term. Potentials which include the quantum corrections have smaller c values than those without this correction. The smaller c value implies that the well depth will be greater and that δ and r_m will be smaller for the potentials with the corrections. For example, in the case of Ar_2 the change in the well depth in the order of 1.38×10^{-23} J. (Values for the depth of the ground state potential well of Ar_2 and Kr_2 found from various intramolecular potential calculations [1, 28, 30, 31, 41–58] are summarized in Table IV.)

Table II
Summary of optimal parameters for the Morse-6 hybrid potential

System	No potential	Parameters								Method of calculation	Ref.
		c	δ 10^{-10} m	r_m 10^{-10} m	ε 10^{-23} J	A 10^{-16} J	λ 10^{10} m^{-1}	C_6 10^{-26} Jnm^6	q_0 10^{-10} m		
1	2	3	4	5	6	7	8	9	10		
Ne-Ne	1	6.0444	3.1993	3.5661	70.294	5.0011	3.7785	60.3012	6.0966	Parameters A, λ, C_6 from SCF calculations, other ones from second virial coefficient (SVC) data.	[1]
	2	6.0472	3.2007	3.5676	69.902	5.0011	3.7785	67.2884	5.9697		
	3	6.0276	3.1904	3.5572	72.696	5.0011	3.7785	0	5.9924		
	4	6.0014	2.7295	3.0447	67.714	4.4204	4.3974	60.3012	4.0945		
	5	6.0020	2.7298	3.0450	67.628	4.4204	4.3994	67.2884	3.8937		
	6	5.9433	2.7031	3.0183	76.059	4.4204	4.3974	0	4.0138		
	7	6.2574	2.6584	2.9529	73.256	7.9794	4.7075	60.3012	3.6621		
	8	6.2255	2.6449	2.9394	78.072	7.9794	4.7075	67.2884	3.4473		
	9	6.2048	2.6361	2.9306	81.380	7.9794	4.7075	0	3.5371		
	10	6.2015	2.6650	2.9629	72.012	6.9750	4.6541	60.3012	3.7066		
	11	6.1740	2.6532	2.9511	76.076	6.9750	4.6541	67.2884	3.4873		
	12	6.1468	2.6415	2.9393	80.339	6.9750	4.6541	0	3.5928		
	13	6.1696	2.6698	2.9696	71.285	6.5151	4.6218	60.3012	3.7383		
	14	6.1454	2.6593	2.9593	74.823	6.5151	4.6218	67.2884	3.5173		
	15	6.1137	2.6456	2.9456	79.727	6.5151	4.6218	0	3.6306		
Ar-Ar	1	5.8608	3.2323	3.6146	226.2981	11.1522	3.6264	622.1549	4.7456		
	2	5.8576	3.2305	3.6128	227.7476	11.1522	3.6264	663.3129	4.5866		
	3	5.8285	3.2145	3.5967	241.4150	11.1522	3.6264	0	4.6740		
	4	5.2046	3.3343	3.7783	196.1195	2.6013	3.1219	622.1549	5.8015		
	5	5.2077	3.3363	3.7803	194.9046	2.6013	3.1219	663.3129	5.6602		
	6	5.1742	3.3148	3.7589	208.3925	2.6013	3.1219	0	5.7336		
	7	5.8037	3.4179	3.8261	209.1656	9.1958	3.3961	622.1549	5.5912		
	8	5.8062	3.4194	3.8276	208.1302	9.1958	3.3961	663.3129	5.4733		
	9	5.7746	3.4008	3.8090	221.6871	9.1958	3.3961	0	5.5318		
	10	5.5020	3.4814	3.9200	195.7329	4.7064	3.1608	622.1549	6.1302		
	11	5.5945	3.4830	3.9216	194.7389	4.7064	3.1608	663.3129	6.0122		
	12	5.4765	3.4653	3.9039	205.9627	4.7064	3.1608	0	6.0634		
Kr-Kr	1	6.1843	3.4904	3.8816	325.9455	30.6722	3.5437	1225.1666	5.1371		
	2	6.1825	3.4894	3.8806	327.1051	30.6722	3.5437	1340.0260	4.9463		
	3	6.1588	3.4759	3.8672	343.0228	30.6722	3.5437	0	5.0056		
	4	5.1162	3.5906	4.0771	271.3865	3.0163	2.8497	1225.1666	6.5834		
	5	5.1195	3.5930	4.0795	269.5504	3.0163	2.8497	1340.0260	6.3880		
	6	5.0941	3.5751	4.0616	283.6181	3.0163	2.8497	0	6.4437		
Xe-Xe	1	6.2268	3.5434	3.9379	538.2725	55.1554	3.5140	2641.7656	4.7009		
	2	6.2071	3.5322	3.9267	559.9332	55.1554	3.5146	0	4.8711		

Table III

Summary of parameters for the Morse-6, -8, -10 hybrid potentials

System	No Pot.	Parameters										Method of calculation	Ref.
		c	δ 10^{-10} m	r_m 10^{-10} m	ε 10^{-23} J	A 10^{-16} J	λ 10^{10} m^{-1}	C_6 10^{-26} J nm^6	C_8 10^{-28} J nm^8	C_{10} 10^{-30} J nm^{10}	q_0 10^{-10} m		
Ar-Ar	1	5.2075	3.3362	3.7802	194.9598	2.6012	3.1219	647.9983	3025.9683	0.0	5.5340	Parameters	
	2	5.2087	3.3369	3.7810	194.5181	2.6012	3.1219	647.9983	3025.9683	18462.52	5.2436	A, λ, C_6, C_8	
	3	5.8149	3.4245	3.8327	204.5408	9.1957	3.3961	647.9983	3025.9683	0.0	5.1819	C_{10}, from	
	4	5.8163	3.4253	3.8335	203.9610	9.1957	3.3961	647.9983	3025.9683	18462.52	5.0821	SCF calcu-	
	5	5.5065	3.4843	3.9229	193.9658	4.7064	3.1608	647.9983	3025.9683	0.0	5.8079	lations,*	
	6	5.5071	3.4846	3.9232	193.7587	4.7064	3.1608	647.9983	3025.9683	18462.52	5.7574	δ, c, r_m, ε,	[41]
Kr-Kr	1	5.1159	3.5905	4.0769	271.4970	3.0163	2.8497	1273.0247	6630.8642	0.0	6.2277	from SVC	
	2	5.1164	3.5908	4.0773	271.2347	3.0163	2.8497	1273.0247	6630.8642	46231.35	6.1694	data without quantum corrections	
Ne-Ne	1′	5.9980	2.7280	3.0432	68.1724	4.3974	4.3974	62.6940	153.3085	0.0	3.5604		
	2′	5.9622	2.7117	3.0269	73.2335	4.3974	4.3974	62.6940	153.3085	523.8552			
	3′	6.1872	2.6286	2.9231	84.2930	7.9795	4.7075	62.6940	153.3085	0.0			
	4′	6.1914	2.6304	2.9249	83.5820	7.9795	4.7075	62.6940	153.3085	523.8552		SVC	
	5′	6.1296	2.6341	2.9319	83.1527	7.0147	4.6541	62.6940	153.3085	0.0			
	6′	6.1338	2.6359	2.9338	82.4514	7.0147	4.6541	62.6940	153.3085	523.8552		with	
	7′	6.0967	2.6338	2.9382	82.4720	6.5151	4.6218	62.6940	153.3085	0.0			
	8′	6.0967	2.6338	2.9382	82.4271	6.5151	4.6218	62.6940	153.3085	523.8552		quantum	
Ar-Ar	1′	5.2051	3.3346	3.7787	195.8986	2.6012	3.1219	647.9983	3025.9683	0.0	5.3619	corrections	
	2′	5.2062	3.3353	3.7794	195.4706	2.6012	3.1219	647.9983	3025.9683	18462.52	5.2536		
	3′	5.8120	3.4228	3.8310	205.7418	9.1957	3.3961	647.9983	3025.9683	0.0	5.1898		
	4′	5.8133	3.4236	3.8318	205.1758	9.1957	3.3961	647.9983	3025.9683	18462.52	5.0918		
	5′	5.5040	3.4827	3.9213	194.9322	4.7064	3.1608	647.0083	3025.9683	0.0	5.8133		
	6′	5.5046	3.4830	3.9216	194.7251	4,7064	3.1608	647.9983	3025.9683	18462.52	5.7633		
Kr-Kr	1′	5.1152	3.5900	4.0764	271.8697	3.0163	2.8497	1273.0247	6630.8642	0.0	6.2295		
	2′	5.1157	3.5903	4.0768	271.6212	3.0163	2.8497	1273.0247	6630.8642	46231.35	6.1714		

* The guide to the literature Ref. [1]

The effect of adding higher-order terms to the long-range portion of the potential on the vibrational energy levels of Ar_2 and Kr_2 we can see from Tables V–VI. These tables compare the vibrational spacings calculated from Morse hybrid potentials with experimental spectroscopic evidence [38, 39] and in the case of Kr_2 with the MSV scattering potential results [57]. Tables V–VI show that vibrational levels are predicted by all the present potentials which include a C_8r^{-8} term in the long range portion. The best results are obtained for the Morse hybrid 2′ (M-hybrid 2′) potential. Parameters of this potential are compared with experimental data in Table VII.

Table IV

Potential well depth ε [J] for Ar_2 and Kr_2

Ar_2			Kr_2		
Potential	$\varepsilon \cdot 10^{-21}$	Ref.	Potential	$\varepsilon \cdot 10^{-21}$	Ref.
Kihara	2.032	[43]	Kihara	2.959	[52]
Kihara	1.973	[44]	Kihara	2.977	[53]
Lennard—Jones(16-6)	2.056	[25]	Lennard—Jones (12-6)	2.366	[54]
Morse	1.831	[45]	Morse	2.527	[42]
exp-6	2.099	[43]	exp-6	2.959	[43]
Morse-6-hybrid	2.084	[1]	Morse-6-hybrid	2.700	[1]
M-6-8	2.112	[28]	M-6-8	2.715	[41]
M-6-8-10	1.955	[41]	M-6-8-10	2.712	[41]
Kingston	2.022	[46]	Dymond-Adler	2.716	[53]
Munn—Smith	2.112	[47, 48]	Rigid—Morse—		
Barker—Pompe	2.039	[31]	Mie—van der Waals	2.561	[56]
Dymond—Alder	1.908	[50]	Barker—Bobetic	2.725	[49]
Barker—Bobetic	1.936	[49]	MSV	2.746	[57]
Barker—Fisher	1.962	[51]	Gordon—Kim	2.485	[58]
Watts					
MSV	1.993	[36]			

Table V

Comparison of the experimental data for the vibrational spacings for the ground electronic state of Ar_2 with calculated from Morse hybrid potentials

v''	$G\left(v''+\frac{1}{2}\right)$ [cm^{-1}]						
	Experiment	1′	2′	3′	4′	5′	6′
0	25.4	24.364	24.338	27.162	27.124	24.607	24.594
1	20.2	20.246	20.224	22.570	22.539	20.447	20.437
2	15.5	16.111	16.094	17.961	17.936	16.272	16.263
3	10.3	11.676	11.664	13.017	12.999	11.792	11.787
4	7.99	6.946	6.939	7.744	7.733	7.015	7.012
5		3.697	3.693	4.121	4.115	3.733	3.731
6		1.465	1.464	1.633	1.631	1.480	1.479

Table VI

Comparison of the experimental data for the vibrational spacings for the ground electronic state of Kr_2 with calculated from Morse hybrid potentials and MSV scattering potentials.

v''	$G\left(v''+\frac{1}{2}\right)$ [cm^{-1}]				
	Experiment	1′	2′	MSV[a]	MSV[b]
0	21.56	20.995	21.015	21.17	21.39
1	19.09	19.237	19.229	19.15	19.26
2	16.76	17.479	16.237	16.86	16.81
3	14.76	15.719	14.602	14.65	14.74
4	12.23	13.961	12.969	12.69	13.10
5	10.49	12.201	11.334	10.80	11.07
6	8.92	10.437	9.700	8.96	9.00
7	6.92	8.662	8.050	7.12	7.11
8	5.54	6.671	6.200	5.38	5.42
9	4.09	4.412	4.10	4.01	3.94
10	2.87	2.982	2.77	2.83	2.69
11	1.86	1.819	1.69	1.80	1.68
12	1.07	0.968	0.90	1.00	0.90

[a] $r_m = 0.411$ [nm]
[b] $r_m = 0.403$ [nm] Ref. [38]

Table VII

Experimental results for Ar_2 and Kr_2

Substance	Potential	Parameters			Ref.
		$\varepsilon \cdot 10^{-21}$ J	r_m nm	δ nm	
Ar_2	Barker—Fisher—Watts	1.962	0.37612	0.33605	[51]
	MSV-II	1.993	0.3715	0.3330	[36]
	MSV-III	1.942	0.376	0.3354	[36]
	M-hybrid 2′	1.954	0.37794	0.3353	
Kr_2	Barker—Bobetic	2.725	0.40152	0.35944	[49]
	MSV	2.746	0.411		[57]
	M-hybrid 2′	2.716	0.40768	0.35903	

The comparison of the Morse hybrid potentials with experimental data and potentials obtained by other workers reveals that the method of calculation of the parameters of the Morse hybrid potential function is adequate for the heavier rare gas systems. For this reason Morse hybrid potentials appear to warrant further application in the description of van der Waals molecules. As a successful example we refer to the KONOWALOW–MUHLHAUSEN paper [59].

Acknowledgement

The author wishes to thank Professor D. D. KONOWALOW for helpful discussion connected with this paper as well as the possibility to visit the Department of Chemistry, State University of New York at Binghamton.

Warm thanks are due to Professor L. WOJTCZAK for reading the manuscript and also to Professor J. KARNIEWICZ, Head of the Institute of Physics, Technical University of Łódź, for kindly supporting these investigations.

References

[1] *Konowalow, D. D., D. S. Zakheim:* J. Chem. Phys. **57**, 4375 (1972).
[2] *Abrahamson, A. A.:* Phys. Rev. **178**, 76 (1969).
[3] *Gaydaenko, V. J., V. K. Nikulin:* Chem. Phys. Letters **7**, 360 (1970).
[4] *Gilbert, T. L., A. C. Wahl:* J. Chem. Phys. **47**, 3425 (1967).
[5] *Matcha, R. L., R. K. Nesbet:* Phys. Rev. **160**, 72 (1967).
[6] *Dalgarno, A., J. H. Morrison, R. M. Pengelly:* Intern. J. Quantum Chem. **1**, 16 (1967).
[7] *Langhoff, P. W., M. Karplus:* J. Chem. Phys. **53**, 233 (1970).
[8] *Starkschall, G., R. G. Gordon:* J. Chem. Phys. **54**, 663 (1971)[a]; **56**, 2801 (1972)[b].
[9] *Gordon, R. G., Y. S. Kim:* J. Chem. Phys. **56**, 3122 (1972).
[10] *Bertoncini, P., A. C. Wahl:* Phys. Rev. Letters **25**, 991 (1970).
[11] *Schaefer, H. F., D. R. Mc Laughlin, F. E. Harris, B. J. Alder:* Phys. Rev. Letters **25**, 988 (1970).
[12] *Mc Laughlin, D. R., H. F. Schaefer:* Chem. Phys. Letters **12**, 244 (1971).
[13] *Tanaka, Y., K. Yoshino:* J. Chem. Phys. **53**, 2012 (1972).; **57**, 2964 (1972).
[14] *Hirschfelder, J. O., C. F. Curtiss, R. B. Bird:* Molecular Theory of Gases and Liquids, J. Wiley & Sons, New York, 1954.
[15] *Whalley, E., W. G. Schneider:* J. Chem. Phys. **23**, 1644 (1955).
[16] *Buckingham, A. D.:* J. Chem. Phys. **23**, 412 (1955).
[17] *Barua, A. K.:* J. Chem. Phys. **31**, 957 (1959).
[18] *Amdur, I., T. F. Schatzki:* J. Chem. Phys. **27**, 1949 (1957).
[19] *Fender, B. E. F., G. D. Halsey, Jr.:* J. Chem. Phys. **36**, 1881 (1962).
[20] *Tee, L. S., S. Gotoh, W. E. Steward:* Ind. Eng. Chem. Fundamentals **5**, 356 (1966).
[21] *Konowalow, D. D., S. L. Guberman:* Ind. Eng. Chem. Fundamentals **7**, 622 (1968).
[22] *Kihara, T.:* Rev. Mod. Phys. **25**, 831 (1953).
[23] *Guggenheim, E. A., M. L. Mc Glashan:* Proc. Roy. Soc. (London) **A 255**, 456 (1960).
[24] *Boys, S. F., I. Shavitt:* Nature **178**, 1340 (1956).
[25] *Dymond, J. H., M. Rigby, E. B. Smith:* J. Chem. Phys. **42**, 2801 (1965).
[26] *Axilrod, B. M.:* J. Chem. Phys. **17**, 1349 (1949); **19**, 24 (1951).
[27] *Mason, E. A., W. E. Rice:* J. Chem. Phys. **22**, 843 (1954).
[28] *Konowalow, D. D.:* J. Chem. Phys. **50**, 12 (1969).
[29] *Hanley, H. J. M., M. Klein:* J. Chem. Phys. **50**, 4765 (1969).
[30] *Klein, M., H. J. M. Hanley:* J. Chem. Phys. **53**, 4722 (1970).
[31] *Barker, J. A., A. Pompe:* Aust. J. Chem. **21**, 1683 (1968).
[32] *Berstein, R. B., F. A. Morse:* J. Chem. Phys. **40**, 917 (1964).
[33] *Bruch, L. W., I. J. Mc Gee:* J. Chem. Phys. **46**, 2959 (1967).
[34] *Siska, P. E., J. M. Parson, T. P. Schafer, Y. T. Lee:* J. Chem. Phys. **55**, 5762 (1971).
[35] *Farrar, J. M., Y. T. Lee, Y. Y. Goldman, M. L. Klein:* Chem. Phys. Letters, **19**, 359 (1973).
[36] *Parson, J. M., P. E. Siska, Y. T. Lee:* J. Chem. Phys. **56**, 1511 (1972).
[37] *Chen, C. H., P. E. Siska, Y. T. Lee:* J. Chem. Phys. **59**, 601 (1973).
[38] *Tanaka, Y., K. Yoshino, D. E. Freeman:* J. Chem. Phys. **59**, 5160 (1973).
[39] *Maitland, G. C., E. B. Smith:* Mol. Phys. **22**, 861 (1970).
[40] *Nesbet, R. K.:* J. Chem. Phys. **48**, 1419 (1968).
[41] *Konowalow, D. D.:* Preprint.
[42] *Konowalow, D. D., J. O. Hirschfelder:* Phys. Fluids **4**, 629 (1961).
[43] *Sherwood, A. E., J. M. Prausnitz:* J. Chem. Phys. **41**, 429 (1964).
[44] *Barker, A., W. Fock, F. Smith:* Phys. Fluids **7**, 897 (1964).
[45] *Konowalow, D. D., S. Carra:* Phys. Fluids **8**, 1585 (1965).

[46] *Kingston, A. E.:* Phys. Rev. **135 A**, 1018 (1964).
[47] *Munn, R. J.:* J. Chem. Phys. **40**, 1439 (1964).
[48] *Munn, R. J., F. J. Smith:* J. Chem. Phys. **43**, 3998 (1965).
[49] *Bobetic, M. W., J. A. Barker:* Phys. Rev. **B 2**, 4169 (1970), **B 5**, 3185 (1972).
[50] *Dymond, J. H., B. J. Alder:* J. Chem. Phys. **51**, 309 (1969).
[51] *Barker, J. A., R. A. Fisher, R. O. Watts:* Mol. Phys. **21**, 657 (1971).
[52] *Weir, R. D., I. Wynn Jones, J. S. Rowlinson, G. Saville:* Trans. Faraday Soc. **63**, 1320 (1967).
[53] *Lin, H. M., R. L. Robinson, Jr.:* J. Chem. Phys. **54**, 52 (1971).
[54] *Stogryn, D. E., J. O. Hirschfelder:* J. Chem. Phys. **31**, 1531 (1959).
[55] *Dymond, J. H.:* J. Chem. Phys. **54**, 3675 (1971).
[56] *Davis, B. W.:* J. Chem. Phys. **57**, 5098 (1972).
[57] *Docken, K. K., T. P. Schafer:* J. Mol. Spectrosc. **46**, 454 (1973).
[58] *Gordon, R. G., Y. S. Kim:* J. Chem. Phys. **56**, 3122 (1972).
[59] *Muhlhausen, C. W., D. D. Konowalow:* Chem. Phys. **7**, 143 (1975).

ФУНКЦИИ МЕЖМОЛЕКУЛЯРНОЙ ПОТЕНЦИАЛЬНОЙ ЭНЕРГИИ ДЛЯ НЕПОЛЯРНЫХ МОЛЕКУЛ

Ц. Малиновска – Адамска

В данной работе обсуждается проблема кривых потенциальной энергии применимых для неполярных молекул. Правильность этих функций (прежде всего Морзе-гидридных кривых) доказывается сравнением вычисленных расстояний между осцилляционными уровнями с экспериментальными значениями. Результаты полученные для параметров межмолекулярных функций применимых для неполярных молекул собранье вместе с экспериментальными данными.

МАТЕМАТИЧЕСКОЕ МОДЕЛИРОВАНИЕ НА ЭВМ ХАРАКТЕРИСТИК IMPATT-ГЕХЕРАТОРОВ

К. М. ДАТИЕВ

Северо-Кавказный Горнометаллургический Институт,
Факультет электронной техники, г. Орджоникидзе, СССР

(Поступило в редакцию в 19 апреля 1979 г.)

В статье издожен метод расчета характеристик IMPATT-генераторов, основанный на численном решении уравнений сохранения заряда совместно с уравнением Пуассона. Результаты моделирования на ЭВМ позволяют за малое время и с хорошей точностью получить информацию об основных характеристик генераторов.

Введение

Теоретическому анализу высокочастотных характеристик лавинно-пролетных диодов посвящены работы как советских, так и зарубежных авторов.

Аналитический метод решения задачи позволяет, при использования ряда допущений, просто и эффективно определять характеристики IMPATT-диода [1, 2]. В работах авторов [3, 4] наряду с аналитическими методами расчета диодов используются методы чусленного анализа, позволяющие решать широкий круг задач, связанных с проектированием твердотельных генераторов.

Несмотря на трудности, связанные со сложностью численных моделей и с необходимостью длительного счета на ЭВМ, использование моделей численного анализа перспективно, так как позволяет избавиться от упрощений, свойсвенных аналитическим методам и учесть основные факторы, влияющие на работу приборов.

В данной работе изложен простой и легкой метод для машинной реализации численный метод решения исходной дифференциальной системы уравнений, позволяющий рассчитать динамические характеристики прибора, приведены результаты некоторых расчетов.

В основе анализа работы полупроводниковых приборов лежит совместное решение уравнений сохранения заряда, уравнения Пуассона и уравнения полного тока.

Для одномерного случая система имеет вид:

$$\frac{\partial n}{\partial t} = \frac{1}{q}\left(\frac{\partial I_n}{\partial x} + \alpha_p I_p + \alpha_n I_n\right)$$

$$\frac{\partial p}{\partial t} = \frac{1}{q}\left(\frac{\partial I_p}{\partial x} + \alpha_p I_p + \alpha_n I_n\right)$$

$$\frac{\partial E}{\partial x} = \frac{q}{\varepsilon}(N_g - N_a + p - n) \tag{1}$$

$$I(t) = I_p + I_n + \varepsilon \frac{\partial E}{\partial t}$$

$$I_n = qnV_n$$

$$I_p = qpV_p,$$

где n, p — концентрация электронов и дырок соответственно
N_g, N_a — концентрация донорных и акцепторных ионов примеси соответсвенно
V_n, V_p — скорости электронов и дырок соответсвенно
I_n, I_p, I — плотность электронного, дырочного и полного тока соответсвенно
E — напряженность электрического поля
α_n, α_p — коэффициенты ударной ионизации для электронов и дырок
q — абсолютное значение заряда электрона
ε — диэлектрическая проницаемость.

Система решается для активной области пространственного заряда IMPATT диода в предположении, что на выводы диода синусоидальное напряжение, наложенное на постоянное смещение

$$U(t) = V_0 + V_1 \sin \omega t \tag{2}$$

Граничное условие для управления Пуассона определяется условием

$$U(t) = \int_{x_э}^{x_g} E(x,t)dx \tag{3}$$

где $x_э$ и x_g — левая и правая границы активной области, задавались либо неподвижными (для проколотых структур), либо определялись из условия равенства нулю напряженности в этих точках. Знаки в исходной системе выбраны так, что электроны движутся слева направо, а дырки справо налево, так что в качестве граничных условий для уравнений сохранения заряда можно взять

$$n(x_э, t) = n_0 \quad p(x_g, t) = p_0 \tag{4}$$

а начальными условиями могут быть

$$n(x, 0) = n_0 \quad p(x, 0) = p_0 \tag{5}$$

где n_0 и p_0 — малые концентрации носителей, обеспечивающие обратные токи в предпробойном режиме.

Решением исходной системы уравнений являются пространсвенно-временные зависимости дырочного и электронного токов и полного тока цепи в зависимости от падения напряжения на переходе. Гармонический анализ этих величин дает значение мощности, отдаваемой в нагрузку, активной и реактивной состовляющих проводимости.

Поскольку исходная система уравнений в частных призводных нелинейна, аналитическое решение задачи возможно лишь при использовании некоторых допущений.

Для численного анализа данной системы использовался метод конечных разностей [5].

Ниже в конечно-разностной форме представлена нормированная система уравнений (напряженность включает в себя сомножитель ε а все концентрации включает в себя сомножитель q):

$$\frac{n_i^j - n_i^{j-1}}{\tau} = \frac{I_{n_i+1}^{j-1} - I_{n_i}^{j-1}}{h} + \alpha_p(E) I_p^{j-1} + \alpha_n(E) I_{n_i}^{j-1}$$

$$\frac{p_i^j - p_i^{j-1}}{\tau} = \frac{I_{p_i-1}^{j-1} - I_{p_i}^{j-1}}{h} + \alpha_p(E) I_{p_i}^{j-1} + \alpha_n(E) I_{n_i}^{j-1}$$

$$\frac{E_i^j - E_{i-1}^j}{h} = N_g - N_a + (p_i^j - n_i^j + p_{i-1}^j + n_{i-1}^j) \cdot 0{,}5 \qquad (6)$$

$$I_{n_i}^j = V_n(E) n_i^j$$

$$I_{p_i}^j = V_p(E) p_i^j$$

$$I^j = 0{,}5 \cdot (I_{p_i}^j + I_{p_i}^{j-1} + I_{n_i}^j + I_{n_i}^{j-1}) + \frac{E_i^j + E_i^{j-1}}{\tau},$$

где надстрочный индекс j обозначает текущую точку по времени, подстроечный индекс i — текущую точку по расстоянию, h — шаг по расстоянию, τ — шаг по времени.

Для сходимости численного решения к точному необходимо выполнения условий

$$h < \frac{1}{\alpha(E_{\max})} \quad \text{и} \quad \tau \leqq \frac{h}{V}. \qquad (7)$$

На первом этапе работы программы в рабочие массивы заносятся начальные и граничные условия. По заданному значению напряженности в точке $E_{\max}$ в предположении, что обьемный заряд мало меняется за один шаг по времени. Значения коэффициентов в каждой точке находятся для $E = E_i^{j-1} + 0{,}5(E_{\max}^j - E_{\max}^{j-1})$.

Определяются для всех точек по расстоянию значения n_i^j, p_i^j, $I_{n_i}^j$, $I_{p_i}^j$, I^j, затем вычисляется падения напряжения в активной области и цикл повторяется для следующего шага по времени. Расчет ведется для нескольких периодов,

пока ток не станет периодической функцией, анализ которой позволяет получить величину мощности, отдаваемой в нагрузку, активной и реактивной проводимостей диода.

Используемый метод расчета прост, легко дополняется членами учитывающими процессы рекомбинации, диффузии. Ниже проводятся результаты расчетов для двухпролетного диода на арсенида галлия проколотой структуры на частоте $2 \cdot 10^{10}$ Гц. Расчет проводился при

$$N_a = N_g = 1{,}9 \cdot 10^{16}\ \text{см}^{-3} \quad x_э = x_g = 1{,}32 \cdot 10^{-4}\ \text{см}$$

$$\alpha_p = \alpha_n = 2{,}07 \cdot 10^5 \exp\left[-\left(\frac{6{,}64 \cdot 10^5}{E}\right)^2\right] \tag{8}$$

$$U = 71 + 21 \cos \omega t.$$

В течении всего периода напряженность поля в пролетных областей обеспечивает дрейф электронов и дырок со скоростями насыщения ($V_n = V_p = 5{,}4 \cdot 10^6$ см сек$^{-1}$)

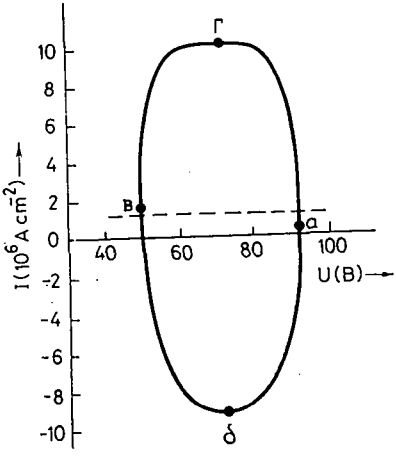

Рис. 1. Зависимость плотности полного тока от напряжения на диоде

На рис. 1. представлена зависимость тока на зажимах прибора от приложенного напряжения, характеризующая фазовые соотношения между ними, пунктиром отмечено значение средней плотности тока. Точка *а* соответствует максимальному значению напряжения: *б, г* среднему и *b* минимальному значению приложенного напряжения. Отрицательная активная проводимость при средней плотности тока 1200 Асм$^{-2}$ составила 33 Ом$^{-1}$ см$^{-2}$, электронный КПД — 17%.

На рис. 2 приводятся распределения поля и плотностей дырочных и электронных токов для моментов времени соответствующих точкам *а, б, в, г* на рис. 1. Объемный заряд носителей заметно понижает поле в зоне лавинного пробоя, импульсы токов формируются к моменту достижения напряжением своего среднего значения. Импульсы, движущиеся в пролетных областях не создают дополнительных максимумов поля достаточных для возникновения лавинного пробоя, к концу периода импульсы частиц выходят из дрейфовой области.

Для того же диода на рис. 3. приведены зависимости отрицательной активной проводимости и электронного КПД от амплитуды переменного напряжения при средней плотности тока 1200 Асм$^{-2}$.

Программа составлена на языке Алгамс для ЭВМ «Минск—22», при быстродействии машины в 5 тысяч операций в секунду, время счета одного периода составляет в среднем 20 минут.

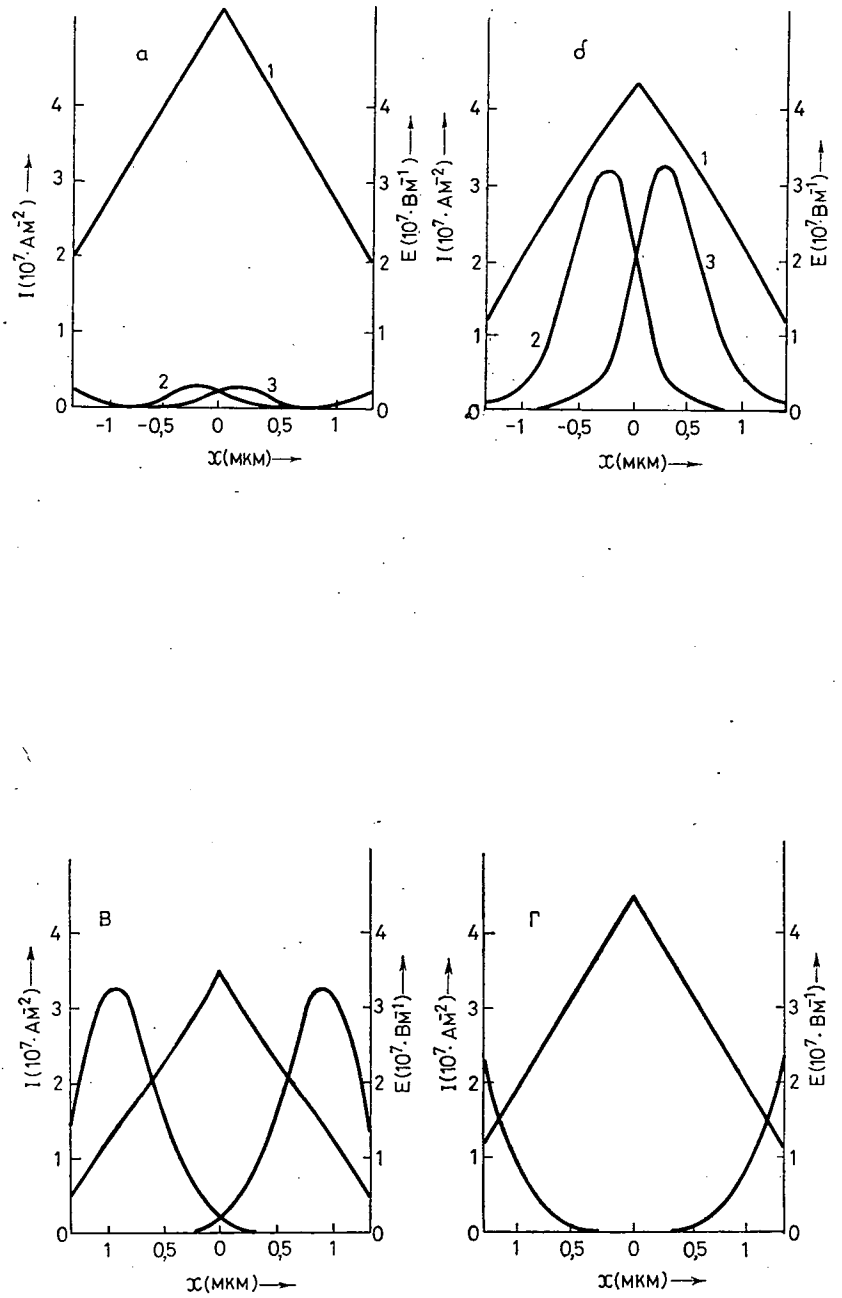

Рис. 2. Распределение электрического поля (1), плотности электронного (2) и дырочного (3) токов в различные моменты периода колебаний

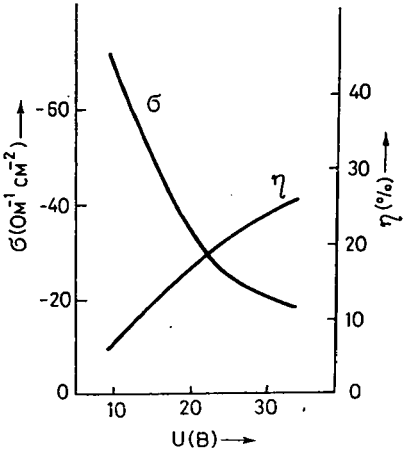

Рис. 3. Зависимость отрицательной активной проводимости (б) и коэффициента полезного действия от амплитуды переменного напряжения

Выводы

Предложений метод анализа прост, легко реализуем на ЭВМ и позволяет с хорощей точностью получить информацию об основных динамических характеристик одно- и двухпролетных IMPATT-диодов в широком диапазоне частот, с заданными распределями концентраций примесей и зависимости коэффициентов лавинного умножения и скоростей от поля.

Метод решения исходной системы дифференциальных уравнений может быть хорошей основой для расчета других полупроводниковых приборов.

Литература

[1] *Тарег, А. С., В. М. Вальд-Перлов:* Лавино-пролетные диоды и их применение в технике СВЧ, М., «Советское радио» 1968.
[2] *Захаров, А. Л.:* Полное описание уточненной модели активной области IMPATT-диода. «Электротехника». «Электронная техника», сер. 2, «Полупроводниковые приборы», 1977.
[3] *Кэррол, Дж.:* СВЧ-генераторы на горячих электронах, М. «Мир», 1972.
[4] *Yu, P., W. Tantraporn:* IEEE Trans. Elec. Dev. **22**, 515 (1975).
[5] *Годунов, С. К., В. С. Рябеньский:* Разностные схемы, М., «Наука», 1973.

COMPUTER SIMULATION OF THE CHARACTERISTIC OF IMPATT DIODES

K. M. Datiev

A computer simulation method is described to calculate the characteristic of IMPATT generators on the basis of Poisson's equation and charge conservation. The method gives a fast and precise information on the characteristics of IMPATT diodes.

DETERMINATION OF THE THICKNESS AND THE REFRACTIVE INDEX OF V_2O_5 THIN FILMS FROM REFLECTANCE INTERFERENCE SPECTRA

By

Á. SÜLI, L. MICHAILOVITS and I. HEVESI

Institute of Experimental Physics, Attila József University, Szeged

(Received March 25, 1979)

The thickness and the refractive index of V_2O_5 thin layers on silicon single-crystal plates were determined from the reflectance interference spectra measured at 45° and 29.2° angle of incidence in the wavelength range of 360 nm—900 nm. The thin V_2O_5 layers were prepared by evaporating vanadium layers of different thickness onto silicon single-crystal plates and oxidizing the vanadium layer at 400° C. For evaluation of the reflectance spectra an approximate calculation was applied. The density of thin layers was determined from the thickness of vanadium measured during the evaporation and from the thickness of vanadium pentoxide layers measured by optical method. For the density of the V_2O_5 films an average value of 3.1 g/cm³ was obtained. A reflectance peak found at about 420 nm was attributed to the V^{4+} concentration present in the vanadium pentoxide.

Introduction

The mechanisms of carrier transport, the voltage dependence of capacitance, and the photoconductivity of V_2O_5-nSi system were reported in earlier communications [1, 2]. We measured some physical parameters of the V_2O_5 layers, but concerning the thickness and refractive index were restricted only to estimations. The subject of the present paper is the determination of the thickness and the refractive index of vanadium pentoxide thin films — prepared by evaporation and subsequent oxidation of vanadium on silicon single-crystal plates — from reflectance interference spectra.

As it is known, if a non-absorbing planparallel slab with a thickness of d and a refractive index of n is bordered on its sides by two non-absorbing media I and II with refractive indices of n_0 and n_1, respectively, ($n_0 < n$; $n_1 < n$ for all wavelengths taken into account), then the light beams *1* and *2* reflected from the upper and the lower surfaces of the slab will interfere (Fig. 1). Due to this interference the intensity of the light beams reflected at α angle will exhibit maxima and minima at the following wavelength:

$$\lambda_{max} = \frac{4d\sqrt{n^2(\lambda_{max}) - n_0^2(\lambda_{max})\sin^2\alpha}}{2k-1} = \frac{A(\lambda_{max})}{2k-1} \tag{1}$$

$$\lambda_{min} = \frac{4d\sqrt{n^2(\lambda_{min}) - n_0^2(\lambda_{min})\sin^2\alpha}}{2k} = \frac{A(\lambda_{min})}{2k}, \tag{2}$$

where $k=1, 2, 3, \ldots$. In Eqs. (1) and (2) the wavelength dependence of the refractive indices should be taken into account. If medium I is air, then $n_0=1$ is true with a good approximation in a wide spectral region.

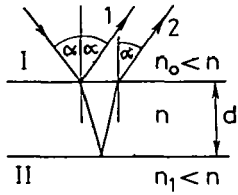

Fig. 1.

For our reflectance spectra we can write;

$$\text{maxima:} \quad \lambda_1 = A(\lambda_1), \quad \lambda_3 = \frac{A(\lambda_3)}{3}$$

$$\text{minima:} \quad \lambda_2 = \frac{A(\lambda_2)}{2} \quad \lambda_4 = \frac{A(\lambda_4)}{4}, \tag{3}$$

i.e. we have taken into account only the first and second order extrema. Knowing the $n=n(\lambda)$ function the thickness of the layers can be calculated from Eqs. (1) and (2). Although the $n(\lambda)$ function is known for the crystallographic directions *a*, *b*, *c* in the case of vanadium pentoxide single-crystal [3–5], we cannot use directly these values of refractive indices, because the prepared layers are certainly not single-crystals, and the optical properties of thin films generally differ from that of bulk materials. The method applied for the evaluation of interference spectrum and for determination of the thickness and the refractive indices of the thin V_2O_5 layers will be discussed in the last section.

Experimental

Vanadium layers (thickness: 57 nm, 52 nm, 45 nm, 20 nm and 11.5 nm) were evaporated onto freshly etched silicon single-crystal plates of 15 mm×15 mm×0.2 mm in size or onto chemically cleaned mica sheets in 5×10^{-6} torr vacuum. The thickness of the condensed metal layer was determined during the evaporation process by a Thin Film Thickness and Deposition Rate Monitor instrument type MSV-1841; made by the Hungarian Research Institute for Precision Engineering. The vanadium covered silicon plates (in the followings referred to as samples) and mica sheets (in the followings referred to as sheets) were held in an oxigen stream of atmospheric pressure in an oven of 400° C temperature. The vanadium layers which differed in thickness were oxidized for different time-periods. From time to time the oxidation process was interrupted and the reflectance spectra of the samples and the sheets were determined.

The reflectance spectra were measured at an angle of $\alpha=45°$ and $\alpha=29.2°$ changing the wavelength of the monochromatic light beam in 5 nm or 10 nm steps in the 360 nm–900 nm range. The intensity ratio of the light reflected from the layer $(I_R(\lambda))$ and incident onto the layer $(I_o(\lambda))$ at the same λ was measured with a PIN silicon photodiode (sensitive area 1 cm², type UDT 500, United Detector Technology Inc.). The output voltage of the FET operation amplifier built in the photodiode housing was detected by a digital voltmeter. The sensitivity of the detector considerably depended on the wavelength, however the relation between the output voltage of the photodiode-amplifier system and the light intensity at all fixed wavelength and intensity used was found to be linear with a good approximation. Therefore,

the reflectance was determined from the relation $R(\lambda)=\frac{I_R(\lambda)}{I_o(\lambda)}=\frac{U_R(\lambda)}{U_o(\lambda)}$, where $U_R(\lambda)$ and $U_o(\lambda)$ denote the measured output voltages. On a given sample the reflectance spectrum minima and maxima could be reproduced within 5 nm in all cases; the maximum relative error of $R(\lambda)$ was 6% in the most unfavourable case.

Results and discussion

During the oxidation process the metallic vanadium gradually transformed to yellow vanadium pentoxide. In an early stage of the oxidation, a peak at about 420 nm appeared in the reflectance spectrum, but interference structure could not be resolved (Fig. 2). In the following only the results obtained with samples in the last stage of oxidation process will be discussed, *i.e.* the oxidation was first stoppey when the yellow colour of V_2O_5 on the sheets which were heat treated parallele with the samples had already appeared. It is reasonable to assume that at this stagd the composition of the layers was very near to that of the vanadium pentoxide, but the layers were not totally stochiometric, especially beyond a certain depth.

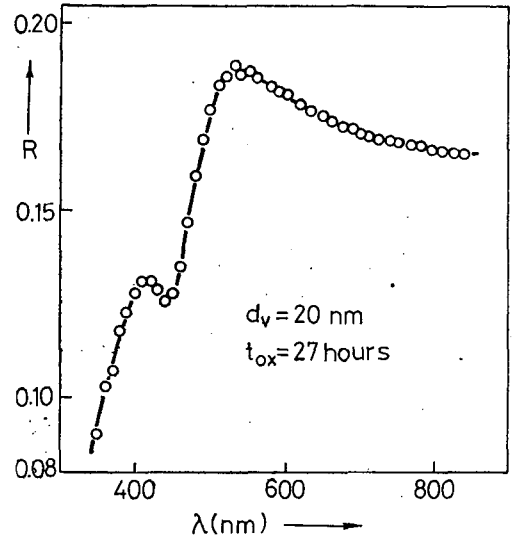

Fig. 2. The reflectance spectrum of a sample measured at $\alpha=45°$ angle of incidence in an early stage of oxidation. d_v and t_{ox} are the thickness of evaporated vanadium layer and the oxidation time, respectively.

In Figs. 3a–d the reflectance spectra of a sample covered with evaporated vanadium layer (thickness $d_v=57$ nm) are shown. The spectra were measured at an angle of $\alpha=45°$ and $\alpha=29.2°$ after an oxidation time (t_{ox}) of 35, 59, 109 and 205 hours, respectively. The shortest wavelength maximum was found at $\lambda_0=430$ nm (Figs. 3a–d). This λ_0 belonging to the first maximum practically did not depend on the angle of incidence, but the wavelength belonging to other maxima and minima were generally shifted towards longer wavelength with decreasing angle of incidence. Quite generally λ_0 was found to be independent of α, whereas the maxima and minima strongly depended on α in all reflectance spectra presented below. As it is seen in Figs. 3a–d the maxima and minima are red-shifted with increasing oxidation time for both angles, however, λ_0 remained constant (see Table I). The reflectance spectra of different samples are shown in Figs. 4–7.

It has to be mentioned that the peak belonging to λ_0 could not be observed in the thinnest layer (Fig. 7), probably due to the overlaping intense maximum.

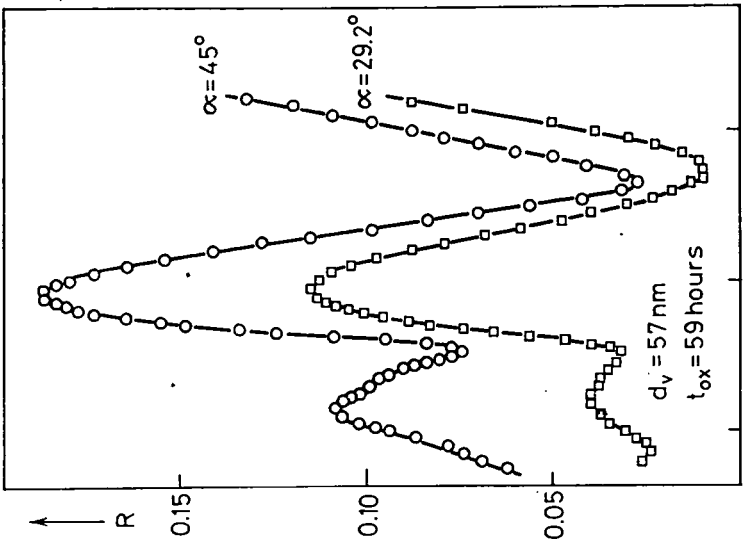
α=45°
α=29.2°
d_v = 57 nm
t_{ox} = 59 hours
R
0.15
0.10
0.05
400
600
800
λ(nm)

Fig. 3b

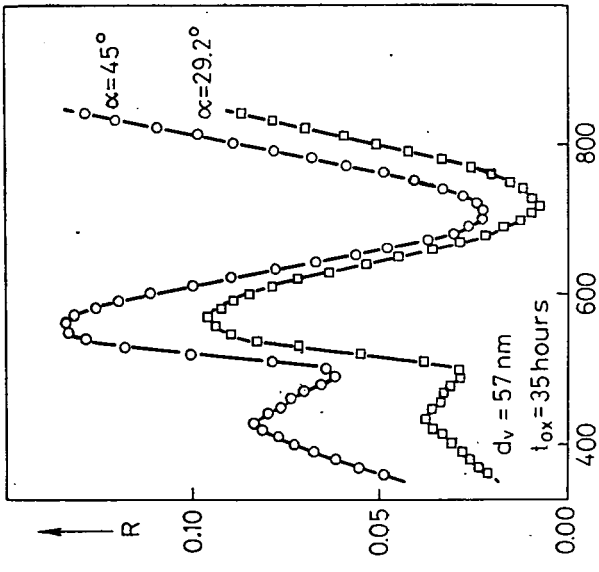
α=45°
α=29.2°
d_v = 57 nm
t_{ox} = 35 hours
R
0.10
0.05
0.00
400
600
800
λ(nm)

Fig. 3a

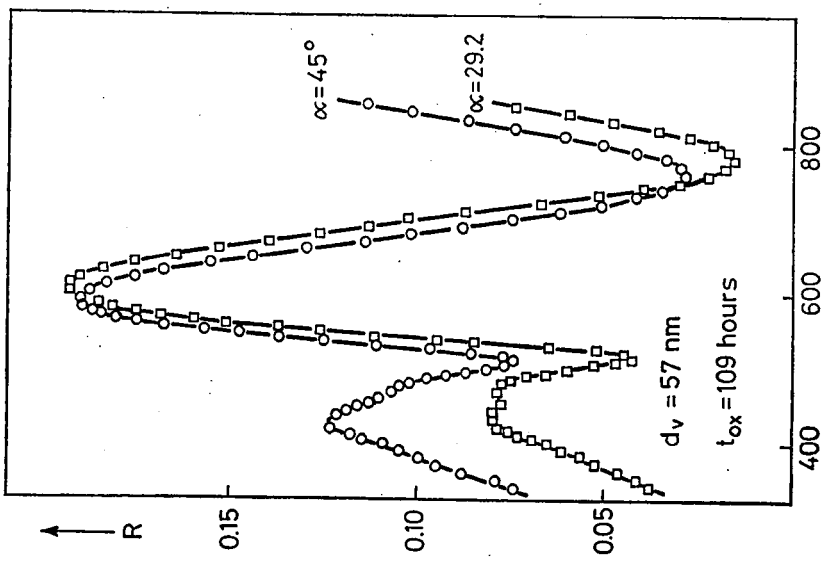
R
0.15
0.10
0.05
400
600
800
λ(nm)
α=45°
α=29.2
d_V = 57 nm
t_{ox} = 109 hours

Fig. 3c

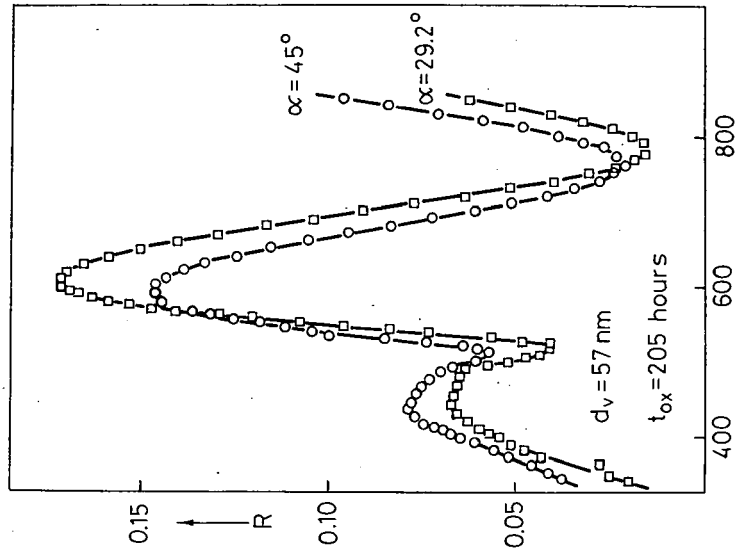
R
0.15
0.10
0.05
400
600
800
λ(nm)
α=45°
α=29.2°
d_V = 57 nm
t_{ox} = 205 hours

Fig. 3d

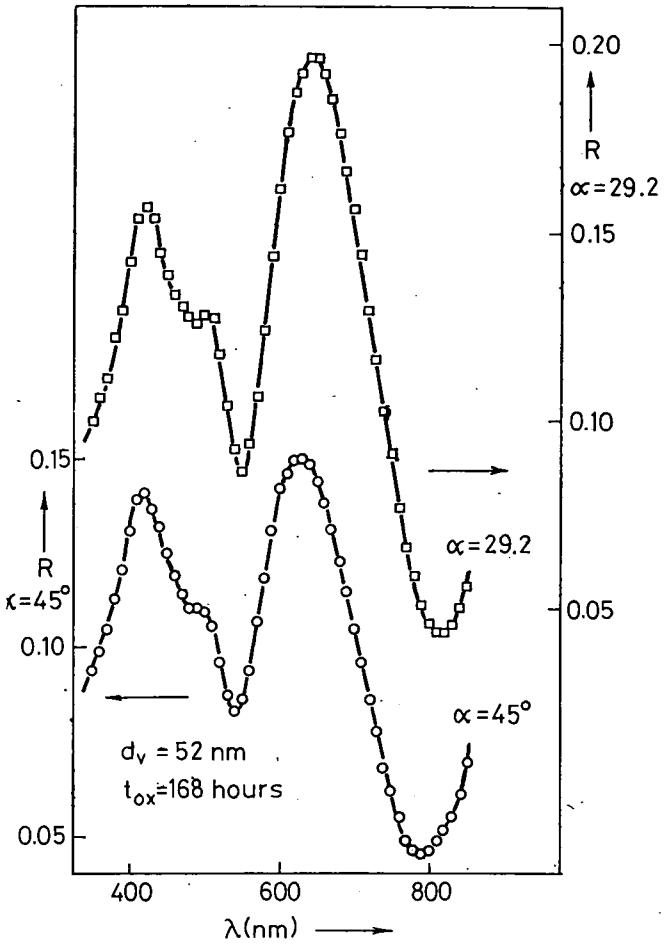

Fig. 4. The reflectance spectrum of a sample measured at an angle of $\alpha=45°$ and $\alpha=29.2°$ after an oxidation time of 168 hours. Scales for $\alpha=45°$ and $\alpha=29.2°$ are given on the left-hand and righthand sides of the figure, respectively.

The reflectance spectra of V_2O_5 films on mica sheets were also determined. The main features of these were as follows:

(i) in the case of all but the thinnest layer (with different d_v and t_{ox}) λ_0 was found to be 415 nm and its amplitude was slightly higher than that observed in the samples;

(ii) in the case of the thinnest layer ($d_v=11.5$ nm and $t_{ox}=40$ hours) the λ_0 maximum could not be observed;

(iii) the maxima and minima within a deviation of 0–20 nm were observed close to the same features of the samples.

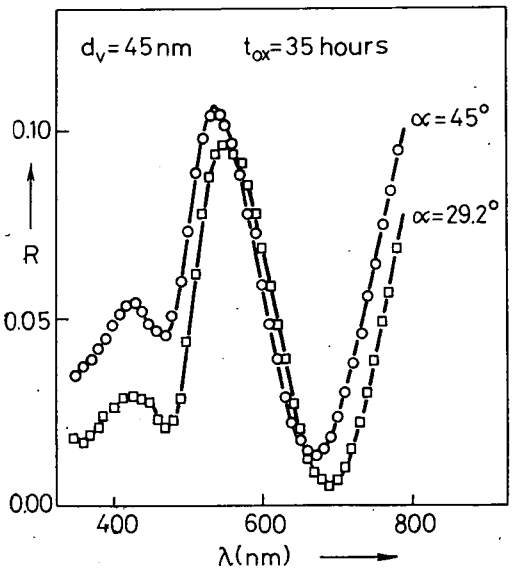
d_v = 45 nm
t_{ox} = 35 hours
α = 45°
α = 29.2°
0.10
R
0.05
0.00
400
600
800
λ(nm)

Fig. 5a

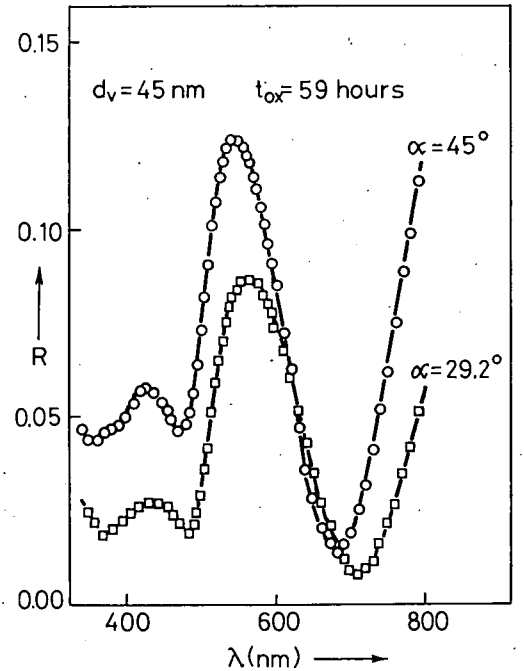
d_v = 45 nm
t_{ox} = 59 hours
α = 45°
α = 29.2°
0.15
0.10
R
0.05
0.00
400
600
800
λ(nm)

Fig. 5b

Because the reflective index of mica is smaller than that of V_2O_5 in the total wavelength range investigated (for instance at $\lambda = 600$ nm the refractive index of mica is between 1.56 and 1.60 depending on crystallographic orientation), the light beam reflected from the V_2O_5-mica interface does not suffer phase change. Since the spectra of the samples and the sheets with the same parameters agreed relatively well with each other as the position of maxima and minima were concerned, we concluded that no phase jump could take place at the V_2O_5-Si interface either. The major part of the light intensity probably reflected from the thin layer between the V_2O_5 and the silicon [1]. If so this thin interface layer should have smaller refractive index than that of the vanadium pentoxide film in the investigated wavelength range; the refractive index of silicon itself is higher than that of V_2O_5 [6]. Had the light thus reflected from the silicon surface, a phase change should have been observed.

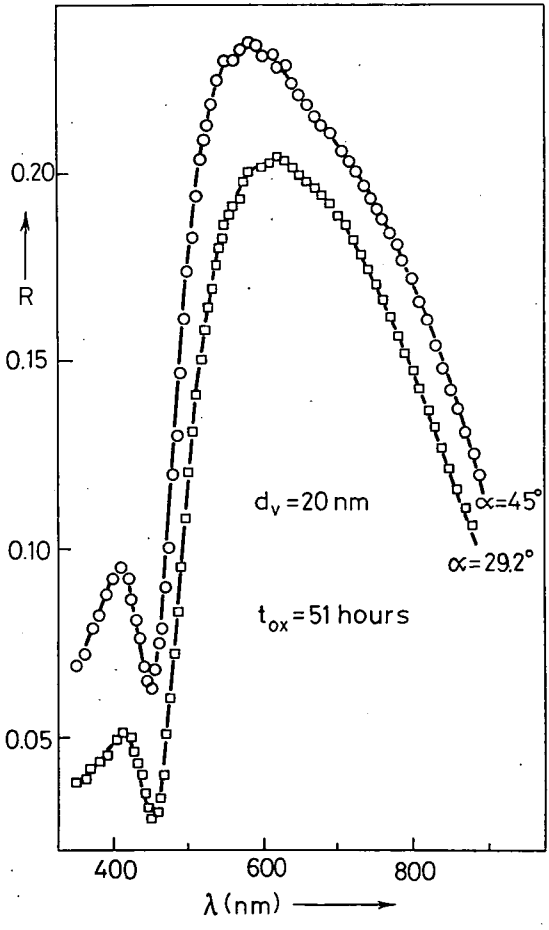

Fig. 6

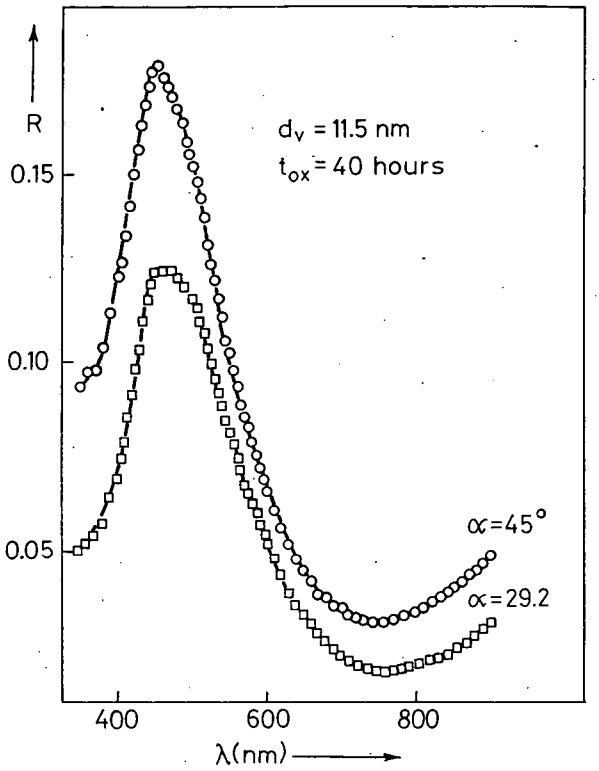

Fig. 7

However, no maximum-minimum interchange was observed indicating that the light was mainly reflected from the thin interface layer.

Taking into account that the vanadium pentoxide single-crystals were found to be non-absorbing* with a good approximation in the wavelength range used [3] the same can hold for V_2O_5 layers, too. Therefore Eqs. (1) and (2) can be applied for the evaluation of the reflectance spectra.

Notation used in Table I: m_d denotes the so called "mass thickness" *i.e.* the mass of vanadium layered on 1 cm^2 area of the silicon substrate. It has to be noted that by longest oxidation times we mean the time period which was necessary to the total oxidation of the vanadium layer at a given thickness. After prolonged oxidation listed in Table I as "longest" no changes could be observed in the reflectance spectra.

On evaluating the reflectance spectra the following assumptions were made:

(i) Eqs. (1)–(2) are valid;

(ii) the $n=n(\lambda)$ function is nearly the same for all V_2O_5 layers investigated and $n(\lambda)$ is a continous function of λ;

(iii) the reflectance peak belonging to λ_0 did not produce interference.

* More exactly: the refractive index n is much more higher than the absorption index k.

Table I

Results of measurements

d_v (nm)	m_d $\left(\times 10^{-5}\frac{g}{cm^2}\right)$	t_{ox} (hours)	(λ_0) (nm)	$\alpha=45°$				$\alpha=29.2°$			
				λ_1 (nm)	λ_2 (nm)	λ_3 (nm)	λ_4 (nm)	λ_1 (nm)	λ_2 (nm)	λ_3 (nm)	λ_4 (nm)
57	6.06	35	430	—	705	555	490	—	720	570	495
57	6.06	59	430	—	730	580	505	—	745	582	505
57	6.06	109	430	—	760	585	510	—	782	603	515
57	6.06	205	430	—	763	590	510	—	785	608	517
52	5.53	168	425	—	790	625	545	—	815	645	550
45	4.79	35	425	—	670	535	465	—	690	550	470
45	4.79	59	425	—	680	545	473	—	710	565	480
20	2.13	51	405	590	446	—	—	620	450	—	—
11.5	1.22	40	—	453	—	—	—	465	—	—	—

For notation $\lambda_1-\lambda_4$ see Eq. (3).

Since we did not know the $n(\lambda)$ function for V_2O_5 thin films there was one way to calculate the thicknesses and refractive indices belonging to different wavelength: inserting simultaneously all the results obtained into an iteration. By averaging and interpolating the values of refractive indices given in the literature [3–5] for different crystallographic directions and wavelength for V_2O_5 single-crystal, an approximate $n=n_h(\lambda)$ function was constructed (dotted line in Fig. 8). First we supposed that

$$\frac{n_h(\lambda_{i45°})}{n_h(\lambda_{i29,2°})}=\frac{n_{(0)}(\lambda_{i45°})}{n_{(0)}(\lambda_{i29,2°})}, \tag{4}$$

where $i=2, 3, 4$; and $n_{(0)}(\lambda)$ is the value of refractive index at wavelength λ in zeroth order approximation. The values of λ_{ix} were taken from the 1st–7th lines of Table I. Using the values standing on the right side of Eq. (4) three different values of thickness were obtained for each sample with the same d_v and t_{ox} from Eqs. (1)–(3). The average of these values was taken as zeroth order approximate value for the thicknesses. Substituting these values into Eqs. (1)–(3) the numerical values of $n_{(1)}(\lambda)$ could be obtained for all λ can be found in the 1st–7th lines of Table I. Inserting the appropriate values of $n_{(1)}(\lambda)$ into the left-hand side of Eq. (4) we got the new values of $\frac{n_{(2)}(\lambda_{i45°})}{n_{(2)}(\lambda_{i29,2})}$. The iterative calculation was continued as long as the values obtained for the thickness were the same in three digits for all λ_i. At last the iteration was expanded over the two samples with thinner V_2O_5 layer (8th and 9th lines in Table I).

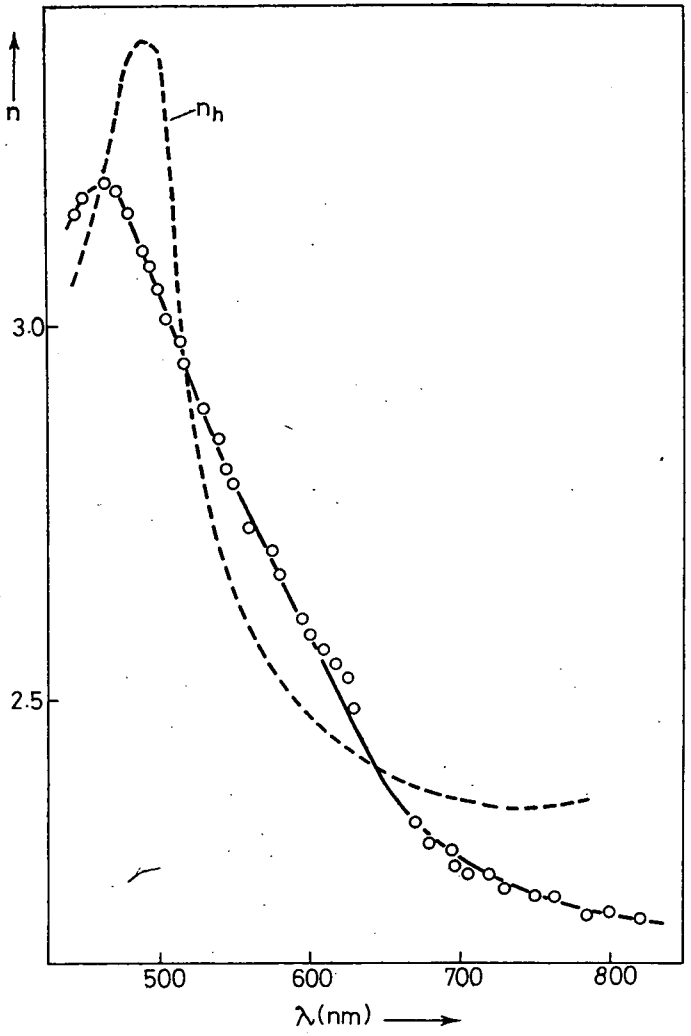

Fig. 8. The calculated values of refractive index for V_2O_5 thin films (empty circles) and the $n_h(\lambda)$ curve (dotted line).

Obviously the results obtained for the thickness and $n(\lambda)$ in this way were independent of $n_h(\lambda)$. If $n_h(\lambda)$ were equal to const. $n(\lambda)$ for example, then the iteration would be completed in the first step. If the form of $n_h(\lambda)$ deviates from that of $n(\lambda)$ the iteration consists of too many steps.

The determination of interference order (k in Eqs. (1)–(2)) was very simple since in Figs. 7 and 6 only one and two extrema could be found, respectively.*

* In Fig. 7 the minimum at about 750 nm is due to the slight increase in the reflectance of the silicon substrate towards the longer wavelength, as measured in Si-SiO_2 system.

Any variation in k implicitely found in Eq. (3) resulted in very unresonable thickness and density values for the vanadium pentoxide layers and, in addition, made the simultaneous evaluation of the reflectance spectra impossible.

In Fig. 8 the calculated values of refractive index (empty circles) and the $n_h(\lambda)$ curve (dotted line) are shown. As it has been expected, the shape of the two curves is similar but the values of the two curves at certain wavelength regions are considerably different.

The obtained results are summarized in Table II. Column 4 of Table II contains the calculated thickness (d) of the vanadium pentoxide layers, while column 5 gives the density calculated from the relation $\varrho=\frac{m_d}{d}$, other columns give the wavelength values recalculated from the refractive indices (Fig. 8) and from the thickness (column 4) obtained by the iterative calculation. Comparing the measured (Table I) and the calculated wavelength values (Table II) for the interference maxima and minima, the agreement is satisfactory except for two λ_1 values in the case of sample with $d_v=20$ nm. The slight increase in reflectance of the substrate towards longer wavelength, the asymmetry of the reflectance peak in Fig. 6 (not experienced by us in other cases), and the poor resolution of the peak may probably contribute to the difference between the measured and calculated values. These factors caused uncertainity in the determination of the λ_1 values.

As it is seen from Table II the thickness of the V_2O_5 layers increase, whereas their density decrease with increasing oxidation time. This thickness increase is about 10% for a sample with $d_v=57$ nm. In the case of the longest oxidizing times presented in Table II the average value of density is 3.1 g/cm³ for V_2O_5 layers of different thickness.

Table II

The obtained results and the recalculated values of wavelength

					$\alpha=45°$				$\alpha=29.2°$			
d_v (nm)	m_d $\left(\times 10^{-5}\frac{g}{cm^2}\right)$	t_{ox} (hours)	d (nm)	ϱ $\left(\frac{g}{cm^3}\right)$	λ_1 (nm)	λ_2 (nm)	λ_3 (nm)	λ_4 (nm)	λ_1 (nm)	λ_2 (nm)	λ_3 (nm)	λ_4 (nm)
57	6.06	35	163	3.72	—	705	553	489	—	719	574	494
57	6.06	59	170	3.56	—	728	580	505	—	745	585	504
57	6.06	109	179	3.39	—	761	595	513	—	781	602	516
57	6.06	205	180	3.37	—	764	595	515	—	784	604	520
52	5.53	168	190	2.91	—	796	620	535	—	816	630	540
45	4.79	34	149	3.21	—	667	540	464	—	678	550	470
45	4.79	59	155	3.09	—	683	553	76	—	694	561	485
20	2.13	51	72	2.96	650	446	—	—	662	450	—	—
11.5	1.22	40	37	3.30	453	—	—	—	460	—	—	—

The reflectance peak at about 420 nm can be assigned according to JOHNSTON [7] to V^{4+} ions present in the vanadium pentoxide which play an important role in determining the conductivity of V_2O_5. This assignment can be supported by our observation that the height of the λ_0 peak could be paralleled with the conductance of the vanadium pentoxide layer.

On the basis of the results presented here we arrived at the following conclusions:

(i) Eqs. (1)–(2) could be applied for the evaluation of reflectance spectra of V_2O_5 layers on silicon substrate;

(ii) the reflected light from the V_2O_5 side of V_2O_5-Si interface did not suffer phase change indicating that a thin interface layer should exist between the V_2O_5 and the silicon with lower refractive index than that of V_3O_5 in the wavelength range investigated;

(iii) after prolonged oxidizing time, which depended on the thickness of the V_2O_5 layer, the refractive index of the V_2O_5 layer was independent of the oxidation time, whereas the thickness and the density changed with the oxidation time;

(iv) the refractive index of the V_2O_5 layers prepared by evaporation and subsequent oxidation of vanadium varied with wavelength as shown in Fig. 8, practically independently of the thickness (in the d_v range investigated);

(v) the density of the V_2O_5 layers prepared was 3.1 g/cm^3, ranging between the density of single crystalline V_2O_5 (3.357 g/cm^3) and that of the amorphous V_2O_5 (2.42–2.69 g/cm^3), but it was nearer to the density of V_2O_5 single-crystals [8].

References

[1] *Mačkus, P., Á. Süli, M. I. Török and I. Hevesi:* Thin Solid Films **42**, 17 (1977).
[2] *Süli, Á., S. D. Kurmashev, L. Michailovits and I. Hevesi:* Acta Phys. et Chem. Szeged **22**, 45 (1976).
[3] *Hevesi, I.,* and *Karvaly:* Acta Phys. Hung. **29**, 182 (1970).
[4] *King, B. W.,* and *L. Suber:* J. Am. Ceram. Soc. **38**, 306 (1955).
[5] *Kenny, N., C. R. Kannewurf and D. H. Whitemore:* J. Phys. Chem. Solids **27**, 1237 (1966).
[6] *Wolf, H. F.:* Silicon Semiconductor Data, Pergamon Press, London, 1969.
[7] *Johnston, W. D.:* J. Am. Ceram. Soc. **48**, 608 (1965).
[8] *Neuberger, M.:* Data Compilation on Vanadium Oxides, National Technical Information Service, U. S. Department of Commerce, Springfield, Virginia 22151, 1971. p. 30.

ОПРЕДЕЛЕНИЕ ТОЛЩИНЫ И КОЭФФИЦИЕНТА ПРЕЛОМЛЕНИЯ ТОНКИХ СЛОЕВ V_2O_5 НА ОСНОВАНИИ ОТРАЖАТЕЛЬНЫХ ИНТЕРФЕРЕНЦИОННЫХ СПЕКТРОВ

А. Шюли, Л. Михайлович и И. Хевеши

Определены толщины и коэффициенты преломления слоев V_2O_5, приготовленных термическим окислением при 400 °C, конденсированных на поверхность монокристаллов кремния, слоев разной толщины ванадия, при $\alpha=45°$ и $\alpha=29{,}2°$ углах падения, с помощью отражательных спектров, снятых в области длин волн 360—900 нм. Для оценки спектров был принят метод приближений. Удельный вес слоев V_2O_5 определяли исходя из толщины конденсированных слоев ванадия и оптических измерений толщины слоев V_2O_5. Средний удельный вес слоев V_2O_5 составлял 3,1 г·см$^{-3}$. Полоса отражения, найденная в области 420 нм, независимая от угла падения света, отнесена к концентрации V^{4+} находящегося в V_2O_5.

PREPARATION OF AMORPHOUS V_2O_5 THIN FILMS BY CHEMICAL VAPOR DEPOSITION METHOD

By

K. BALI, L. MICHAILOVITS and I. HEVESI

Institute of Experimental Physics, Attila József University, Szeged

(Received January 30, 1979)

Amorphous vanadium pentoxide thin films have been prepared by chemical vapor decomposition of $VOCl_3$ with H_2O in inert atmosphere at room temperature. The films crystallize at around 240°C irreversibly. The d. c. electrical resistivity in the amorphous state is approximately 1–2 orders of magnitude lower than in the polycrystalline state.

Vanadium pentoxide, V_2O_5, is known to contain both V^{4+} and V^{5+} ions and the electronic conduction is due to the hopping motion of the unpaired 3d electron from V^{4+} to V^{5+} ions (small polaron hopping). Due to the difficulty of preparing pure vitreous V_2O_5 most of the previous studies on its semiconducting properties were carried out on glasses containing vanadium pentoxide as a component. Until now vacuum deposition [1–3] and splat cooling [4–6] have been succesfully applied to prepare amorphous V_2O_5.

Chemical vapor deposition (CVD) proved to be a convenient method for growing crystalline vanadium oxides [7]. Relatively high reaction temperatures (above 600° C) are needed to grow single crystals of good quality. Since the decomposition of $VOCl_3$ vapor with H_2O vapor is a strongly exothermic process, the reaction already takes place at room temperature according to the equation:

$$2\,VOCl_3 + 3\,H_2O \rightarrow V_2O_5 + 6\,HCl.$$

Based on this reaction the CVD method can be applied to obtain amorphous vanadium pentoxide. In this paper we report the successful preparation of amorphous V_2O_5 thin films by chemical vapor decomposition of $VOCl_3$ with H_2O in inert atmosphere.

The schematic diagram of the apparatus used is shown in Fig. 1. The vapor of $VOCl_3$ (FLUKA; Switzerland) and H_2O thermostated at 22° C was led to the reaction chamber by high purity N_2 gas flow. To avoid the chemical reaction of water vapor traces in the $VOCl_3$ containing ampulla, the carrier gas was led through an LN_2 baffle. As substrate material quartz plates (HERASIL I; Germany) were used. The colour of the freshly prepared films varied from yellow to orange depending on the reaction time typically 10 through 20 minutes. The thickness of the films determined by optical method was of some thousand Å.

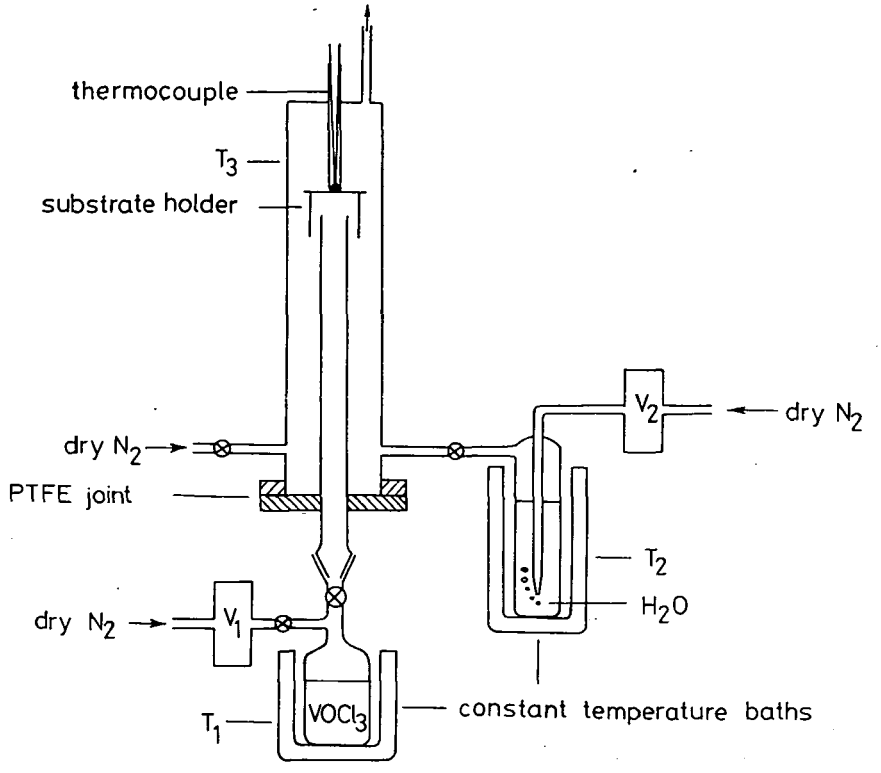

Fig. 1. V_1, V_2-flowmeters (Rotameter MFG. Co. Ltd. England) ⊗-PTFE valves (Corning, England) $T_1=T_2=T_3=22°$ C, $V_1=1$ lit/hours, $V_2=0.7$ lit/hours

LIVAGE *et al.* pointed out that the solubility of the two phases is extremely different. Crystalline V_2O_5 can not be dissolved in water while the amorphous oxide readily dissolves [5, 6]. Our films prepared by the CVD method easily dissolved in water, yielding strongly acidic solution with pH $\sim$ 2, in accordance with the results of LIVAGE and COLLONGUES. The results of microscopic examination in polarized light and electron diffraction pictures unambigously verified that these films were amorphous.

The crystallization temperature of the amorphous oxide obtained by splat cooling is between 180 and 200° C [5, 6]. The crystallization is an irreversible, strongly exothermic process. Because the crystallization can be followed by electrical measurements, we studied the temperature dependence of the d.c. electrical resistivity of the amorphous V_2O_5 thin films from room temperature up to 300° C in dry O_2 atmosphere. The platinium electrode were deposited on the substrates by vacuum evaporation before the preparation of the films. Applying a constant heating rate of 0.5° C/min, a decrease in the conductivity could be observed at around 240° C in each case. We found a ratio of $10–10^2$ between the conductivity of the two phases. The material of the films heated above 240° C was insoluble in water. The

microscopic re-examination in polarized light demonstrated, that the films had been crystallized (Fig. 2).

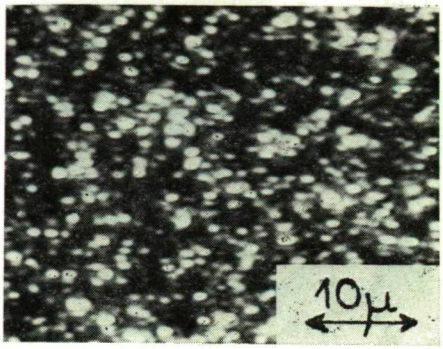

Fig. 2

To determine more precisely the value of the crystallization temperature the influence of the annealing was studied on initially amorphous films. The samples were held for 3 hours at different temperatures: (a) 180° C, (b) 200° C, (c) 220° C, and (d) 240° C. The resistivity of the samples was steadily measured during this annealing process. Samples (a), (b), and (c) exhibited no changes in the resistivity, while the resistivity of sample (d) increased by approximately two orders of magnitude. The microscopic examination showed that the film when annealed at 240° C crystallized completely.

Summing up we conclude that the chemical vapor decomposition of $VOCl_3$ with H_2O in inert atmosphere at room temperature proved to be a reliable method for preparing amorphous vanadium pentoxide thin films. The films crystallize at around 240° C irreversibly. The d.c. electrical conductivity in the amorphous state is approximately two orders of magnitude higher than in the polycrystalline state.

References

[1] *Kennedy, T. N., R. Hakim and J. D. Mackenzie:* Mat. Res. Bull. **2**, 193 (1967).
[2] *Rjanjel, E. F., V. I. Gaman and V. M. Kaligina:* Izv. Vuz. Fiz. no. 2, **102** (1976).
[3] *Allersma, T., R. Hakim, T. N. Kennedy and J. D. Mackenzie:* J. Chem. Phys. **46**, 154 (1967).
[4] *Kahn, A., J. Livage and R. Collongues:* phys. stat. sol. (a) **26**, 175 (1974).
[5] *Rivolen, L., A. Revcolevschi, J. Livage and R. Collongues:* J. Non-Cryst. Solids **21**, 171 (1976).
[6] *Livage, J. and R. Collongues:* Mat. Sci. Eng. **23**, 297 (1976).
[7] *Takei, H.:* Jap. J. Appl. Phys. 7(8), **827** (1968).

ПРИГОТОВЛЕНИЕ АМОРФНЫХ ТОНКИХ СЛОЕВ V_2O_5 МЕТОДОМ РАЗЛОЖЕНИЯ ГАЗОВОЙ ФАЗЫ

К. Бали, Л. Михайлович и И. Хевеши

Описано приготовление тонких слоев V_2O_5 путем химического разложения газовой фазы $VOCl_3$ с H_2O в инертном газе при комнатной температуре. Пленки кристаллизируются около 240 °C по необратимому пути. Электрическое сопротивление аморфного состояния по постоянному току ниже на 1—2 порядка по сравнению сопротивлением поликристаллического состояния.

DIELECTRIC ABSORPTION STUDIES IN SOME α-SUBSTITUTED BENZYL CYANIDES IN DILUTE SOLUTION

By

S. K. SAXENA, C. K. MISRA*, J. P. SHUKLA & M. C. SAXENA

Department of Physics, Lucknow University, Lucknow, India

(Received 5th March, 1979)

Dielectric absorption studies on four α-substituted benzyl cyanides namely α-butyl benzyl cyanide, α-heptyl benzyl cyanide & α-cyano stilbene have been made. The observed α values being sufficiently high, indicate the existence of more than a single relaxation process occurring in the system. When further resolved, the dielectric dispersion yielded relaxation time $\tau(1)$ and $\tau(2)$ which are sufficiently different from one another, showing the presence of the molecular and some other process. In some cases the enthalpies of activation and the other energy parameters have also been evaluated. It has been concluded that the dielectric relaxation takes place due to both molecular and group processes except for the case of α-benzyl benzyl cyanide, where the enthalpy of activation for the group process has been found to be very low.

Introduction

Dielectric absorption studies are very helpful in probing the molecular flexibility or rigidity which is of vital importance for the investigations on carcinogenic activity. FISCHER and his collaborators [1] studied benzyl chloride for its dielectric behaviour and concluded that the nonrigidity is an important feature of the molecule. PURCEL et al. [2] studied the dielectric relaxation of benzyl chloride in the dilute solution of benzene and analysed the data in terms of the two relaxation times; Cole-Cole's molecular relaxation time τ_1 (=23.7 ps) and the group relaxation time τ_2 (=2.3 ps). KLAGES and KNOBLOCH [3] investigated for dielectric behaviour, some substituted benzyl halides including benzyl chloride for which they obtained $\tau_1=14.6$ ps and $\tau_2=1.6$ ps with the contribution due to the group relaxation ($C_2=0.3$). FOREST and SMYTH [4] investigated benzyl cyanide in dilute solution and below 40° C obtained two relaxation times. HASSAN et al. [5] studied microwave absorption in some benzyl derivatives *i.e.* $C_6H_5CH_2X$ (=Cl, Br, CN and NH_2) in pure liquid state and analysed the data in terms of the two relaxation processes. For benzyl cyanide the dielectric data of FOREST and SMYTH [4] in the dilute solution of benzene and HASSAN et al. [5] in the pure liquid state above 40° C give very surprising results by showing the absence of group rotation.

Due to the interesting results obtained on benzyl cyanide the authors in the present work have chosen four higher homologues of α-substituted benzyl cyanides

* Department of Physics, B. S. N. V. Degree College, Lucknow.

namely α-butyl benzyl cyanide, α-heptyl benzyl cyanide, α-benzyl benzyl cyanide and α-cyano stilbene for the dielectric and thermodynamic investigations in the dilute solutions of benzene. The permittivity data have been analysed by GOPALA KRISHNA [6], HIGASI [7], KOGA and NAKAMURA [8] methods. The results show that at x-band nonrigidity is an important feature of the molecules under investigation over the range of temperature (288–320° K) investigated.

Experimental: The dielectric constant (ε') and the dielectric loss (ε'') of the dilute solutions of a polar solute in the nonpolar solvent have been measured over a range of temperature at x-band described elsewhere [9] by a technique due to ROBERTS and VON HIPPEL [10] and later modified by DAKIN and WORKS [11]. The static dielectric constant ε_0 of solutions have been measured at 300 KHz by a dipole meter based on the principle of heterodynbeat method. The refractive indices (Na light) of all the solutions have been measured by an Abbe's Refractometer. The measurements for ε' & ε'' are accurate up to $\pm 2\%$ and $\pm 5\%$ respectively.

Materials: The chemicals have been obtained from the Central Drug Research Institute, Lucknow, India and the solvent (A.R. grade) has been obtained from E. Merck (Germany). The chemicals have been distilled twice before use.

Method: The permittivity data have been analysed by the GOPALA KRISHNA method [6] for the evaluation of the dielectric relaxation time (τ_{GK}) using the equations

$$X = P + Y/\omega\tau_{GK} \tag{1}$$

where $P = \left(\frac{\varepsilon_\infty - 1}{\varepsilon_\infty + 2}\right)$ has been assumed to be constant for the dilute solutions; $W = \frac{2\pi C}{\lambda}$ and

$$\left.\begin{aligned} X &= \frac{\varepsilon'^2 + \varepsilon''^2 + \varepsilon' - 2}{(\varepsilon' + 2)^2 + \varepsilon''^2} \\ Y &= \frac{3\varepsilon''}{(\varepsilon' + 2)^2 + \varepsilon''^2} \end{aligned}\right\} \tag{2}$$

The slope $\left(\frac{dy}{dx}\right)$ of equation (1) gives the relaxation time

$$as\ \tau_{GK} = \frac{\lambda}{2\pi C}\frac{dy}{dx}; \tag{3}$$

The most probable relaxation time τ_{OH} and the distribution parameter (α) have also been determined by HIGASI method [7] using the equations

$$\left.\begin{aligned} \tau_{OH} &= \frac{1}{\omega}\left[\frac{A^2 + B^2}{C^2}\right]^{\frac{1}{2(1-\alpha)}} \\ 1 - \alpha &= \frac{2}{\pi}\tau_{an}^{-1}\left(\frac{A}{B}\right) \end{aligned}\right\} \tag{4}$$

where

$$\left.\begin{aligned} A &= a''(a_0 - a_\infty) \\ B &= (a' - a_\infty)(a_0 - a') - a''^2 \\ C &= (a' - a_\infty)^2 + a''^2 \end{aligned}\right\} \tag{5}$$

The quantities a_0, a', a'' and a_∞ are the slopes of the straight line plots of the respective dielectric quantity $\varepsilon_0, \varepsilon', \varepsilon''$ and $\varepsilon_\infty = n_D^2$ against the concentrations in the dilute solution range and are defined as

$$\begin{aligned} \varepsilon_0 &= \varepsilon_{01} + a_0 W_2 \\ \varepsilon' &= \varepsilon_1' + a' W_2 \\ \varepsilon'' &= a'' W_2 \\ \varepsilon_\infty &= \varepsilon_{1\infty} + a_\infty W_2 \end{aligned}$$

in which subscript 1 refers to the pure solvent and O to the static frequency, ∞ to the high frequency or optical frequency measurements, W_2 is the weight fraction of the solute.

The absorption processes have further been resolved by the recent HIGASI, KOGA and NAKAMURA method [8] in terms of two independent Debye type relaxation times $\tau_{(1)}$ and $\tau_{(2)}$ defined by the equation

$$\tau_{(1)} = \frac{a''}{\omega(a' - a_\infty)} \tag{7}$$

$$\tau_{(2)} = \frac{1}{\omega}\left[\frac{a_0 - a'}{a''}\right]. \tag{8}$$

The slopes a_0, a', a_∞ and a'' are defined by the set of equations (6).

It has been found [12–14] that the relaxation time $\tau_{(2)}$ leads to that for the Cole-Cole's molecular relaxation process τ_1 and $\tau_{(1)}$ has been found to be an implicit function of group relaxation time τ_2, τ_1 and weight factor C_2 for the group rotation process; any difference beyond experimental error in the value of $\tau_{(1)}$ and $\tau_{(2)}$ for a molecule is indicative of more than one relaxation process present in the system.

The activation energy parameters for the dipole relaxation process have been estimated using Eyring's theory of rate process [15]. The enthalpy of activation corresponding to the relaxation time τ_{GK}, τ_{OH}, $\tau_{(1)}$, $\tau_{(2)}$ and $\tau_0 = \sqrt{\tau_{(1)}\tau_{(2)}}$ have been estimated from the slopes of plots of $\log \tau_{GK}T$, $\log \tau_{OH}T$, $\log \tau_{(1)}$. T, $\log \tau_{(2)}$. T and $\log \tau_0 T$ against $-1/T$ respectively.

Results and Discussion: The slopes of the dielectric quantities *vs* concentration plots *i.e.* a_0, a', a'' and a_∞ at different temperatures of the molecule under investigation are reported in Table I. The relaxation time $\tau_{(1)}, \tau_{(2)}, \tau_0 = \sqrt{\tau_{(1)}\tau_{(2)}}$, τ_{GK}, τ_{OH} and the distribution parameter of the molecules at different temperatures are presented in Table II. The enthalpies of activation $\Delta H\tau_{(1)}, \Delta H\tau_{(2)}, \Delta H\tau_0, \Delta H\tau_{GK}$ and $\Delta H\tau_{OH}$ corresponding to the relaxation time $\tau_{(1)}, \tau_{(2)}, \tau_0, \tau_{GK}$ and τ_{OH} have been tabulated in Table III. In Table IV. the activation parameters for the dipole reorientations associated with the relaxation times τ_{GK} and τ_{OH} have been compared.

α-Butyl Benzyl Cyanide (A)

The examination of Table II. shows that the molecule has an appreciable value of the distribution parameter ranging from (0.09–0.22) in the temperature range of (288–320° K) and the most probable relaxation time τ_{OH} evaluated using Higasi method for the molecule has been found to be 23.5 p.s. at 288° K. The occurrence of large distribution parameter in the molecular system indicates the non-rigidity of the molecule in the microwave region under investigation. The dielectric dispersion, was therefore, further resolved in terms of two independent Debye type relaxation times $\tau_{(1)}$ and $\tau_{(2)}$. It is found that the molecular relaxation time $\tau_{(2)}$ is 30.0 p.s. and $\tau_{(1)}$ associated with the relaxation process other than the molecular

Table I

The slopes a_0, a', a'', a_∞ and dipole moment of molecules in dilute solution of Benzene

Compound	Temp. K	a_0	a'	a''	a_∞
α-Butyl benzyl cyanide (A)	288	14.0	5.00	5.50	0.58
	296	12.5	4.75	4.76	0.40
	304	11.1	4.50	3.90	0.39
	312	8.5	4.00	3.12	0.37
	320	6.5	3.50	2.63	0.30
α-Heptyl benzyl cyanide (B)	296	18.0	5.00	5.71	0.28
	304	14.0	4.70	4.70	0.25
	312	12.05	4.00	4.44	0.15
	320	10.00	3.33	4.00	0.75
α-Benzyl benzyl cyanide (C)	288	16.00	3.13	3.80	0.75
	296	12.00	2.77	3.00	0.62
	304	10.50	2.50	2.66	0.54
	312	9.3	2.20	2.50	0.32
α-Cyano stilbene (D)	296	12.50	3.60	3.10	0.48
	304	11.80	3.30	2.90	0.35
	312	8.50	2.80	2.40	0.25
	320	6.15	2.18	1.90	0.08

is 18.4 p.s. at 288° K. An appreciable difference between $\tau_{(1)}$ and $\tau_{(2)}$ supports the presence of two independent relaxation processes occurring in the molecule. The longer relaxation time (30 p.s.) would correspond to the molecular rotation of butyl benzyl cyanide whereas the second process would be expected to be due to the internal rotation of 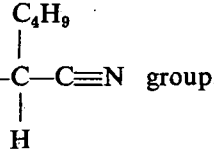 group. Similar conclusions have been made by MISRA and SAXENA [16] on some substituted benzaldehydes.

A comparison of τ_{OH} (Higasi) and $\tau_0=\sqrt{\tau_{(1)}\tau_{(2)}}$ (Higasi, Koga and Nakamura) shows a close agreement, as both represent the most probable (average) relaxation time parameters. A close agreement between τ_{OH} and $\tau_0=\sqrt{\tau_{(1)}\tau_{(2)}}$ observed by MISRA et al. [17] on some substituted amides in dilute solution supports

Table II

Relaxation times of the molecules using Higasi, Higasi, Koga and Nakamura method and Gopala Krishna Method

Temp. K	Higasi Method		Higasi, Koga & Nakamura Method			Gopala Krishna Method
	τ_{OH} ps	α	$\tau_{(1)}$ ps	$\tau_{(2)}$ ps	$\tau_0=\sqrt{\tau_{(1)}\tau_{(2)}}$ ps	τ_{GK} ps
			α-Butyl Benzyl cyanide (A)			
288	23.5	0.09	18.9	30.0	23.8	26.6
296	22.4	0.12	16.7	27.1	21.3	24.4
304	22.2	0.20	14.5	25.8	19.3	22.5
312	17.8	0.17	13.1	22.6	17.2	20.7
320	15.4	0.20	12.5	19.0	15.4	17.5
			α-Heptyl benzyl cyanide (B)			
296	33.2	0.18	18.4	34.4	25.2	30.2
304	27.3	0.20	16.1	30.1	22.0	25.5
312	25.4	0.14	17.6	27.6	22.0	22.1
320	24.4	0.12	14.3	26.5	19.4	20.7
			α-Benzyl Benzyl cyanide (C)			
288	56.7	0.15	24.3	51.6	35.4	26.6
296	53.4	0.17	21.3	45.7	31.2	20.4
304	51.6	0.21	20.6	45.2	30.5	19.0
312	46.3	0.15	20.3	45.0	30.2	17.7
			α-Cyano stilbene (D)			
296	44.2	0.29	15.0	43.7	25.7	22.1
304	41.1	0.29	14.9	42.0	25.0	19.0
312	33.0	0.27	14.3	36.2	22.7	16.6
320	30.0	0.25	13.8	31.9	21.0	14.7

Table III

Activation energies calculated for the relaxation times $\tau(1)$, $\tau(2)$, τ_0, τ_{OH} *and* τ_{GK} (*in* kJ mol^{-1})

Compound	$\Delta H\,\tau(1)$	$\Delta H\,\tau(2)$	$\Delta H\,\tau_0$	$\Delta H\,\tau_{OH}$	$\Delta H\tau_{GK}$
α-Butyl Benzyl cyanide (A)	5.3	8.0	6.4	6.4	5.6
α-Heptyl Benzyl cyanide (B)	—	—	—	8.0	8.0
α-Benzyl Benzyl cyanide (C)	—	—	—	5.1	4.8
α-Cyano Stilbene (D)	1.7	11.9	6.4	10.6	9.6

Table IV

Relaxation times, free energy of activation, energy, enthalpy, and entropy of activation by Higasi and Gopala Krishna method

Compound	Temp. K	τ_{OH} ps	τ_{GK} ps	Using Higasi parameters			Using G. K. parameters		
				ΔF_e kJ mol^{-1}	ΔH_e kJ mol^{-1}	ΔS_e J/deg^{-1} mol^{-1}	ΔF_e kJ mol^{-1}	ΔH_e kJ mol^{-1}	ΔS_e J/deg^{-1} mol^{-1}
α-Butyl Benzyl cyanide (A)	288	23.5	26.6	11.7		−18.4	12.1		−22.5
	296	22.4	24.4	12.1		−19.2	12.1		−21.7
	304	22.2	22.5	12.1	6.4	−18.8	12.1	5.6	−20.1
	312	17.8	20.7	12.1		−18.4	12.5		−22.2
	320	15.4	17.5	12.1		−17.9	12.5		−21.7
α-Heptyl Benzyl cyanide (B)	288	—	30.2	13.0		—	12.5		−15.8
	296	33.2	25.5	13.0		−16.7	12.5		−15.0
	304	27.3	22.1	13.4	8.0	−16.3	12.5	8.0	−14.6
	312	25.4	21.0	13.4		−17.1	12.5		−14.6
	320	24.4	20.8	13.8		−16.7	13.0		−15.85
α-Benzyl Benzyl cyanide (C)	288	56.7	26.6	13.8		−30.1	12.1		−25.4
	304	53.4	20.4	14.2	5.1	−30.9	12.1	4.8	−24.2
	312	51.6	19.0	14.6		−31.8	12.5		−24.6
	329	45.3	17.7	14.6		−30.9	12.5		−24.2
α-Cyano Stilbene (D)	296	44.2	22.1	13.8		−10.4	11.7		−7.1
	304	44.1	19.0	13.8	10.6	−10.4	12.1	9.6	−7.9
	312	33.0	16.6	13.8		−10.0	12.1		−8.1
	320	30.0	14.8	14.2		−11.3	12.1		−8.2

the present observations. Also τ_{GK} (26.6 p.s.) has been found to be slightly longer than τ_0 (23.8 p.s.) or τ_{OH} (23.5) and comparatively smaller than $\tau(2)$ the relaxation time considered to be for molecular rotation. This is due to the fact that τ_{GK} gives an average of the different relaxation mechanisms involved in the system and thus has a smaller value.

The enthapies of activations (ΔH) associated with the different modes of rotations are given in Table III $\Delta H\,\tau_{(1)}$ and $\Delta H\,\tau_{(2)}$ for **A** have been found to be 5.3 and 8.0 kJ mol^{-1} respectively. These two values are respectively due to the group and the molecular relaxation processes. The enthalpies of activation $\Delta H\tau_{OH}$ and $\Delta H\tau_0$ 6.4 kJ mol^{-1} corresponding to Higasi and the average relaxation due to Higasi *et al.* have been found to be in very close agreement; where as that due to Gopala Krishna relation, $\Delta H\tau_{GK}$ is slightly different from the former two values.

An examination of Table IV. shows that the free energies of activation ΔF_e in the range of temperature (288°–320° K) evaluated, using τ_{GK} and τ_{OH} parameters are comparable. The entropy values have been found to be negative suggesting the presence of cooperative orientations [18] resulting from the steric forces.

α-Heptyl Benzyl Cyanide (B)

For this molecule also appreciable value of the distribution parameter α (0.12–0.20) has been observed. The value of the most probable relaxation time τ_{OH} has been found to be 33.2 p.s. at 296° K. The appreciably high value of the distribution parameter suggests the presence of more than one relaxation process. Absorption corresponding to these processes have thus further been resolved in terms of two independent Debye type dispersions defined by $\tau_{(1)}$ and $\tau_{(2)}$ using Higasi, Koga & Nakamura [8]. The two observed relaxation times are sufficiently different from one another suggesting further the probable flexibility of the molecule in the microwave region under investigation. As can be seen from Table II., the resolved relaxation times $\tau_{(1)}$ and $\tau_{(2)}$ at 296° K are found to be 18.4 and 34 p.s. respectively. The first process, having smaller relaxation time, would be assigned to the internal rotation of the group; whereas the second process, having longer relaxation time, would be expected to be due to the molecular rotation. τ_{GK} (30.2 p.s.) has been found to be smaller than that for molecular process $\tau_{(2)}$ (34.4 p.s.). Also the other two average processes giving rise to the most probable relaxation times at 296° K *i.e.* τ_{OH} (33.2 p.s.) and τ_0 (25.2 p.s.) are comparatively smaller than that for the molecular process. However these values are not in very good agreement to one another. The difference can not be ruled out within the experimental errors and also because of broad dispersions associated with the above two processes.

A comparison of $\tau_{(1)}$ and $\tau_{(2)}$ of **B** with that of the corresponding values of **A** shows that $\tau_{(2)}$ (=34.4 p.s.) for this molecule is longer than $\tau_{(2)}$ (=30.0 p.s.) for the previous one, which is smaller in molecular size, showing that the process occurring is due to the molecular rotation. The second process, which could be associated to the internal rotation of the group has no significant variation from the corresponding process in **A**.

In this case also, an attempt to evaluate different enthalpies of activation was made. However, due to irregular variations, the evaluation of $\Delta H\tau_{(1)}$ and $\Delta H\tau_{(2)}$ could not be done properly. The enthalpies, using Gopala Krishna and Higasi relaxation time values were however calculated and the two parameters $\Delta H\tau_{GK}$ (8.00 kJ mol^{-1}) and $\Delta H\tau_{OH}$ (8.00 kJ mol^{-1}), are in very good agreement.

Entropy values for the molecules are found to be negative suggesting the presence of the cooperative process [18].

α-Benzyl Benzyl Cyanide (C)

Having obtained the distribution parameter α in the range of (0.15–0.21) and the most probable relaxation time τ_{OH} as 56.7 p.s. at 288° K, the absorption process has been further resolved by Higasi, Koga and Nakamura method [8] in terms of the two independent relaxation times and the parameters observed were $\tau_{(1)}$ (=25.6 p.s.) and $\tau_{(2)}$ (=51.6 p.s.) respectively at 288° K. The relaxation time for the overlapped process has been calculated as $\tau_0=\sqrt{\tau_{(1)}\tau_{(2)}}$ and been found to be 35.4 p.s. at 288° K.

The dielectric relaxation time associated with the molecular process $\tau_{(2)}$ was 51.6 p.s. whereas that associated with the internal rotation was $\tau_{(1)}$=25.6 p.s. A comparison of the relaxation time values obtained by Higasi's τ_{OH} 56.7 p.s. and

Gopala Krishna's τ_{GK} 26.6 p.s. method show that τ_{OH} is predominantly due to the molecular relaxation process whereas τ_{GK} corresponds to the other process probably arising from the internal rotation of the group. Also $\tau_{OH} > 2\tau_{GK}$, which is similar to the behaviour observed by MATHUR et al. [19] in the case of some substituted anilines.

On comparing the relaxation time of this molecule with the relaxation time of α-Heptyl benzyl cyanide it is found that τ_{OH}, $\tau_{(1)}$, $\tau_{(2)}$ and $\tau_0 = \sqrt{\tau_{(1)}\tau_{(2)}}$ for the former molecule are longer than for the latter molecules whereas in both the molecules the substitution at α-position has the same number of carbon atoms but with different spatial configuration. It is interesting to point out here that in α-Heptyl benzyl cyanide the substituted heptyl group has seven carbon atoms arranged in a linear chain whereas in α-benzyl benzyl cyanide the substituted benzyl group at α-position has also seven carbon atoms but arranged in a cyclic form. The difference in the relaxation time in these molecules may be attributed to the difference in the geometry of the substituted group.

The enthalpy parameters in response to the relaxation processes $\tau_{(1)}$ and $\tau_{(2)}$ could not be ascertained due to some irregular variation in these parameters with respect to the temperature. The other two enthalpy parameters corresponding to τ_{OH} and τ_{GK} are not very accurate. However a comparison shows that $\Delta H\tau_{OH} > \Delta H\tau_{GK}$.

For this molecule also the entropy of activation has been found to be negative. The free energy of activation evaluated using τ_{GK} and τ_{OH} shown in Table IV, and are different being greater for τ_{OH} than for τ_{GK}.

α-*Cyano Stilbene* (*D*)

This molecule gives the distribution parameter α — in the range of (0.29–0.25) and this value decreases with the increase of temperature. τ_{OH} for the molecule has been found to be 44.2 p.s. at 296° K. Due to the high value of α the dielectric dispersion has been resolved in terms of two independent relaxation times $\tau_{(1)}$ and $\tau_{(2)}$. The average relaxation time τ_0 obtained as the geometrical mean of $\tau_{(1)}$ and $\tau_{(2)}$ has been found to be 25.7 p.s. at 296° K.

On comparing the relaxation times evaluated using Gopala Krishna method and Higasi method it is found that $\tau_{OH} > \tau_{GK}$. Similar observations have been made by KRISHNAJI et al. [20]. Lower value of τ_{GK} as compared to τ_{OH} is probably due to the fact that in the evaluation of τ_{GK} it has been assumed that the molecule follows single Debye type dispersion and the Cole-Cole's distribution parameter α is zero or nearly zero.

The enthalpy of activation corresponding to the various modes of rotation have been evaluated and the value 11.9 kJ mol^{-1} for $\Delta H\tau_{(2)}$ corresponds to those for the molecular rotation $\Delta H\tau_{OH}$ (10.6 kJ mol^{-1}) and $\Delta H\tau_{GK}$ (9.6 kJ mol^{-1}) giving the most probable enthalpy values observed for the average dispersion and are comparable to one another. $\Delta H\tau_{(1)}$ (1.7 kJ mol^{-1}) corresponding to the dispersion occurring from the process other than the molecular one, is too low and can not be predicted to be due to the internal motion of the group. However, it could be said to have arisen from some segmental motion of the longer group.

Acknowledgements

Thanks are due to Dr. NITYA NAND the Director of C.D.R.I., Lucknow, for arranging the compounds and providing the library facilities. One of us (S.K. Saxena) is grateful to the University Grant Commission for the award of the fellowship in the "Teacher Fellowship Programme".

References

[1] *Fischer, E.:* Z. Natur. **4a**, 707 (1949).
[2] *Purcell, W. P., K. Fish, C. P. Smyth:* J. Chem. Phys. **82**, 6299 (1960).
[3] *Kleges, G., P. Knobloch:* Z. Natur. **20**, 210 (1965).
[4] *Forest, E., C. P. Smyth:* J. Chem. Phys. **86**, 3474 (1964).
[5] *Hassan, A., A. Das, A. Ghatak:* Ind. J. Phys. **45**, 558 (1971).
[6] *Gopala Krishna, K. V.:* Trans. Faraday Soc. **53**, 767 (1957).
[7] *Higasi, K.:* Bull. Chem. Soc. Japan **39**, 2157 (1966).
[8] *Higasi, K., Y. Koga, M. Nakamura:* Bull. Chem. Soc. Japan **44**, 988 (1971).
[9] *Vyas, A., M. C. Saxena:* J. Sci. and Ind. Res. **14B**, 1613 (1957).
[10] *Roberts, S., A. von Hippel:* J. Appl. Phys. **17**, 610 (1946).
[11] *Dakin, T. W., C. N. Works:* J. Appl. Phys. **18**, 789 (1947).
[12] *Chitoku, K., K. Higasi, M. Nakamura, Y. Koga, H. Takahashi:* Bull. Chem. Soc. Japan **44**, 994 (1971).
[13] *Singh, B., J. K. Viz:* Bull. Chem. Soc. Japan **49**, 2870 (1976).
[14] *Viz, J. K., I. Krishna, K. K. Srivastava:* Bull. Chem. Soc. Japan **46**, 17 (1973).
[15] *Glasstone, S., K. J. Laidler, H. Eyring:* "The Theory of Rate Processes", McGraw Hill Book Co., New York, p. 548. 1941.
[16] *Misra, C. K., M. C. Saxena:* Acta Phys. et Chem. Szeged **24**, 357 (1978).
[17] *Misra, C. K., J. P. Shukla, M. C. Saxena:* Adv. Molecular Relaxation Process, (due to appear).
[18] *Branin, F. H. (Jr.), C. P. Smyth:* J. Chem. Phys. **20**, 1120 (1952).
[19] *Mathur, A.:* Study of the Behaviour of Polar Molecules in Microwave Region, 1975, Ph.D. Thesis, Lucknow University, Lucknow.
[20] *Krishnaji, S. C. Srivastava, Dina Nath:* Bull. Chem. Soc. Japan **43**, 2805 (1970).

ИЗУЧЕНИЕ ДИЭЛЕКТРИЧЕСКИХ ПОТЕРЬ В НЕКОТОРЫХ α-ЗАМЕЩЕННЫХ БЕНЗИЛЦИАНИДОВ В РАЗБАВЛЕННЫХ РАСТВОРАХ

С. К. Саксена, Ц. К. Мисра, Й. П. Шукла и М. Ц. Саксена

Изучены диэлектрические потери для четырех α-замещенных бензилцианидов. Наблюдаемые значения «α» достаточно высоки, что указывает на наличие не одного релаксационного процесса в системе, носящих молекулярный и другой характер. Сделан вывод, что диэлектрическая релаксация относится как к молекулярным, так и групповым процессам.

DEACTIVATION BEHAVIOUR OF ARENES AND HETEROARENES XVI. FLUORESCENCE SELF-QUENCHING OF ANTHRACENE-LIKE COMPOUNDS BY EXCIMER FORMATION

by

J. BENDIG, B. HENKEL and D. KREYSIG

Humboldt-Universität, Sektion Chemie, Bereich Organische Photochemie,
DDR-104 Berlin, Hessische Str. 1—2.

(Received 5th December, 1978)

Using frontal fluorescence excitation, fluorescence quantum yields are accessible even at large fluorophor concentrations provided there is total absorption. This allows to determine the quenching rate constants of fluorescence self-quenching. A suitable method is presented and tested on anthracene and some of its derivatives (2-Me-, 9-Me-, 9-Ph-), the acridizinium ion and 6,7-benzoquinoline. The Stern—Volmer plots agree within the experimental accuracy to those obtained for concentration-dependent fluorescence lifetimes (determined from decay curves and external fluorescence quenching) Consequently a dynamic mechanism has to be formulated for the self-quenching processes examined.

As opposed to other fluorophors studied, the rate constant of self-quenching for 9-phenyl-anthracene is appreciably smaller than the rate constant of diffusion. This effect is ascribed to steric hindrance of excimer formation.

Introduction

Decreasing fluorescence quantum yields with rising concentration, along with shorter fluorescence lifetimes, are typical for the fluorescence behaviour of many aromatic compounds [1–5]. Detailed studies showed that self-quenching according to (1) is caused by the formation of excimers and their deactivation (radiative k_f^E; non-radiative k_d^E).

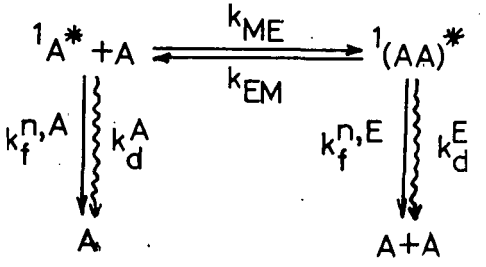

The degree of self-quenching (2) depends on the relationship between the rate constants of all deactivation steps or excimer formation and their back-reactions.

$$\frac{\varphi_{f,0}^A}{\varphi_f^A} = \frac{\tau_{f,0}^{w,A}}{\tau_f^{w,A}} = 1 + k_q^{AA}\tau_f^{w,A}[A] \qquad (2)$$

$\varphi_{f,0}^{A}$; φ^{A} — limit-value of the fluorescence quantum yield at low concentrations ($[A] < 1 \cdot 10^{-5}$ mol l^{-1}) or in the case of self-quenching.

$\tau_{f,0}^{w,A}$; $\tau_{f}^{w,A}$ — unaffected and affected fluorescence decay time, *resp.*, due to self-quenching.

For the rate constant of self-quenching k_q^{AA} holds expression (3).

$$k_q^{AA} = \frac{k_{ME} k_f^{w,E}}{k_{EM} + k_f^{w,E}} \tag{3}$$

$k_f^{w,E}$ — fluorescence decay time of the excimer with

$$k_f^{w,E} = k_f^{n,E} + k_d^E. \tag{4}$$

The studies known from the literature of self-quenching of fluorescence are based on concentration-dependent fluorescence lifetimes [6–8]. To prove that fluorescence quenching (1) is purely dynamic, requires to check the validity of (2) to the effect that plotting of the lifetimes and the fluorescence quantum yields will give both values the same Stern–Volmer plots [2, 3, 9, 10]. However, conventional fluorescence observation by right angle excitation does not allow to determine the fluorescence quantum yield at high concentrations owing to the strong filter effect [11, 12] under these conditions of excitation and important reabsorption and reemission influences [12, 13]. Recent investigations into the fluorescence behaviour with frontal fluorescence excitation [12] show that the reabsorption and reemission effects are stable and correctable for this geometrical arrangement (Fig. 1). Based on these results a procedure will be presented which enables the self-quenching at rising concentration to be evaluated on the basis of the fluorescence quantum yields.

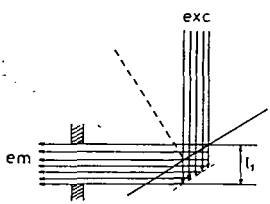

Fig. 1. Optical arrangement in the case of frontal fluorescence excitation

As can be seen from eq. (3) basically two border-line cases exist for the degree of self-quenching:

(i) Deactivation of the excimer is much faster than the back-reactions to $^1A^*$ and A ($k_f^{w,E} \gg k_{EM}$). Under these conditions self-quenching of fluorescence should be diffusion-controlled [14].

$$k_q^{AA} \approx k_{ME} \approx k_{\text{diff}} = \frac{8RT}{2000\eta} \tag{5}$$

(ii) The back-reaction k_{EM} is faster than the deactivation of the excimer ($k_{EM} \gg k_f^{w,E}$). In this case (6) the extent of fluorescence quenching depends in addition on the location of the equilibrium ($K_c^{ME} = k_{ME}/k_{EM}$), and it holds (7).

$$k_q^{AA} = \frac{k_{ME}}{k_{EM}} k_f^{w,E} = K_c^{ME} k_f^{w,E} \tag{6}$$

$$0 \leqq k_q^{AA} < k_{\text{diff}} \tag{7}$$

With reference to the self-quenching of the fluorescence of anthracene (*An*) [2, 4] it is further examined to what extent this self-quenching is affected by exocyclic substitution (2-methylanthracene (*2-Me-An*), 9-methylanthracene (*9-Me-An*), 9-phenylanthracene (*9-Ph-An*)) and endocyclic substitution (acridizinium ion (*Az*), 6,7-benzoquinoline (*BQ*)).

Experimental

The anthracenes used in this study, were commercial products (for purification see [15]). Acridizinium perchlorate was synthesized according to [16] and 6,7-benzoquinoline according to [17]. The solvents were purified by standard procedures [18].

The fluorescence measurements were made on a MPF-2A spektro-fluorimeter (Hitachi–Perkin–Elmer) at 298 K under aerobic conditions. The excitation angle was 30° (*cf.* Fig. 1). The fluorescence decay curves were recorded by excitation with a nitrogen laser ($\lambda = 337.1$ nm) using a Boxcar integrator (for details see [19]).

For the quenching tests $[Q] = 1 \cdot 10^{-1} \ldots 1 \cdot 10^{-4}$ mol l^{-1} of quencher were added. The self-absorption of the quenchers was in all cases $< 1\%$ of the fluorophor absorption intensity at excitation wavelength.

For all linear plots, calculations were carried out to adjust for errors in the straight lines.

Results

For studying self-quenching of fluorescence by frontal excitation there must be total absorption inside the path length l_1. This total absorption depends on a minimum concentration ($[A]_t$) [12] which does not permit to determine $\varphi_{f,0}$ or an adequate relative fluorescence intensity $I_{f,0}$ because of the presence of self-quenching. Consequently eq. (2) has to be applied in the form of (8).

$$\frac{1}{I_f^A} = \frac{1}{I_{f,0}^A} + \frac{k_q^{AA} \tau_{f,0}^{w,A}}{I_{f,0}^A} [A]. \tag{8}$$

By plotting the reciprocal relative fluorescence intensities *versus* fluorophor concentration, a straight line is obtained, and the quenching rate constant k_q^{AA} is determined from the quotient obtained from the slope and ordinate section, divided by the fluorescence decay time, $\tau_{f,0}^{w,A}$ (Table I).

Table I

Fluorescence quantum yields and fluorescence lifetimes of investigated compounds

	Solvent	$\varphi_{f,0}^A$	$\tau_{f,0}^{w,A}$ [ns]
An	benzene	0.26[a]	4.3[a]
2-Me-An	benzene	0.30	4.8
9-Me-An	benzene	0.33	5.2[a]
9-Ph-An	benzene	0.53	5.1[a]
Az	methanol	0.52[b]	4.4[b]
BQ	ethanol	0.62	11.6

[a] [2]; [b] [20].

Figures 2–7 show the functions (8) for the studied fluorophors. Linearity is observed above a given concentration $[A]_t$, as expected, whereas below $[A]_t$ the recorded fluorescence intensities are smaller than suggested by the plotted straight line. This is attributable to the fact that the condition of total absorption inside l_1 (Fig. 1) is no longer satisfied for $[A] < [A]_t$. This also explains the change of shape of the fluorescence band in this concentration range, since the otherwise stable reabsorption effect is becoming weaker, as indicated by the growing intensity in the short-wave part of the spectrum (Fig. 8).

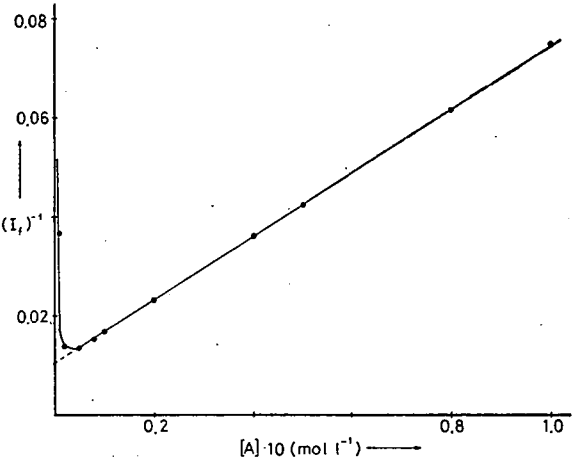

Fig. 2. Relative fluorescence intensity as a function of concentration (anthracene in benzene)

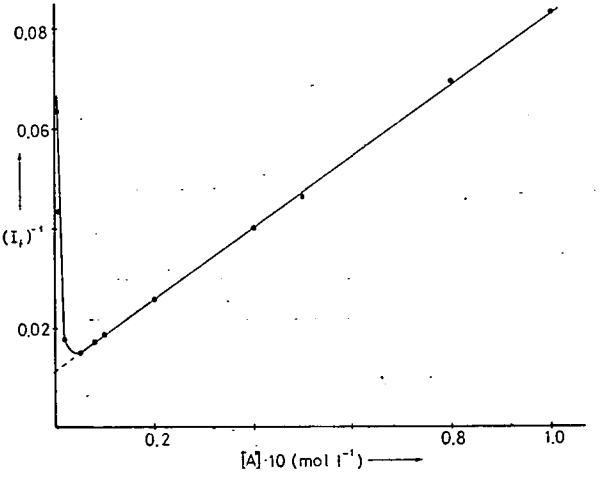

Fig. 3. Relative fluorescence intensity as a function of concentration (2-methylanthracene in benzene)

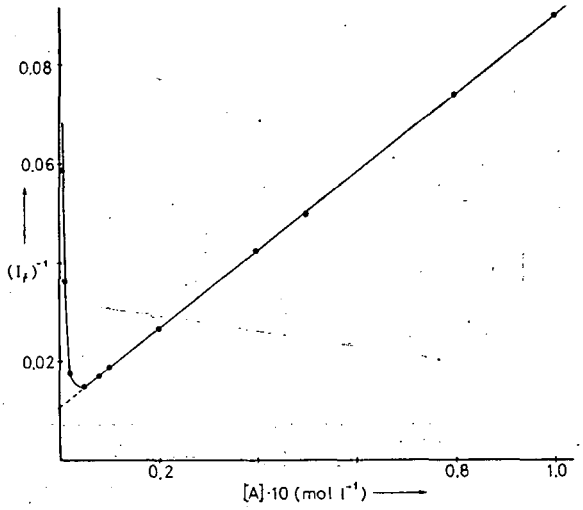

Fig. 4. Relative fluorescence intensity as a function of concentration (9-methylanthracene in benzene)

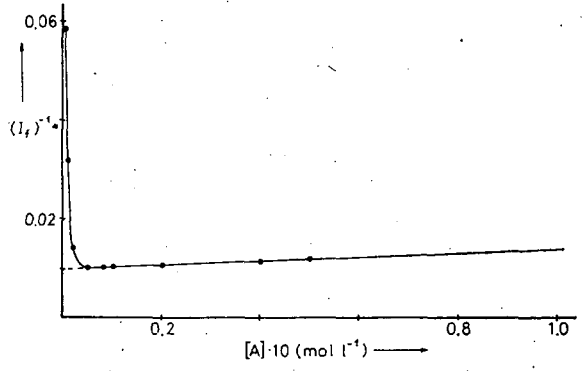

Fig. 5. Relative fluorescence intensity as a function of concentration (9-phenylanthracene in benzene)

The fluorescence quantum yield $\varphi_{f,0}^{A}$ (Table I) can be assigned to the relative fluorescence intensity $I_{f,0}^{A}$ obtained by extrapolation. The resultant fluorescence quantum yields φ_f^A are collected as a function of concentration in Table II. The lifetimes τ_f^w for the fluorophors *Az* and *BQ* were calculated from the fluorescence decay times (Table II). The Stern–Volmer plots according to (2) obtained from these concentration-dependent lifetimes, yield straight lines (Fig. 9). From the slope of these lines the quenching rate constants were calculated (see in Table III).

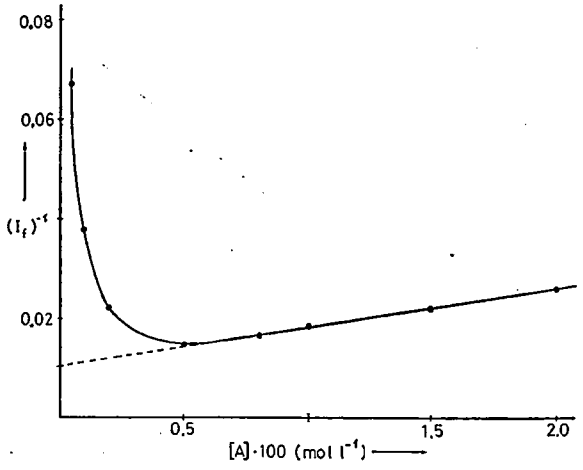

Fig. 6. Relative fluorescence intensity as a function of concentration (acridizinium ion in methanol)

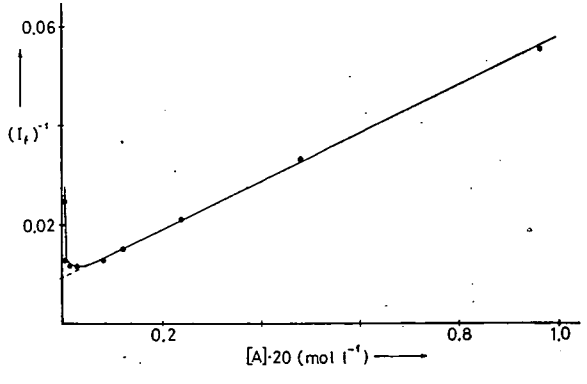

Fig. 7. Relative fluorescence intensity as a function of concentration (6,7-benzoquinoline in ethanol)

Further the fluorescence lifetimes at different fluorophor concentrations by quenching with an external quencher Q were determined (9).

$$\frac{I_{f,0}}{I_f} = 1 + k_\zeta^{AQ}\tau_f^{w,A}[Q]. \tag{9}$$

For *An, 2-Me-An, 9-Me-An* and *9-Ph-An* methyl iodide was used as quencher, for which case the mechanism (10) holds [23].

$$^1A^* + Q \rightleftharpoons (\overset{\delta+}{^1A^*}\ldots\overset{\delta-}{Q}) \rightarrow {}^3A^* + Q. \tag{10}$$

Table II

Fluorescence quantum yields and fluorescence lifetimes (in ns) at different concentrations

[A] [mol l^{-1}]	*An*		*2-Me-An*		*9-Me-An*		*9-Ph-An*		*BQ*		*Az*		
	φ_f	$\tau_f^{w a)}$	φ_f	$\tau_f^{w a)}$	φ_f	$\tau_f^{w a)}$	φ_f	$\tau_f^{w a)}$	φ_f	$\tau_f^{w b)}$	φ_f	τ_f^{w} I[a]	II[b]
$1 \cdot 10^{-4}$	0.26	4.3	0.30	4.8	0.33	5.2	0.53	5.1	0.61	11.5	0.52	4.4	4.4
$1 \cdot 10^{-3}$	0.25	4.0	0.28	4.5	0.31	4.9	0.53	5.1	0.57	10.7	0.48	4.1	4.0
$2 \cdot 10^{-3}$	0.23	3.8	0.27	4.2	0.29	4.6	0.53	5.0	0.53	9.8	0.45	3.8	3.8
$5 \cdot 10^{-3}$	0.20	3.3	0.23	3.6	0.24	3.8	0.52	5.0	0.43	7.9	0.38	3.2	3.3
$8 \cdot 10^{-3}$	0.18	2.9	0.20	3.1	0.21	3.3	0.51	4.9	0.35	6.6	0.33	2.8	2.8
$1 \cdot 10^{-2}$	0.16	2.6	0.18	2.9	0.19	3.0	0.51	4.9	0.33	6.2	0.30	2.5	2.5
$1.5 \cdot 10^{-2}$	0.14		0.15		0.16		0.50		0.26		0.25	2.1	2.1
$2 \cdot 10^{-2}$	0.12	1.9	0.13	2.0	0.14	2.1	0.49	4.6	0.22	4.2	0.21	1.8	1.8
$4 \cdot 10^{-2}$	0.08	1.2	0.09	1.3	0.09	1.4	0.46	4.2	0.14	2.6			
$5 \cdot 10^{-2}$	0.06	1.0	0.07	1.1	0.07	1.1	0.44	4.1	0.11	2.1			
$8 \cdot 10^{-2}$	0.04		0.05		0.05		0.40						
$1 \cdot 10^{-1}$	0.04		0.04		0.04		0.38						
$5 \cdot 10^{-1}$									0.01	0.2			

[a] Calculated from the fluorescence quenching results.
[b] Decay times.

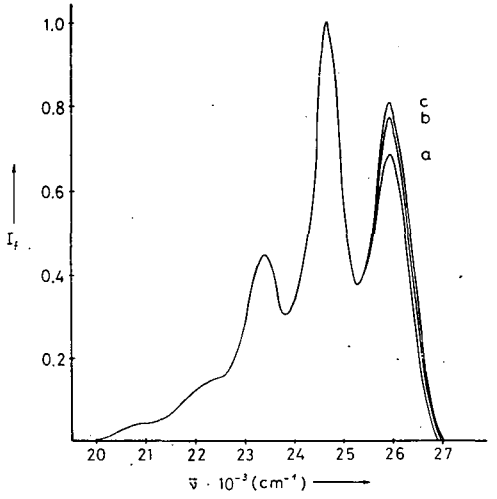

Fig. 8. Fluorescence spectra of anthracene at different concentrations (frontal fluorescence excitation)
$a = 5 \cdot 10^{-3}$ mol l^{-1}, $b = 2 \cdot 10^{-3}$ mol l^{-1},
$c = 1 \cdot 10^{-0}$ mol l^{-1}

Table III

Rate constants of fluorescence self-quenching k_q^{AA} for the investigated fluorophors and rate constants of diffusion (all in $10^9\ l\ mol^{-1}\ s^{-1}$)

Fluorophor	Solvent	k_q^{AA}			k_{diff}[d]
		I[a]	II[b]	III[c]	
An	benzene	14.1		14.6	16.0
2-Me-An	benzene	13.0		14.0	16.0
9-Me-An	benzene	13.6		13.7	16.0
9-Ph-An	benzene	0.8		1.0	16.0
Az	methanol	16.8	16.5	16.5	18.0
BQ	ethanol	8.9	8.1		9.2

[a] Calculated by the fluorescence quantum yields.
[b] Calculated by fluorescence decay times.
[c] Calculated by fluorescence lifetimes result from quenching investigations.
[d] [21].

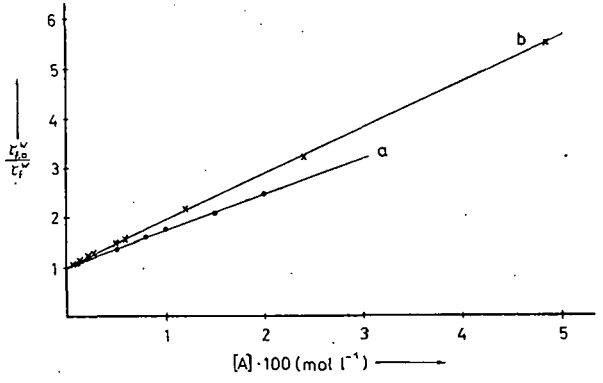

Fig. 9. Stern—Volmer plots of fluorescence lifetimes as obtained from fluorescence decay measurements; for *Az* in methanol (*a*) and for *BQ* in ethanol (*b*)

The fluorescence of the acridizinium ion was quenched by naphthalene (11) [5, 22].

$$^1A^{+*} + Q \rightleftharpoons (^2A^{\cdot} \ldots {}^2Q^{+\cdot}) \rightarrow A + Q. \qquad (11)$$

The values of k_q^{AQ} required for interpretation, were determined by means of fluorescence quenching at $[A] \leqq 1 \cdot 10^{-5}$ mol l^{-1} with reference to $\tau_{f,0}^w$ (Table I) and summarized in Table IV.

The Stern–Volmer plots using the τ_f^w-values found by external quenching are shown in Fig. 10. The resultant quenching rate constants k_q^{AA}, using (2), are likewise included in Table III.

Table IV

Rate constants of fluorescence quenching k_q^{AQ} for the investigated fluorophor/quencher pairs (in 10^9 l mol^{-1} s^{-1})

Fluorophor	Solvent	Quencher	k_q^{AQ}
An	benzene	methyliodide	6.2
2-Me-An	benzene	methyliodide	6.1
9-Me-An	benzene	methyliodide	5.9
9-Ph-An	benzene	methyliodide	4.1
Az	methanol	naphthalene	16.1[a]

[a] [22].

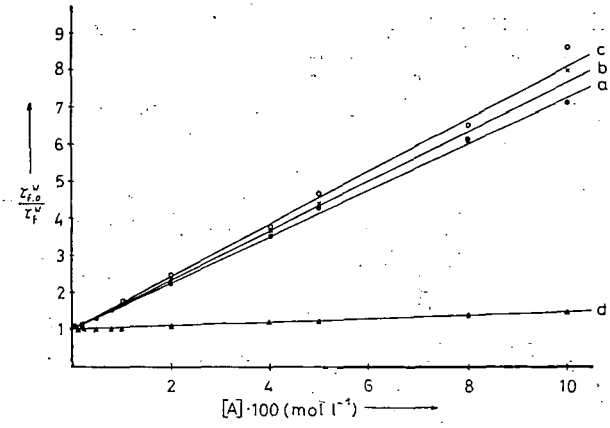

Fig. 10. Stern—Volmer plots of fluorescence lifetimes, obtained from external fluorescence quenching; for *An* (●, *a*), *2-Me-An* (*x*, *b*), *9-Me-An* (*o*, *c*) and *9-Ph-An* (▼, *d*) in benzene

Discussion

The linear dependencies obtained between $(I_f)^{-1}$ and $[A]$ for $[A] > [A]_t$ (Figs. 2–7) confirm the validity of (8). This result and the fact that the $k_{q_1}^{AA}$-values are identical within the experimental accuracy with those determined from fluorescence lifetimes (Table III) prove the applicability of the approach by which self-quenching with frontal excitation is studied by means of the fluorescence quantum yield.

As stated previously, frontal excitation requires a minimum concentration $[A]_t$. Hence self-quenching can be studied only in the concentration range (12), which will be relatively narrow (Fig. 6) with sparingly soluble fluorophors ($[A]_{\text{saturated}}$ low).

$$[A]_{\text{saturated}} \geqq [A] > [A]_t. \tag{12}$$

As a result, the evaluation will be difficult, especially extrapolation $[A] \to 0$ for (8). By contrast, concentration range (13) can be utilised when evaluating the fluorescence lifetime.

$$[A]_{\text{saturated}} \geqq [A] > 0. \tag{13}$$

Table III shows that there is good agreement for the values of k_q^{AA} obtained by the three methods outlined above. It may be concluded that self-quenching of fluorescence is in all cases a dynamic process. Diffusion control is observed in all cases, apart from *9-Ph-An*, as shown by comparing k_q^{AA} with k_{diff} of the solvents studied (Table III). Hence it may be followed that for the compounds *An, 2-Me-An, 9-Me-An, Az* and *BQ*, deactivation of the excimer proceeds at a considerably faster rate than the back-reaction k_{EM}, that is to say, it holds (5). In the case of *9-Ph-An* very weak fluorescence self-quenching is observed which implies that (6) holds here. The relationship $k_{EM} \gg k_f^{w,E}$ may be explained either by steric hindrance of complex formation because of the twisted phenyl substituent or by the slower deactivation rate of the excimer as compared to the other fluorophors[1]. Investigations which studied the potential ability to form π-π-molecular complexes [24] have shown a comparatively small association constant to be typical of the *9-Ph-An* in this case. Hence it may be assumed that steric hindrance of excimer formation caused by twisting of the phenyl ring relative to the π-plane of the anthracene [28] accounts for the weak tendency toward excimer formation and concomitant self-quenching. This steric effect is not observed in methylanthracene. This group, which takes up little space, has no effect because of the relatively large intermolecular distances in the excimer (0.3... 0.5 nm [2])[2].

Endocyclic substitutions (*Az, BQ*) are observed to have no noticeable influence on the rate constant k_q^{AA}. Hence it is concluded that the expected destabilization of the excimer by repulsion (free electron pairs, positive charges) is compensated by an improved ability of forming excimers or a very rapid deactivation (formation of photo-dimers, for instance) of the excimer. The favourable position of the endocyclic substitution is of great importance in this context as it does not cause the meso-positions to be blocked like in N-methylacridinium ion or acridine. This problem will be discussed in a report to be published later.

* * *

We are grateful to Herr M. Näther, Zentralinstitut für Optik and Spektroskopie der Akademie der Wissenschaften der DDR and Herr K. Wilda, Sektion Mathematik/Physik der PH Potsdam, for the determination of the fluorescence decay times.

References

[1] *Stevens, B.:* Adv. Photochem. **8**, 161 (1971).
[2] *Birks, J. B.:* Photophysics of Aromatic Molecules, Wiley-Interscience, London, 1970.
[3] *Davidson, R. S.:* in Molecular Association, Vol. 1 (ed. R. Foster), Academic Press, London, 1975.
[4] *Ledwith, A.:* in The Exciplex (ed. M. Gordon, W. R. Ware) Academic Press, New York, 1975.
[5] *Bendig, J., B. Geppert, S. Helm, D. Kreysig:* Adv. Mol. Relax. Interaction Processes **12**, 289 (1978).
[6] *Itoh, M., T. Mimura, T. Okamoto:* Bull. Chem. Soc. Japan **47**, 1078 (1974).
[7] *Itoh, M., T. Mimura:* Chem. Phys. Lett. **24**, 551 (1974).

[1] Unlike *An, 9-Me-An* [1—4], *2-Me-An* [25], *Az* [26] and *BQ* [27], where this reaction contributes substantially to a rapid excimer deactivation ($k_f^{w,E}$), *9-Ph-An* does not photodimerise (in the absence of an energy transferring agent) [29].

[2] This statement concerns only the formation of excimers and does not apply to photodimers [24].

[8] *Aladekomo, J. B.:* J. Luminescence **6**, 83 (1973).
[9] *Weller, A.:* Progress in Reaction Kinetics **1**, 187 (1961).
[10] *Bendig, J., D. Kreysig:* Z. physik. Chemie (Leipzig) **259**, 551 (1978).
[11] *Parker, C. A., W. T. Rees:* Analyst **85**, 587 (1960).
[12] *Bendig, J., D. Kreysig:* Z. physik. Chemie (Leipzig) **260**, 149 (1979).
[13] *Bendig, J., C. Csongár, D. Kreysig:* Z. physik. Chemie (Leipzig) **260**, 312 (1979).
[14] *Parker, C. A.:* Photoluminescence of Solutions, Elsevier Publ., Amsterdam, 1968.
[15] *Sauer, J., J. Bendig, M. Siegmund:* Z. Chem. **17**, 308 (1977).
[16] *Bradsher, C. K., T. W. G. Solomons, F. R. Vaugham:* J. Org. Chem. **25**, 757 (1960).
[17] *Albert, A., D. J. Brown, M. Duewell:* J. Chem. Soc. 1284 (1948).
[18] *Riddick, J. A., W. A. Burger:* in Techniques of Chemistry (ed. A. Weissberger), Vol. 2: Organic Solvents, 3rd edition, Wiley-Interscience, New York, 1970.
[19] *Becker, W., S. Dähne, K. Teuchner, K. Seliger:* Exp. Tech. Physik **23**, 297 (1975).
Dähne, S., W. Becker, M. Sorge, K. Teuchner: Z. Chem. **16**, 134 (1976).
[20] *Bendig, J., S. Helm, D. Kreysig:* J. prakt. Chem. **319**, 807 (1977).
[21] *Murov, S. L.:* Handbook of Photochemistry, Marcel Dekker Inc. New York, 1973.
[22] *Bendig, J., B. Geppert, S. Helm, D. Kreysig:* Teor. Eksp. Khimija, **14**, 629 (1978).
[23] *Werner, T. C.:* Fluorescence News **9**, 1 (1976).
[24] *Bendig, J., Kreysig, G. Templer:* J. Prakt. Chem. **318**, 861 (1976).
[25] *Bendig, J.:* unpublished results.
[26] *Bendig, J., B. Geppert, D. Kreysig:* J. prakt. Chem. **320**, 739 (1978).
[27] *Bendig, J., B. Henkel, D. Kreysig:* in preparation.
[28] *Hamilton, T. D. S.:* Photochem. Photobiol. **3**, 153 (1964).
[29] *Bouis-Laurent, H.:* J. Chem. Soc. Chem. Commun. 906 (1973).

ПУТИ ДЕЗАКТИВАЦИИ АРЕНОВ И ГЕТЕРОАРЕНОВ, XVI. САМОТУШЕНИЕ ФЛУОРЕСЦЕНЦИИ СОЕДИНЕНИЙ ТИПА АНТРАЦЕНА ПРИ ОБРАЗОВАНИИ ЭКСИМЕРОВ

Ю. Бендиг, Б. Хенкель, Д. Крейзиг

В случае высокой концентрации флуоресцирующего вещества можно определить квантовые выходы флуоресценции при полном поглощении. Таким образом возможно определения констант скорости самотушения флуоресценции. Соответствующая методика представлен, в данной работе и успешно испытана на примере антрацена и его производных (2-Me-, 9-Me-9-P-), иона акридиция и 6,7-бензхинолина. Полученные таким образом соотношения Штерна-Фольмера совпадают в пределах ошибки с кривыми из зависимости времени жизни от концентрации (определяемые из кривых затухания флуоресценции и тушения посторонними тушителями). Следовательно, можно предположить динамический механизм самотушения.

Константа скорости самотушения 9-фенилантрацена в отличие от других изученных веществ намного меньше константы скорости диффузии, что объясняется стерическими затруднениями при образовании эксимеров.

RÖNTGENDIFFRAKTOMETRISCHE UNTERSUCHUNGEN DES EINBAUS VON SILBERIONEN IN ZEOLITHE DES Y-TYPS

Von

K. VARGA und I. KIRICSI
Lehrstuhl für Angewandte Chemie der Attila-József-Universität, Szeged

und

GY. ARGAY
Zentralforschungsinstitut für Chemie der Ungarischen Akademie der Wissenschaften, Budapest

(Eingegangen am 21. März 1979)

Es wurden AgNaY Zeolithproben von verschiedenen Ag-Gehalten durch Ionenaustausch hergestellt, und auf Grund der Röntgendiffraktogramme dieser Proben wurden die von den Ag^+-Ionen eingenommenen Positionen *bzw.* die Reihenfolge der Besetzung der gegebenen Ionenpositionen mit der Strukturfaktoranalyse bestimmt. Die von Verfassern ausgearbeiteten Rechenprogramm ist für die Auswertung der Röntgendiffraktogramme jedes Zeolithes des Faujasite-Typs geeignet.

Einleitung

Die katalytischen Eigenschaften der Zeolithe werden entscheidend durch Art und Menge der darin befindlichen Kationen beeinflußt. Von großer Wichtigkeit sind deshalb einerseits die Untersuchung des Ionenaustauschvermögens, andererseits die Analyse der Verteilung *bzw.* Anordnung der darin befindlichen Kationen. Was die erste Frage betrifft, so ist heute schon sehr viel über die Bedingungen des Austauschs einwertiger Kationen bekannt, und auch der Austausch der sich wesentlich komplizierter verhaltenden mehrwertigen Kationen ist zu kontrollieren und zu steuern. Man kann sagen, daß das Ionenaustauschvermögen im wesentlichen als geklärt angesehen werden kann [1].

Der zweite Problemkreis, die Frage der Anordnung (der in der Elementarzelle eingenommenen Positionen) der Kationen ist in vielen Fällen noch nicht geklärt, und in vielen Teilfragen weichen die Meinungen der einzelnen Autoren voneinander ab. Verhältnissmäßig wenig Kenntnisse haben wir über die sich in den eine komplizierte Struktur aufweisenden Faujasiten abspielenden Ionenaustauschprozesse. Darüber wird auch heute noch gearbeitet, siehe *z. B.* [2]. In Tab. I sind die früheren Ergebnisse über die Anordnung von durch Ionenaustausch in Y-Zeolith eingebrachten Kationen zusammengefaßt.

Zur Bestimmung der Positionen der sich in der Kristallstruktur der Zeolithe *bzw.* in den Hohlräumen des Zeolithgitters befindlichen austauschbaren Kationen ist die röntgendiffraktometrische Methode am geeignetsten. Die am Einkristall aufge-

Tabelle I

Verteilung der Kationen in der Elementarzelle von Zeolithen des Y-Types

Kationenpositionen		Na^+	K^+	Ag^+	Cu^{++}	Ni^{++}
symbol	anzahl	[3]	[4]	[3]	[5]	[6]
S_I	16	7,5	12	16	3,4	12
$S_{I'}$	32	19,5	14,2	10,7	10,4	1,1
$S_{II'}$	32	—	—	—	—	—
S_{II}	32	30	30	28,3	21 Na	21 Na

nommenen Diffraktogramme liefern verhältnismäßig viele und genaue Informationen. Die Zeolithe des Y-Typs sind jedoch mikrokristallin, und nur in Ausnahmefällen lassen sich solche Einkristalle erhalten, deren Ausmaße für Röntgeneinkristalluntersuchungen ausreichend sind. Somit kommt bei der röntgendiffraktometrischen Untersuchung von Zeolithen der Pulver-aufnahme-Technik eine besonders große Bedeutung zu [7, 8].

In der vorliegenden Arbeit haben wir den Versuch unternommen, auf Grund der Pulverdiffraktogramme von Zeolithen des Y-Typs mit verschiedenen Ionenaustauschgraden durch Strukturanalyse die Reihenfolge des Einbaus von Kationen und den Besetzungsgrad der Ionenpositionen zu bestimmen.

Wir haben den Eintausch von Silberionen untersucht. Die Wahl dieses Ions ist durch mehrere Umstände gerechfertigt: alle Kationen des NaY sind durch das einwertige Ag^+-Ion austauschbar und der Austausch verläuft mit ausreichender Geschwindigkeit. Der Eintausch von Ag^+-Ionen ist auch hinsichtlich der röntgendiffraktometrischen Untersuchung vorteilhaft, da der atomare Streufaktor verhältnismäßig groß ist.

Herstellung der AgNaY-Proben

Bei der Herstellung der Zeolithe mit vershiedenen Silbergehalten wurde von einem aus der Sowjetunion stammenden NaY-Zeolith ausgegangen, der von L. I. Piguzova (Inst. Neft. Prom., Moskau) synthetisiert wurde. Aus röntgenmikroanalytischen und röntgenfluorescenzspektroskopischen Daten wurde die Zusammensetzung der Elementarzelle zu

$$Na_{58,1}Ca_{0,3}(Ti, Fe, K)_{0,76}Al_{60,7}Si_{131,3}O_{384} \cdot 256\,H_2O,$$

berechnet.

Der Austausch der Na^+-Ionen des Ausgangszeoliths gegen Ag^+-Ionen wurde nach BEYER [9] auf folgende Weise ausgeführt: je 10 g NaY-Zeolith wurden einen Tag mit 1000 ml einer 0,1 N, 0,05 N, 0,02 N, 0,08 N bzw. 0,003 N $AgNO_3$-Lösung äquilibriert. Die Proben wurden danach durch ein Glasfilter filtriert und mit dest. Wasser bis zur Ag^+-Ionenfreiheit gewaschen, durch Durchsaugen von Luft getrocknet und bis zur Verwendung im Exsikkator über Schwefelsäure aufbewahrt. Die Silberkonzentration der Filtrate wurde nach der klassischen Volhard-Methode bestimmt und daraus der Gleichgewichts-Silbergehalt der Zeolithproben berechnet. Es wurden die in Tab. II angeführten AgNaY-Zeolithe erhalten. Mit diesen Proben wurden die röntgendiffraktometrischen Untersuchungen ausgeführt.

Tabelle II

Silbergehalt der Zeolithproben

Probennummer	mval Ag^+/g hydratisierter Zeolith	Ag^+ pro Elementarzelle	Ionenaustauschgrad
1	0,0	0,0	0,0
2	0,267	4,66	7,7
3	0,714	12,5	20,5
4	1,59	27,7	46,7
5	2,73	47,6	78,5
6	3,10	54,1	89,1

Aufnahme der Röntgendiffraktogramme

Die Diffraktogramme der Zeolithproben wurden mit einem Phillips-Pulverdiffraktometer im Bereich $2\theta = 3° - 54°$ bei eine Registriergeschwindigkeit von 1°/min aufgenommen. Die Breite (Divergenz) des Strahlenbündels betrug 1°. Die Untersuchungen wurden mit Cu-K_α-Strahlung ausgeführt ($\lambda = 1{,}5418$ Å) [10].

Die aufgenommenen Diffraktogramme zeigten etwa 40 Reflexionen, aus denen nach der Methode der kleinsten Fehlerquadrate die Parameter der kubischen Elementarzelle berechnet wurden. Es wurde festgestellt, daß der Austausch gegen Silberionen keine Veränderungen der Elementarzellengröße zur Folge hat, die für die in Tab. II. angeführten sechs Zeolithproben erhaltenen Werte streuten um den Wert $a = 24{,}681$ Å.

Zur Bestimmung der Positionen der eingebauten Silberionen wurde die Intensität der einzelnen Reflexionen durch graphische Integration bestimmt. Diejenigen Reflexionen, denen eindeutig nur ein einziger Gitterebenen-Index zuzuordnen war, sind in Tab. III angeführt, wo die Werte I_{rel} die mit 1000 multiplizierten, auf I_{ill} bezogenen gemessenen Intensitäten I_{hkl} bedeuten.

Berechnung der Strukturfaktoren

Die Strukturfaktor-Analyse wurde gemäß der für Pulveraufnahmen gültigen Gleichung

$$I \sim Lp\,P\,A_s|F|^2$$

ausgeführt, in der

$Lp = \dfrac{1+\cos^2 2\theta}{2\sin 2\theta}$: der trigonometrische Faktor,

P: die Multiplizität,

A_s: der Absorptionsfaktor,

F: der Strukturfaktor,

$\sim$: das Proportionalitätszeichen

sind.

Tabelle III

Intensitäten und Strukturfaktoren der gemessenen Reflexionen

h	k	l	θ	Probe 1		Probe 2		Probe 3		Probe 4		Probe 5		Probe 6	
				I_{rel}	F_{gem}	I_{rel}	F_{gem}	I_{rel}	F_{gem}	I_{rel}	F_{gem}	I_{rel}	F_{gem}	I_{rel}	F_{gem}
1	1	1	3,125	1000	431	1000	431	1000	431.	1000	431	1000	431	1000	431
2	2	0	5,10	189	250	258	293	129	207	97	179	58	139	21	83
3	1	1	5,925	88	140	211	218	234	229	119	163	56	112	15	58
3	3	1	7,83	220	295	282	335	190	275	137	233	91	190	33	114
4	4	0	10,18	136	430	158	458	55	273	32	208	0	0	0	0
6	2	0	11,40	46	199	78	259	65	237	51	209	33	168	11	97
5	3	3	11,825	253	485	358	577	280	510	396	607	577	733	236	468
4	4	4	12,50	13	202	10	177	0	0	0	0	20	250	10	177
6	4	2	13,51	161	315	293	425	280	415	208	358	160	314	70	207
7	3	3	14,81	41	247	132	444	77	339	50	273	30	212	24	189
8	4	0	16,22	58	325	165	548	197	599	245	668	258	685	131	488
6	6	4	17,05	66	366	114	481	106	464	106	464	91	430	29	242
9	3	1	17,33	45	217	97	319	86	300	99	322	102	327	47	222

Die Bestimmung des Absorptionsfaktors ist ziemlich umständlich, aber sein Wert ändert sich unter den gegebenen Bedingungen praktisch nicht. Diese Größe wurde deshalb — als konstanter Proportionalitätsfaktor — bei den Berechnungen nicht berücksichtigt. Die Werte für Lp und P wurden dem 1. und 2. Band der International Tables entnommen [11]. Die Werte der gemessenen (relativen) Strukturfaktoren konnten damit auf Grund der Gleichung

$$F_{gem} = 10^3 \sqrt{\frac{I_{rel}}{Lp\,P}}$$

erhalten werden (s. Tab. III).

Die zu den einzelnen Kristallgitterebenen gehörenden Strukturfaktoren sind auf Grund der Fourier-Analyse nach der Gleichung

$$|F_{hkl}|^2 = \left(\sum_{n=1}^{N} f_n A_n\right)^2 + \left(\sum_{n=1}^{N} f_n B_n\right)^2$$

zu berechnen;

f_n: Streukoeffizienten der einzelnen Atome,

A_n; B_n: trigonometrische Strukturfaktoren,

N: Anzahl der Atome in der Elementarzelle.

Die Streukoeffizienten sind auf Grund des Zusammenhanges

$$f_n = f_n^0 \exp\left(-b \sin^2\theta/\lambda^2\right)$$

zu berechnen. Der Temperaturkoeffizient b ist nicht streng konstant. In erster Näherung ist er zwar als konstant zu betrachten ($b=5$), aber im Rechenprogramm tritt er als Veränderliche auf.

Die Werte für f_n^0 wurden den International Tables entnommen [12]. Die Streukoeffizienten für die Silber-, Natrium- und Sauerstoffatome waren direkt in Abhängigkeit von 0 angegeben, die Werte für die T-Atome wurden entsprechend dem Si/Al-Verhältnis aus den Streukoeffizienten von Silicium und Aluminium durch Interpolation erhalten.

Die trigonometrischen Strukturfaktoren sind Funktionen der (h, k, l) Indizes und daneben auch der die Position der einzelnen Atomarten bestimmenden (x_n, y_n, z_n) — kurz: (x, y, z) — Koordinaten. Im Falle der für die Struktur der Zeolithe des Faujasit-Typs charakteristischen Raumgruppe Fd3m gilt:

$$A_n = 8 \cos^2 2\pi \frac{h+k}{4} \cdot \cos^2 2\pi \frac{k+l}{4} \cdot G \quad \text{und} \quad B_n = 0,$$

wobei G die trigonometrische Funktion von (x, y, z) und (h, k, l) bedeutet [13].

Rechenprogramm

Unter Verwendung der voranstehend angegebenen Beziehungen der Strukturfaktor-Berechnung wurde ein Lösungsalgorithmus und ein entsprechendes FORTRAN-Rechenprogramm aufgestellt. Die Berechnungen wurden mit dem Computer CDC 3300 ausgeführt.

Im INPUT-Teil wurden nach der Eingabe der Zahl der Reflexionen R und der Atomarten M *bzw.* der Atome N die (hkl)-Indizes für $r=1, \ldots, R$ und die Streukoeffizienten $(m=1, \ldots, M)$ eingegeben, und anschließend noch die Bezeichnung der Atompositionen für $n=1, \ldots, N$, die laufende Nummer der Streu-

Tabelle IV

Die in der Elementarzelle von Zeolithen des Faujasit-Typs vorliegenden Atome und Positionen

Laufende Nummer	Bezeichnung des Atoms bzw. der Position	Zahl der Positionen in der Elementarzelle	Ortskoordinaten [8]		
			x	y	z
1	T Si, Al	192	0,0380	0,3050	0,1244
2	01	192	0,0000	−0,1040	0,1040
3	02	192	0,0020	−0,1410	0,0020
4	03	192	0,0780	−0,0360	0,0780
5	04	192	0,0720	0,3250	0,0720
6	OW1 H_2O	96	0,0190	−0,2310	0,2690
7	OW2 H_2O	96	0,0420	−0,2080	0,3320
8	Na1	96	0,0000	0,0000	0,0000
9	Na2	32	0,0710	0,0710	0,0710
10	Na3	32	0,2120	0,2120	0,2120
11	Ag1 = S_I	16	0,0000	0,0000	0,0000
12	Ag2 = $S_{I'}$	32	0,0710	0,0710	0,0710
13	Ag3 = S_{II}	32	0,2120	0,2120	0,2120
14	Ag4 = $S_{II''}$	32	0,2460	0,2460	0,2460
15	Ag5 = $S_{II'}$	32	0,1770	0,1770	0,1770

Tabelle V

Berechnete Strukturfaktoren

h	k	l	F_{Gitter}	F_{Wasser}	F_{Na}	F_{NaY}	F_{Ag^1}	F_{Ag^2}	F_{Ag^3}	F_{Ag^4}	F_{Ag^5}
1	1	1	−2117	654	−419	−1882	−374	−927	−511	−56	−865
2	2	0	1236	77	−277	1036	−0	−903	−314	−3	−940
3	1	1	802	−545	−56	199	372	−392	−230	−18	−615
3	3	1	−1307	−321	79	1548	370	525	537	92	75
4	4	0	−1447	515	286	645	737	66	492	1460	100
6	2	0	455	156	−260	351	0	−514	−670	−11	−444
5	3	3	−1357	−294	15	−1636	368	−712	416	−17	737
4	4	4	−386	412	220	246	736	−14	283	1450	−26
6	4	2	−885	−22	−61	−969	0	109	−387	−11	115
7	3	3	−635	133	224	−278	−369	731	660	238	−330
8	4	0	786	280	162	1229	740	285	−284	1443	333
6	6	4	−795	−19	−170	−985	0	63	−841	−33	55
9	3	1	390	−161	319	548	371	544	546	129	487

koeffizienten und die (x, y, z)-Ortskoordinaten. Die für die Berechnungen benutzten Daten sind in Tab. IV angegeben.

Die *Strukturfaktor-Matrix* hat die Ausmaße $N \times R$. Die Elemente bedeuten die der Reflexion der laufenden Nummer r zuzuschreibenden Strukturfaktor-Beiträge des in der n-ten Position, also auf den (x_n, y_n, z_n)-Plätzen befindlichen Atoms. Die Berechnung erfolgt in einem Doppelzyklus: innerhalb des Zyklus $r=1, \ldots, R$ wird die Operation $F_n = f_n A_n$ auf Grund der voranstehend angegebenen Zusammenhänge $(B \equiv 0)$ für jeden festgelegten (hkl)-Index und $n=1, \ldots, N$ ausgeführt. Das Programm bewahrt die Strukturfaktor-Matrix auf.

In Tab. V sind die die Grundlage für die Modellierung darstellenden Strukturfaktoren zusammengefaßt. Das Rechenprogramm speichert selbstverständlich die Strukturfaktoren F_n für jede Atomart und jede Position gesondert, aber der Übersichtlichkeit wegen wurden die Beiträge der T-Atome und der verschiedenen Gittersauerstoffatome in F_{Gitter}, die Beiträge der Sauerstoffatome der Wassermoleküle in F_{Wasser} und die Beiträge der in drei verschiedenen Positionen vorliegenden Na-Ionen in F_{Na} zusammengefaßt. Die Summe aller dieser Beiträge enthält F_{NaY}.

Die Modellierung des Austauschs der Silberionen erfolgte so, daß bei gleichzeitiger Verminderung des Besetzungsgrades der Na-Positionen damit äquivalente Mengen von Ag^+-Ionen auf die 5 potentiellen Positionen durch Erhöhung der Besetzungsgrade „gebracht" werden. So werden nach der Berechnung der Struktur faktor-Matrix auf einer einzigen Karte N Besetzungsgrade eingegeben, und das Programm berechnet für jede Reflexion den Strukturfaktor $F_{\text{ger}} = \sum F_n$. Diejenige Besetzungsgrade-Kombination wird als real akzeptiert, bei der die Werte F_{gem} und F_{ger} für jede gemessene Reflexion praktisch gleich sind.

Ergebnisse und Schlußfolgerungen

Abb. 1 illustriert die Ergebnisse und zugleich auch das Verfahren. Die ersten Kolonnen repräsentieren die gemessenen Strukturfaktoren, die zweiten *bzw.* dritten Kolonnen (einfach schraffiert) die Strukturfaktoren eines gelungenen *bzw.* offensichtlich schlechten Modells. Die Höhe der mittleren (unschraffierten) Kolonnen folgt gut der Höhe der aus den Meßdaten berechneten (doppelt schraffierten) Kolonnen, nur bei der (733)-Reflexion ist eine geringe Abweichung festzustellen. Die Höhe der dritten Säule weicht dagegen in vier Fällen — bei den Reflexionen (220), (311), (440) und (444) — deutlich von den gemessenen Werten ab und ist auch bei den Reflexionen (840) und (664) zu beanstanden.

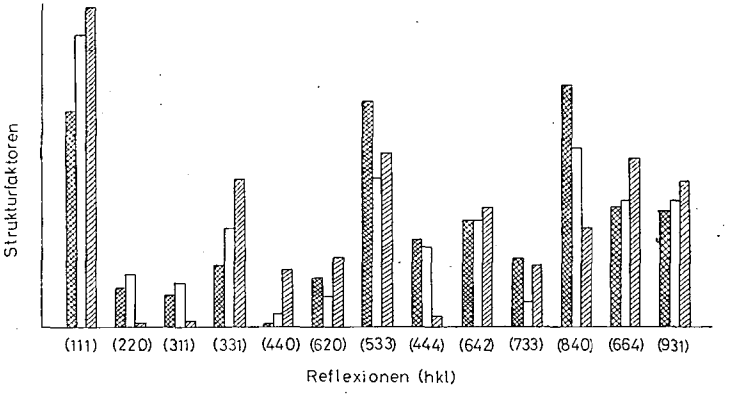

Abb. 1. Der Vergleich der gemessenen Strukturfaktoren (doppelt schraffierte Kolonnen) mit der berechneten Strukturfaktoren eines gelungenen (unschraffierte Kolonnen) bzw. offensichtlich schlechten (einfach schraffierte Kolonnen) Modells

Dieses herausgegriffene Beispiel zeigt, daß die Silberionen bei vollständigem Austausch alle 16 S_I-Positionen der Elementarzelle des Faujasits einnehmen. Die Ergebnisse der Modellisierung der übrigen Proben führten zu der Schlußfolgerung, daß die S_I-Positionen schon bei geringeren Austauschgraden besetzt werden. Die Silberionen nehmen sogar — unabhängig vom Silbergehalt — S_I-Positionen ein, solange das prinzipiell möglich ist, und erst danach werden die weniger bevorzugten $S_{I'}$- bzw. S_{II}-Positionen besetzt. Diese Tendez stellt sich auch bei dem Vergleich der in Abb. 2 dargestellten Meßergebnisse und der in Tab. V angegebenen gemessenen Strukturfaktoren heraus.

Aus der Abbildung ist zu ersehen, daß die (840)-Reflexion in Abhängigkeit vom Silbergehalt anfangs stark, danach langsamer ansteigt und schließlich abnimmt, was in Übereinstimmung mit den Werten der Tabelle ist: der berechnete Wert F_{NaY} ist eine große positive Zahl, und wenn der zunächst ebenfalls große Wert F_{Ag1} hinzukommt, so ist eine größere Erhöhung zu erwarten, später dagegen — wenn der kleinere, positive Wert von F_{Ag2} hinzukommt — eine geringere Erhöhung. Schließlich ist auch die Abnahme verständlich, da F_{Ag3} negativ ist. Die (533)-

Reflexion nimmt anfangs — die Meßunsicherheiten in Betracht gezogen — nicht zu, da F_{Ag1} eine kleine positive und F_{NaY} eine große negative Zahl ist, später aber nimmt sie stark zu, da F_{Ag2} ebenfalls eine große negative Zahl ist. Am Ende schließlich fällt die Kurve ab, da F_{Ag3} positiv ist.

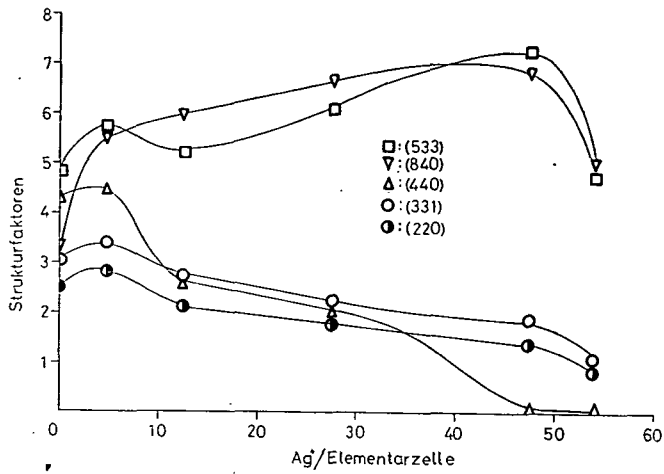

Abb. 2. Die Abhängigkeit der aus den Meßdaten berechneten Strukturfaktoren vom Ag^+-Gehalt des Zeolithes

Die Abnahme der Reflexionen (220) und (331) mit steigendem Silbergehalt sind auf ähnliche Weise erklärbar. Was das Verhalten der (440)-Reflexion betrifft, so ist die Abnahme verständlich, da F_{NaY} negativ und alle F_{Ag} positiv sind, aber daneben ist auch der einen geringen Anstieg aufweisende mittlere Teil der Kurze zu erklären, da F_{Ag2} ein sehr kleiner Wert ist.

Diese qualitativen Erwägungen können noch verfeinert werden, wenn auch die Strukturfaktoren der im Verlaufe des Austauschs eliminierten Na-Ionen berücksichtigt werden. Die geringeren Anomalien dagegen lassen sich auf die Unsicherheit der Positionen des stets zugegenen Wassers zurückführen.

Die Modellierung kann nach der Berechnung der vollständigen Strukturfaktor-Matrix sehr schnell, also in großer Zahl ausgeführt werden, nur eine vernünftige Vorgabe der Besetzungsgrade der Ionen-positionen ist erforderlich. Unserer Meinung nach sind röntgendiffraktometrische Untersuchungen von entsprechend vorbereitetem Versuchmaterial (Zeolithproben) geeignet, mit Hilfe gut durchdachter Modellierungsreihen auf zahlreiche solche ungeklärte Fragen Antwort zu geben, die bei der Untersuchung der Ionenaustauscheigenschaften von Zeolithen, insbesondere hinsichtlich der von den Ionen eingenommenen Positionen, auftauchen.

Literatur

[1] *Breck, D. W.:* Zeolite Molecular Sieves John Wiley, New York.
[2] *Costenoble,M. L., W. J. Mortier, J. B. Uytterhoeven:* J.C.S. Faraday I., **74**, 466 (1978).
[3] *Eulenberger, G. R., D. P., Schomaker, J. G. Keil,:* J. Phys. Chem., **71**, 1812 (1967).
[4] *Uytterhoeven, J. B.:* J. Phys. Chem., **76**, 650 (1972).

[5] *Gallezot, P., B. Imelik,:* C. R. Acad. Sci. Ser. C, **272**, 261 (1971).
[6] *Gallezot, P., B. Imelik:* J. Catal., **26**, 481 (1972).
[7] *Gallezot, P., Y. Ben Taarit, B. Imelik:* J. Catal. **26**, 295 (1972).
[8] *Fichtner-Schmittler, H.:* Proc. of 8th Hung. Diffr. Conf., 1976, Tihany, p. 66.
[9] *Beyer, H. K., P. A. Jacobs, J. B. Uytterhoeven:* J.C.S. Faraday I., **42**, 647 (1976).
[10] *Kálmán, A.:* Mérés és automatika, **8**, 215, 322 (1960); **11**, 41, 80 (1963).
[11] International Tables for *X*-ray Crystallography The Kynoch Press, Birmingham,
Band I, S 32—33 (1952);
Band II, S 268 (1959).
[12] loc. cit. [11], Band IV. S 71 (1974).
[13] loc. cit. [11], Band I. S 519 (1952).

ИЗУЧЕНИЕ РЕНТГЕНО-ДИФРАКЦИОННЫМ МЕТОДОМ ВНЕДРЕНИЯ ИОНОВ СЕРЕБРА В ЦЕОЛИТЫ ТИПА У.

К. Варга, И. Киричи и Дь. Аргаи

Авторы приготовили образцы AgNaY цеолитов с различным содержанием серебра и на основании рентгено-дифрактограм с применением структурно-факторного анализа установили места и очередность внедрения ионов Ag^+. Разработанная авторами программа для ЭВМ пригодна для расчета дифрактограм любых фаужазитного типа цеолитов.

SATURATED HETEROCYCLES, XXI*
SYNTHESIS OF 2,3-TRIMETHYLENE- AND TETRAMETHYLENE--4-OXO-PYRIDO[1,2-*a*]PYRIMIDINE-7-, 8- AND 9-CARBOXYLIC ACID DERIVATIVES WITH POTENTIAL PHARMACOLOGICAL ACTIVITY

By

F. FÜLÖP**, G. BERNÁTH**

Institute of Organic Chemistry, József Attila University, Szeged

and

I. HERMECZ and Z. MÉSZÁROS

CHINOIN Pharmaceutical and Chemical Works Ltd., Budapest, Hungary

(Received 23rd Apr. 1979)

From substituted 2-aminopyridines and ethyl-(2-cyclopentanone- or 2-cyclohexanonecarboxylates), 7-, 8- or 9-carboxylic acid derivatives of 2,3-trimethylene- and tetramethylene-4-oxo-pyrido-[1,2-*a*]pyrimidine were synthesized using polyphosphoric acid or phosphortrichloride-oxide and polyphosphoric acid mixture as condensing agent.

The 4-oxo-pyrido[1,2-*a*]pyrimidines, their synthesis, chemical and pharmacological behaviour have been the subject of our extensive study for more then ten years [1, 2]. The compounds excelled in analgetic activity. One of them, *"Probon"* (**1**) has since been introduced in Hungary, as a new analgetic.

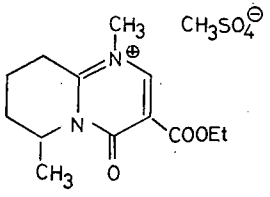

1

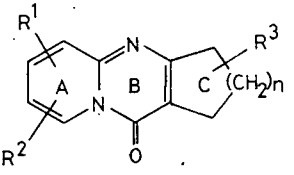

2

* For previous parts of this Series, see: Part XI: F. Fülöp, I. Hermecz, Z. Mészáros, Gy. Dombi, G. Bernáth: J. Heterocyclic Chem. **16**, 457 (1979); Part XII: G. Bernáth, F. Fülöp, Gy. Jerkovich, P. Sohár: Acta Chim. (Budapest) **101**, ... (1979), in press; Part XIII: P. Sohár, L. Gera, G. Bernáth: Organic Magnetic Resonance, in press; Part XIV: L. Gera, G. Bernáth, P. Sohár: Acta Chim. (Budapest), in press; as part XV is regarded: B. Ribár, A. Petrović, Gy. Göndös, G. Bernáth: Cryst. Struct. Comm. **8**, 671 (1979). The parts XXXIX—XLIII of the Series „Stereochemical Studies", G. Bernáth, A. Kálmán *et al.*, Cryst. Struct. Comm. **9**, (1980), in press are also considered to be Parts XVI—XX of the Series „Saturated Heterocycles".

** Present address: Institute of Pharmaceutical Chemistry, University Medical School, 6720 Szeged, Eötvös u. 6, Hungary.

In our previous publication [3] we reported the synthesis and some chemical reactions of the 2,3-polymethylene-derivatives (**2**) of the 4-oxo-pyrido[1,2-*a*]pyrimidines. The substituents of **2** ($n=1-4$) were: alkyl, hydroxyl, nitro, and halogen. According to the expectation, most of the derivatives had considerable, and some of them significant analgetic activity [4]. In the case of $n=2$, compounds **2** comprize the pyrido[2,1-*b*]quinazoline ring, which is a frequent and essential structural element of some plant alkaloides [5].

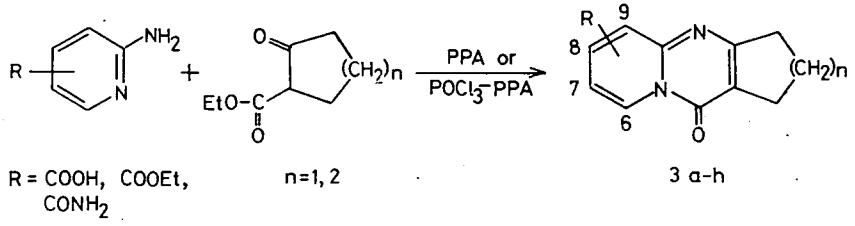

As a continuation of the previous work, here we give an account on some new derivatives of **2**, in which the pyridine ring bears carboxy-group substituent. These compounds may possibly also be of biological interest. Recently some pyrido[2,1-*b*]quinazolin-carboxylic acids, with aromatic "C" ring, have been reported [6–8] to exhibit significant antiallergic — first of all antiasthmatic — effect, and they showed activity — in contrast to *"Intal"* — also after oral administration.

In the synthesis we started from the corresponding substituted 2-amino-pyridine and alicyclic ethyl β-keto-carboxylates (the ring size of the esters was 5 and 6). The carboxy-substituted 2-amino-pyridines, not available commercially, were prepared by known methods [9–11]. The condensation reaction was carried out by either the method of SHUR and ISRAELSTAM [12], using polyphosphoric acid (PPA), or by the method reported by MÉSZÁROS *et al.* [1], using phosphortrichloride-oxyde and polyphosphoric acid mixture ($POCl_3$—PPA) as condensing agent. Independent of the size of the alicyclic ring of the δ-ketocarboxylate, both methods were appropriate for the preparation of the pyrido-pyrimidines, although the PPA method proved to give better yields and purer products in this case. The yields are shown in Table I.

The resulting pyrido[1,2-*a*]pyrimidines (**3a-h**) are insoluble in water. The esters dissolve readily, while the carboxylic acids and the amides are rather insoluble in common organic solvents. The structures were proved by elementar analysis and by spectroscopic methods. The data of the elementar analysis and the UV and IR characteristics are given Tables I and II, respectively.

Some reactions of the carboxyl group of the 7-substituted 2,3-tetramethylene derivatives were carried out. The **3c** ester and the **3d** amide were hydrolysed into the **3b** carboxylic acid in a 2% aqueous hydrochloric acid solution at 100° C. The **3d** carboxylic acid was converted into ester in good yield, in boiling ethanolic hydrochloric acid solution and the carboxamide **2d** was formed quantitatively from the ester on the effect of methanolic ammonia solution.

Table I

Physical characteristics and analytical data for compounds **3a-h**

Compound	R	*n*	Formula, Molecular weight	M. p. (°C) Solvent for recrystallization	Analysis (%) Cald./Found			Yield (%	
					C	H	N	PPA	$POCl_3$-PPA
3a	7-COOH	1	$C_{12}H_{10}N_2O_3$ 230.22	325[a] DMF	62.60 62.74	4.38 4.46	12.17 12.06	55	40
3b	7-COOH	2	$C_{13}H_{12}N_2O_3$ 244.24	255-258 ethanol	63.92 63.84	4.95 5.00		51	44
3c	7-COOEt	2	$C_{15}H_{16}N_2O_3$ 272.29	100-102 ether	66.16 66.20	5.92 6.02		67	49[b]
3d	7-$CONH_2$	2	$C_{13}H_{13}N_3O_2$ 243.26	313-315 DMF	64.18 64.22	5.39 5.61	17.28 17.01	41	
3e	8-COOEt	2	$C_{15}H_{16}N_2O_3$ 272.29	92-93 ether	66.16 66.24	5.92 5.81		81	52[b]
3f	9-COOH	1	$C_{12}H_{10}N_2O_3$ 230.22	189-193[c] ethanol	62.60 62.56	4.38 4.44	12.17 12.30	48[b]	
3g	9-COOH	2	$C_{13}H_{12}N_2O_3$ 244.24	202-204 ethanol	63.92 63.96	4.96 4.96	11.47 11.59	46	
3h	9-COOEt	2	$C_{15}H_{16}N_2O_3$ 272.29	143-144 ethanol	66.16 66.20	5.92 5.87		63	

[a] Under decomposition
[b] The reaction mixture was treated with ethanol
[c] Lit. [13] m.p.: 191-3 °C, yield: 58%

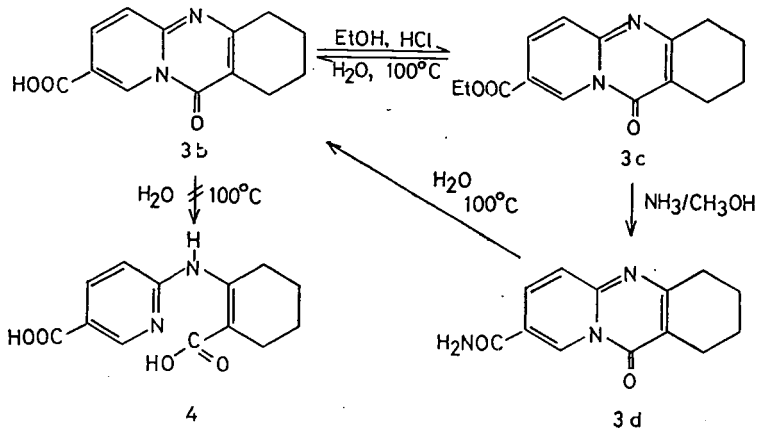

The compounds **3a-h** are weak bases. The hydrochlorides could only be prepared from the ester derivatives, while those of the carboxylic acids and the amides — though they could be prepared —, the parent bases were deliberated under the conditions of the recrystallization.

Table II

UV and IR characteristics of compounds **3**

Compound	R	*n*	UV Absorption Maxima (log ε) [nm]		IR ν_{max} (cm^{-1})
3a	7-COOH	1	344 (—)	236 (—)	1720, 1695
3b	7-COOH	2	344 (2.99)	235 (3.28)	1725, 1695
3c	7-COOEt	2	345 (4.08)	238 (4.43)	1730, 1685, 1500
3d	7-$CONH_2$	2	344 (—)	235 (—)	1685, 1495, 1450, 1415
3e	8-COOEt	2	370 (3.89)	264 (4.07)	1730, 1670
3f*	9-COOH	1	335 (3.97)	268 (4.14) 262 (4.13)	1725, 1695, 1585
3g	9-COOH	2	330 (3.93)	260 (5.05)	1730, 1695, 1595, 1490
3h	9-COOEt	2	336 (4.00)	259 (4.08)	1735, 1670, 1485

* Lit [13] IR (in $CDCl_3$): *v* 1700—2500 (broad *s*), 1720-1670 (broad *s*), 1575 (*s*), 1530 (*s*) 1500—1415 (broad *s*) cm^{-1}.

The pharmacological behaviour of the compounds is under investigation [14].

Experimental

Melting points were determined on a Boetius apparatus, and are uncorrected. The IR spectra were taken in KBr pills with a Unicam SP 200 spectrometer. The UV spectra were recorded in ethanolic solution on a Unicam SP 800 spectrophotometer.

2,3-Tetramethylene-4-oxo-pyrido[1,2-a]pyrimidine-7-carboxylic acid (**3b**)

a) *in PPA:*

3.4 g (20 mmol) of 2-Carbethoxycyclohexanone and 2.76 g (20 mmol) of 6-amino-nicotinic acid were stirred and heated in 20 g of polyphosphoric acid, on a water bath for 1.5 hrs. Than the hot reaction mixture was carefully diluted with 10–20 ml of water, and neutralized under cooling with a 10% aqueous ammonia solution. After 1 hr of standing, the resulting crystals were collected, washed with water and dried. The product (2.5 g, 51%) was crystallized from ethanol.

Compounds **3a, c-h** were obtained similarly. For yields and melting points see Table I.

b) *in $POCl_3$—PPA mixture:*

2-Carbethoxycyclohexanone (3.4 g, 20 mmol) and 6-amino-nicotinic acid (2.76 g, 20 mmol) were heated and stirred in a mixture of phosphortrichloride-oxyde (5.6 ml, 60 mmol) and polyphosphoric acid (1.4 g) on a water bath for 1.5 hrs. After the cease of the hydrochloric acid evolution, ice-cold water was dropwise added to the hot reaction mixture, and it was afterwards neutralized with 10% aqueous ammonia solution. After 1 hr of standing the resulting crystals were collected, washed with water and dried. The product (2.15 g, 44%) was crystallized from ethanol. The product showed no melting point depression with the sample obtained in the PPA ring closure.

Compounds **3a, c, e** were prepared similarly. For yields see Table I.

Ethyl 2,3-tetramethylene-4-oxo-pyrido[1,2-a]pyrimidine-7-carboxylate (**3c**)

1 g of 2,3-Tetramethylene-4-oxo-pyrido[1,2-*a*]pyrimidine-7-carboxylic acid (**3b**) was refluxed for 3 hrs in a 20% ethanolic hydrochloric acid solution. The solution was evaporated, the crystalline residue was dissolved in 20 ml of water, and neutralized with saturated aqueous sodium hydrocarbonate solution. The resulting yellow crystals (0.92 g, 82%) were crystallized from ether, m.p.: 99–101 °C. The product did not show melting point depression with the ester **3c** obtained in the PPA or $POCl_3$—PPA ring closure.

2,3-Tetramethylene-4-oxo-pyrido[1,2-a]pyrimidine-7-carboxamide (**3d**)

1 g of Ethyl 2,3-tetramethylene-4-oxo-pyrido[1,2-*a*]pyrimidin-7-carboxylate (**3c**) was dissolved in 10 ml of saturated methanolic ammonia solution. The amide (**3f**) started to precipitate in 10 minutes. The reaction mixture was left overnight. The crystals were collected (0.84 g, 94%), and purified by crystallization from dimethyl-formamide to obtain pale yellow crystals, m.p.: 312–5 °C. The product did not show melting point depression with the corresponding amide obtained by the PPA ring closure.

References

[1] *Mészáros, Z., J. Knoll, P. Szentmiklósi, Á. Dávid, G. Horváth, I. Hermecz:* Arzneim.-Forsch. **22**, 815 (1972).
[2] *Mészáros, Z.:* Kémiai Közlemények **50**, 173 (1978).
[3] *Bernáth, G., F. Fülöp, I. Hermecz, Z. Mészáros, G. Tóth:* J. Heterocyclic Chem. **16**, 137 (1979).
[4] *Hermecz, I., F. Fülöp, Z. Mészáros, G. Bernáth, J. Knoll,:* Hung. Pat. Appl. CI 1766, 19th Aug. 1977.
[5] *Armarego, W. L. F.:* Quinazolines (In the Series of Fused Pyrimidines Ed.: A. Weissberger) Part I., Interscience Publishers, New York, 1967.
[6] *Schwender, C. F., B. R. Sunday:* Ger. Offen 2.645.110; C. A. **87**, 23 327x (1977).
[7] *Schromm, K., A. Mentru, E. O. Renth, A. Fuegner:* Ger. Offen 2.557.425; C. A. **87**, 117 898m (1977).
[8] *Yale, H. L.:* US Pat. 3.965.100; C. A. **85**, 177 477s (1976).
[9] *Oakes, V., R. Pascoe, H. N. Rydon:* J. Chem. Soc. **1956**, 1045.
[10] *Ferrari, G., E. Marcon:* Farmaco Pavia Ed. sci. **13**, 485 (1958); C. A. **53**, 7162b (1959).
[11] *Vejdelek, Z. J.:* Chem. Listy **46**, 770 (1952); C. A. **47**, 11 191i. (1953).
[12] *Shur, M., S. Israelstam:* J. Org. Chem. **33**, 3015 (1968).
[13] *Yale, H. L.:* J. Heterocyclic Chem. **14**, 207 (1977).
[14] *Knoll, J. et al.:* To be published.

НАСЫЩЕННЫЕ ГЕТЕРОЦИКЛЫ. XXI. СИНТЕЗ 2,3-ТРИМЕТИЛЕН- И ТЕТРАМЕТИЛЕН-4-ОКСО-ПИРИДО[1,2-*a*]ПИРИМИДИНО-7-, 8- И 9 - КАРБОКСИЛЬНЫХ ПРОИЗВОДНЫХ С ВЕРОЯТНОЙ ФАРМАКОЛОГИЧЕСКОЙ АКТИВНОСТЬЮ

Ф. Фюлеп, Г. Бернат, И. Гермец и З. Месарош

Из замещенных 2-аминопиридинов и этил-(2-циклопентанон- или 2-циклогексанон карбоксилатов), 7-, 8- или 9-карбоксильных производных были синтетизированы 2,3-триметилен- и тетраметилен-4-оксо-пиридо[1,2-*a*]пиримидины с применением в качестве конденсирующих агентов полифосфорной кислоты или смеси фосфортрихлорного окисла и полифосфорной кислоты.

A kiadásért felelős: Dr. Tandori Károly
1979
A kézirat nyomdába érkezett: 1979. Május. Megjelenés: 1979. November
Példányszám: 550. Ábrák száma: 34. Terjedelem: 7,5 (A/5) ív
Készült monószedéssel, íves magasnyomással, az MNOSZ 5601—50/A szabványok szerint
79-2975 — Szegedi Nyomda — F. v.: Dobó József igazgató

Information for Contributors

1. Manuscripts should be submitted to Prof. Pál Fejes, Institute of Applied Chemistry, József Attila University, Szeged, Rerrich tér 1, Hungary, H-6720.
2. The manuscripts must not exceed in any case 32 pages (Figures, legends, Tables and Summary included). Manuscripts should be submitted in duplicate.
3. The format of the text: A/4, double spaced, 25 lines per page and 50 characters per line. Title: all capital characters; underlined twice. Subtitle(s) should be written in new line(s) in normal writing, underlined also twice, first characters: capital. (See the following example).

STEREOCHEMICAL STUDIES

Studies on Cyclic-2-Hydroxycarboxylic Acids

By

PÁL KISS

Research Institute for Industrial Chemistry, Budapest
(Received.....)

4. After these comes the summary, which is followed by the text proper. If the parts of the paper are separated by secondary titles like: Introduction, Experimental etc., the following rule holds: secondary titles of equal rank are to be written in new lines, the first word with capital letter, otherwise running text underlined once.
   Example:
   Introduction
   Experimental part
5. The names of the authors in the running text are written in capital letters. Exceptions are the names in connection with scientific instruments, etc. where only the first letter should be capital.
6. Citations in the text with reference to the selected literature at the end of the paper are to be made with squared brackets, like: [5], [4, 9], [4—9].
7. To make printing easier, mathematical formulas are to be simplified as much as possible. Reference to mathematical equations is made by numbers in parenthesis, like: (16).
8. Tables should be typed on separate pages. Please supply numbers and titles for all tables (Numbering occurs with Roman numerals: Table I).
   Throughout the whole text the IUPAC nomenclature should be used.
   Insert of Tables in the text will be indicated at the appropriate place of the margin, like this: Table I.
9. Figures must be drawn clearly with Chinese ink on oily drawing paper, the thickness of lines as well as size of letters and symbols should be selected with care, the minimum size is nearly 0,3 cm.
   The maximum width of Figures is 24 cm, however, Figures of width equal or less than 12 cm are preferred.
   Please, use upwright writing on the Figures.
   In the case of real numbers points are used instead of commas.
   The place of Figures in the text is indicated on the margin like this: Figure 13.
   Please supply legends for all figures and compile these on separate sheets. Indicate only the number of the Figures in the original drawing, for this purpose use blue pencil.
10. Literature will be given under the heading References, like this: (on a separate sheet at the end of the manuscript)
    [1] Allinger, N. L., M. T. Tribble: J. Phys. Chem. 33, 1565 (1976).
    [2] Abraham, J. K., H. S. Hoover: Principles of Competitive Oxidation. Mc Graw-Hill, New York, 1977, p. 133.

INDEX